Regulation of the Hedgehog signalling pathway by Patched1 interacting proteins

Cintli Carina Morales Alcalá

Submitted in accordance with the requirements for the degree of

Doctor of Philosophy

The University of Leeds

School of Medicine

Faculty of Medicine and Health

April 2021

The candidate confirms that the work submitted is their own, except where work which has formed part of jointly authored publications has been included. The contribution of the candidate and the other authors to this work has been explicitly indicated below. The candidate confirms that appropriate credit has been given within the thesis where reference has been made to the work of others.

The work in Chapter 3 of the thesis has appeared in publication as follows:

Chen, X., Morales-Alcala, C.C. and Riobo-Del Galdo, N.A. 2018. Autophagic Flux Is Regulated by Interaction Between the C-terminal Domain of PATCHED1 and ATG101. *Molecular Cancer Research.* **16**(5), pp.909–919.

I was responsible for generation of the results in figure 3.E of this publication.

The contribution of the other authors in the published paper are as follows:

Conception and design: X. Chen, N.A. Riobo-Del Galdo

Acquisition of data: X. Chen.

Analysis and interpretation of data: X. Chen, N.A. Riobo-Del Galdo

Writing, review, and/or revision of the manuscript: N.A. Riobo-Del Galdo

Acknowledgements

I must thank my supervisor Dr Natalia Riobo-Del Galdo, for giving me the opportunity to work in her lab and for the advice and guidance she gave throughout the completion of this project.

I must also thank my co-supervisors Dr Heiko Wurdak and Dr Francesco Del Galdo for the insight they offered, particularly during the first and second year of my PhD.

I want to express my gratitude to the National Council on Science and Technology of Mexico (CONACyT) and the former Leeds Institute of Cancer and Pathology for the support that I received via the CONACyT and LICAP scholarships that allowed me to carry out with my PhD studies.

I thank my amazing lab team, particularly Ioanna, Alex and Dom. My years in the lab would not have been the same without this lot, who besides being my first source to share ideas and solve lab related doubts, were also the most fun to hang around and who, after more than 5 years of knowing each other, have become true friends.

I also thank all my friends that one way or another made my PhD a more happy experience, especially Nel, that has been on the other line on the phone every time I needed to vent, cry and share good news (yes, there were some of those too), I will forever dread the day when we finally play “yo nunca, nunca”… you know way too much.

I want to thank Dan, I couldn’t have dreamt of a better partner in crime/dance partner/fellow foodie, that even in my worst days managed to put a smile on my face and helped keep me sort of sane during the writing period, always making sure I didn’t have cereal for dinner. I am so happy that for more than a year now, you were the only person I was legally allow to hug.

Finally and very importantly, I am so grateful to my family for all the support and encouragement they have always given me. Particularly my mum, I don’t know what would I have done without all the calls, the virtual hugs and the lighting of candles during all these years. And also to my sister Cintia, who always has the best advice and is willing to bet on me no matter what; I really, really hope to soon owe you an all-inclusive holiday. Thank you both so much for always believing in me and being by my side every step of the way.

Abstract

The Hedgehog (Hh) receptor Patched1 is a well-established tumour suppressor. Its C-terminal domain (CTD) interacts with autophagy-related protein 101 (ATG101) to inhibit autophagic flux. The first part of my research focused on understanding this interaction. In Chapter 3, I show that endogenous Patched1 is sufficient to restrain autophagic flux. On Chapter 4, I investigated the functional consequences of three somatic mutations found in the CTD in human cancer databases. Results show that two of these lose the interaction with ATG101 causing an apparent increase in autophagic flux. These results strengthen a tumour suppressor role of Patched1 in addition to, and independently of, its function as Smoothened repressor.

In Chapter 5, I validated and characterised the physical interaction between Integral membrane protein 2A (ITM2A) and Patched1. While the findings indicate that ITM2A, like Patched1, inhibits autophagic flux, the results suggest that they work independently.

Unexpectedly, ITM2A had a negative effect on the stability of Patched1, which suggested a crosstalk with the Hh canonical pathway. Further analysis revealed that ITM2A negatively regulates Gli1 and Gli2 transcriptional activity. In Chapter 6, I showed a potential inhibitory function of Itm2a on autophagic flux during myogenic differentiation. Partial silencing of Itm2a delayed both myogenic differentiation and upregulation of cyclin D3 necessary for cell cycle exit of myoblasts. Proteomic analysis was used to find potential ITM2A-interacting proteins, which suggest a potential role in regulation of CDK1 and CDK2NA and of selective autophagy, which will be explored in future studies.

In summary, this doctoral research uncovered a novel role of ITM2A as a negative regulator of the canonical Hh pathway and as a Patched1-binding partner. Results suggest that ITM2A might be a specific regulator of selective autophagy during skeletal muscle differentiation as opposed to a more general role of Patched1 through its interaction with ATG101.

Table of Contents

Contents

List of Figures

List of Tables

Abbreviations

ATG	autophagy related
BCC	basal cell carcinoma
BCNS	basal cell nevus syndrome
bHLH	basic helix-loop-helix
BOC	Brother of CDO
BSA	bovine serum albumin
CDK	cyclin-dependent kinase
CDKI	CDK inhibitor
CDO	Cell adhesion molecule Downregulated by Oncogenes
Co-IP	Co-immunoprecipitation
CTD	C-terminal domain
Dhh	Desert Hedgehog
Disp	Dispatched
DMEM	Dulbecco’s modified eagle medium
DMOS	dimethyl sulfoxide
DNA	deoxyribose nucleic acid
eGFP	enhanced green fluorescence protein
ER	endoplasmic reticulum
FBS	foetal bovine serum
FIP200	focal adhesion kinase family interacting protein of 200 kDa
GABARAP	GABA type A receptor-associated protein
GAPDH	glyceraldehyde-3-phosphate dehydrogenase
Gli	Glioma associated oncogene
GPCR	G-protein coupled receptor

GSK3β	glycogen synthase kinase 3β
Hh	Hedgehog
Ihh	Indian Hedgehog
ITM2A	integral membrane protein 2A
LIR	LC3 interaction region
MAP	microtubule-associated proteins
MEFs	mouse embryonic fibroblasts
MHC	myosin heavy chain
MRF	myogenic regulatory factor
mRNA	messenger ribonucleic acid
mTOR	mechanistic target of rapamycin
mTORC1	mTOR complex 1
PBS	phosphate buffered saline
Ptc	Drosophila Patched
Ptch1	mouse Patched
PTCH1	Human Patched1
PTCH2	Human Patched2
Raptor	mTOR, rapamycin-associated protein of TOR
Rictor	Rapamycin insensitive companion of TOR
RNA	ribonucleic acid
RND	resistance nodulation division
RPM	revolutions per minute
SDS-PAGE	sodium dodecyl sulphate polyacrylamide gel electrophoresis
Shh	Sonic Hedgehog
siRNA	small interference RNA
Smo	Smoothened

SSD	sterol sensing domain
TBS	tris-buffered saline
UBA	ubiquitin-associated
UBL	ubiquitin-like
ULK	uncoordinated-51-like kinase
VPS34	vacuolar protein sorting 34
WCL	whole cell lysate

Chapter 1

Literature Review

Chapter 1

Literature Review

1.1 Hedgehog Signalling Pathway

The correct functioning of multicellular organisms relies on highly orchestrated signalling pathways and their regulation is important for the cellular response to the ever-changing cellular environment. Dysregulation of these signalling cascades is linked to different human pathologies (Lodish et al., 2000; Valdespino-Gómez, et al., 2015). The Hedgehog (Hh) signalling pathway is a major regulator of embryonic development in vertebrates and invertebrates (McMahon et al., 2003). The *Hh* gene was first identified in a study designed to find embryonic mutants in *Drosophila melanogaster.* The *Hh* gene was shown to be involved in the patterning and in the polarity of the segments during *Drosophila* development (Wieschaus and Nüsslein-Volhard, 1980). Later, vertebrate homologues of the *Hh* gene were identified, including the mammalian members of the Hh family Sonic, Indian and Desert Hh (Echelard et al.,1993; Ingham and McMahon, 2001). The role of Hh signalling in embryonic development involves cell specification, cell proliferation, cell differentiation and cell survival. The Hh signalling pathway is involved in the formation of most of mammals' organs. The effect of Hh signalling is dependent on the cell type, on the concentration (since it acts as a morphogen) and on the time the cells are subjected to Hh stimulus (Ingham and McMahon, 2001). Hh signalling is also involved in the maintenance of homeostasis and regeneration of different adult structures, and aberrant signalling has been linked to tumorigenesis and different types of cancer in mammals (Petrova and Joyner, 2014; Bangs and Anderson, 2017).

1.1.1 Core components of the Hh signalling pathway

Functional Hh proteins are produced by the autocatalytic cleavage of the Hh precursor (45 kDa). This cleavage results in the generation of two fragments. The N-terminal fragment (Hh-N) has a molecular weight of around 20 kDa while the C-terminal fragment (Hh-C) has a molecular weight of around 25 kDa. The amino terminal fragment is involved in the signalling activity of the protein, while the C-terminal fragment plays a role in the autocatalytic cleavage of the precursor form of the Hh protein and aids in the cholesterol modification carried out during the processing of the Hh-N fragment. During processing, the N-terminal fragment is modified by covalent addition of a cholesterol moiety to the carboxyl group of its C-terminus. Additionally, after cholesterol binding, maturation of Hh-N also includes the attachment of a palmitate group into its N-terminal cysteine. The efficient processing of the Hh proteins is necessary for their functionality (Lee et al., 1994; Bumcrot et al., 1995; Porter et al., 1995; Porter et al., 1996; Pepinsky et al.,1998). Once the Hh-N fragment has been processed and secreted, it remains anchored in the plasma membrane. The release of the lipid-modified and functional Hh protein from the producing cell is carried out by the 12-pass transmembrane protein Dispatched (Disp) that functions as a sterol transporter protein. Hh proteins are secreted to the extracellular matrix and can exert their activity locally and also be diffused over long distances to reach the target cells (Burke et al., 1999; Ma et al., 2002; Yang et al., 2015).

Similar to most of the components of the Hh signalling pathway, *Patched* (*Ptc*) was first described in *Drosophila* and characterised as a gene that encodes for a large multi-pass transmembrane protein expressed during embryogenesis and involved in the regulation of cell patterning (Nakano et al., 1989; Hidalgo and

Ingham, 1990; Ingham, 1991). Later, its role as the receptor and repressor of the Hh signalling pathway was established (Ingham et al., 1991; Chen and Struhl, 1996; Stone et al.,1996).

There are two mammalian homologues of *Drosophila* Ptc: Patched1 (PTCH1) and Patched2 (PTCH2). PTCH1 is the most abundant and the most broadly studied mammalian receptor of the Hh pathway. *PTCH1* is a tumour suppressor gene that encodes for a 12-pass transmembrane protein. PTCH1 is negatively regulated by the Hh proteins and, in the absence of Hh ligands it actively represses the activity of Smoothened (Smo). PTCH1 localises in the plasma membrane, its C-terminal domain (CTD) and N-terminus are intracellular while its two large loops are located extracellularly and physically interact and bind to the Hh proteins to activate the pathway. PTCH1 has similarity with the resistance nodulation division (RND) family of bacterial transporters, commonly used to pump lipophilic substrates through membranes. PTCH1 also contains a putative sterol sensing domain (SSD) of about 180 amino acids long that is involved in cholesterol trafficking (Capdevila et al., 1994; Stone et al.,1996; Loftus et al., 1997; Johnson et al., 2002; Taipale et al., 2002; Rohatgi et al., 2007; Robbins et al., 2012).

The CTD of PTCH1 is involved in the regulation of important functions. Studies show that the soluble CTD is enough to exhibit the pro-apoptotic phenotype observed when full length PTCH1 is expressed. The CTD regulates the intracellular localization of PTCH1 and also its turnover (Thibert et al., 2003; Lu et al., 2006; Kawamura et al., 2008).

Mutations that render PTCH1 inactive and that lead to the unregulated activation of the Hh signalling pathway are linked to abnormalities in the developmental

stage and to different types of cancer. In particular, mutations in human PTCH1 are linked to the development of basal cell nevus syndrome (BCNS), also referred to as Gorlin's syndrome, characterised by minor skeletal defects and high incidence of medulloblastoma and basal cell carcinoma (BCC). Somatic mutations of PTCH1 are causal of almost 90% sporadic BCC, the most common skin cancer (Hahn et al., 1996; Johnson et al., 1996; Epstein, 2008).

PTCH2 is another receptor of the Hh signalling pathway. It shares ~50% of homology with PTCH1. The CTD is the least conserved part between these two proteins. *PTCH2* gene encodes for a slightly smaller protein, compared to PTCH1, that exhibits lower activity for inhibition of SMO in the absence of Hh protein. The expression pattern and signalling varies between PTCH1 and PTCH2. Nonetheless, the transcription of PTCH2, as well as the expression of PTCH1, depends on the activation of Gli transcription factors and serves as a negative feedback (Kawamura et al., 2008; Robbins et al., 2012).

The Hh signalling pathway also requires the expression of co-receptors that bind to the Hh ligands. These co-receptors are conserved between *Drosophila* and mammals. The first Hh co-receptor to be identified was Interference Hedgehog (Ihog). It was described as a positive regulator of the Hh pathway in *Drosophila*. A second co-receptor, Brother of Ihog (Boi), was also identified in *Drosophila*. Boi is a homologue of the Ihog protein that carries out the same function as Ihog. Ihog is a type I (single pass) transmembrane protein. Ihog's intracellular domain is not conserved while its larger extracellular region is composed of four immunoglobin-like (Ig) domains and two fibronectin type III (FNIII) domains. The interaction of Ihog with Hh ligands is mediated by the first FNIII domain (FN1)

while the interaction of this co-receptor with Ptc is through its second FNIII domain (FN2) (Lum et al., 2003; Yao et al., 2006; Zheng et al., 2010).

There are two mammalian homologues of Ihog: Cell adhesion molecule Downregulated by Oncogenes (CDO) and Brother of CDO (BOC). These interact with the Hh ligand through their FNIII domain in a fashion comparable to the one described for Ihog. CDO and BOC are type I transmembrane proteins, their extracellular region contains four or five Ig domains, respectively, and two or three FNIII domains, respectively. Expression of these co-receptors is involved in the activation of the Hh signalling pathway, their activity is redundant to each other and silencing of both co-receptors does not completely abolish activation of the Hh signalling (Okada et al., 2006; Tenzen et al., 2006; Yao et al., 2006). Growth arrest-specific 1 (GAS1) is a third co-receptor of the vertebrate Hh pathway. Different from CDO and BOC, GAS1 is a cell surface protein that does not contain a transmembrane domain, instead localises to the cellular membrane by a glycosylphosphatidylinositol (GPI) anchor. As CDO and BOC, GAS1 is a positive regulator of Hh signalling. Abrogation of GAS1 expression is characterised by a reduced Hh signalling, however it does not inhibit it completely (Allen et al., 2007; Martinelli and Fan, 2007; Beachy et al., 2010). The importance of these three co-receptors in the mammalian Hh signalling pathway was appreciated in a study that showed that a Shh mutant, that retains the interaction with PTCH1 but that is unable to bind to any of the co-receptors (CDO, BOC and GAS1) cannot activate the pathway (Izzi et al., 2011).

The *Smoothened* (*Smo*) gene was first identified in *Drosophila* as a polarity gene required for embryonic cell patterning. *Smo* encodes for a 7-transmembrane protein that is structurally similar to G-protein coupled receptors (GPCRs). Its role

in the Hh signalling was first thought to be the receptor of the pathway, later it was shown that Smo mediates the activation of Hh signalling by triggering the activation of downstream components. The activity of Smo is regulated downstream Hh and Ptc. In *Drosophila*, the C-tail of Smo is rich in Ser/Thr phosphorylation sites and this fragment mediates its role in the Hh pathway. The binding of the Hh protein to Ptc induces the phosphorylation of the C-tail of Smo, which in turn produces a change in the conformation state of Smo, promoting its multimerisation. Smo is then translocated to the plasma membrane (Alcedo et al., 1996; van den Heuvel and Ingham, 1996; Hammerschmidt et al., 1997; Chen et al., 2002).

SMO is the only mammalian homologue of *Drosophila* Smo. The most conserved regions of the protein, between *Drosophila* and mammals, are the transmembrane domains, while the most variable region is the C-tail. Mammalian SMO is also phosphorylated upon Hh ligand stimulation and transported into the primary cilium where it accumulates. However, the components involved in its phosphorylation differ from the ones involved in *Drosophila*. Nonetheless, SMO phosphorylation also induces a conformational change required for its activation (Huangfu and Anderson, 2006; Briscoe and Thérond, 2013).

1.1.2 Overview of the regulation of the Hh signalling pathway in *Drosophila*

In *Drosophila*, the Hh signalling pathway is activated when the Hh protein binds to Ptc. In the absence of ligand, Ptc constitutively represses the activity of the Smo (Alcedo, et al., 1996). When Smo is repressed by Ptc, the kinesin-like protein Costal 2 (Cos2) forms a complex with Cubitus interruptus (Ci), Fused (Fu)

and Suppressor of fused (Su(fu)). In this complex Ci is phosphorylated by protein kinase A (PKA), casein kinase 1 (CK1) and glycogen synthase kinase 3β (GSK3β), it is also retained in the cytoplasm and processed into its repressor form (CiR). In the presence of the Hh ligand, Ptc releases Smo inhibition, Smo is then stabilised and phosphorylated by CK1, casein kinase 2 (CK2), G protein-coupled receptor kinase 2 (Gpcrk2) and PKA. Active Smo interacts with Cos2 and Ci is released from the complex. Active full-length Ci is then translocated to the nucleus where it regulates the signalling pathway by activating the transcription of the Hh target genes (Robbins et al., 1997; Chen et al., 1999; Wang et al., 2000; Lum et al., 2003; Zhao et al., 2007; Yang et al., 2015).

1.1.3 Canonical Hh signalling pathway in vertebrates

The core components and the general mechanisms of the Hh signalling pathway are highly conserved. However, there is variability in the specific design of the pathway between different species. The vertebrate Hh signalling pathway requires extra components that are not found in *Drosophila*. In vertebrates, Hh signalling greatly depends on the presence of an additional organelle: the primary cilium. The primary cilium is a highly specialised microtubule-based organelle that forms from the basal body as immotile flagella on the surface of most cells that are not undergoing cell division (Simpson et al., 2009; Yang et al., 2015; Bangs and Anderson, 2017).

Although the presence of primary cilia has not been widely described in immune cells, it has been shown that a region known as the immune synapse, could potentially function as the equivalent of the primary cilium in these cells. The immune synapse is the region used by immune cells to interact with target cells

(Stinchcombe and Griffiths, 2014; Prosser and Morrison, 2015). Furthermore, the presence of primary cilia in lymphocytes was described *in-vitro*. Jurkat T-lymphocytes and NALM-6 B cells were serum starved to induce the formation of functional primary cilia (Prosser and Morrison, 2015).

The primary cilium has an important role in the coordination of extracellular and intracellular signals of a number of signalling cascades involved in development, among them the Hh pathway (Simpson et al., 2009; Yang et al., 2015; Bangs and Anderson, 2017).

In contrast to Hh signalling in *Drosophila* that is regulated by a single Hh ligand, mammalian Hh signalling is activated by three ligands: Sonic Hedgehog (Shh), Indian Hedgehog (Ihh) and Desert Hedgehog (Dhh) (Echelard et al.,1993; Riddle et al., 1993; Ingham and McMahon, 2001). These Hh proteins are expressed in different tissues and, among them, Shh is the most widely expressed. Shh has important functions in the nervous system including specification of different cell types, control of the cell fate and the patterning of the limbs and digits (Zhu et al., 2008). Ihh is expressed and required for the development of bone and cartilages and plays important roles in cytotoxic T cell function (de la Roche et al., 2013). In some tissues, Shh and Ihh have similar functions. Dhh is expressed in male gonads, where it is required for development of germ cells and in Schwann cells where it controls the development peripheral nerves sheaths. These three Hh ligands bind to PTCH1, albeit with a different potency and therefore there is variability in the response observed with each protein (Bitgood et al., 1996; Young et al., 1996; Pathi et al., 2001; Cai et al., 2008).

In the absence of Hh ligand, PTCH1 is located in the primary cilium repressing SMO activity and inhibiting SMO transport into the cilium. When the Hh proteins

are present, PTCH1 is inhibited, excluded out of the primary cilium, internalised and degraded (along with the Hh ligand). Binding to the Hh ligand alleviates PTCH1 suppression of SMO which renders SMO free to move into the primary cilium. Accumulation of SMO within the cilia triggers the events required for the regulation of the Glioma-associated oncogene (Gli) family of zinc finger transcription factors, the vertebrate homologue of Ci. The Gli family of proteins are the downstream effectors of the Hh signalling pathway in vertebrates **(Figure 1.1)** (Kinzler et al., 1988; Rohatgi et al., 2007; Nozawa et al., 2013).

There are three Gli proteins: Gli1, Gli2 and Gli3; and each fulfils a specific function to regulate the Hh pathway. While Gli2 and Gli3 have dual roles in the regulation of the pathway, full length Gli1 is expressed as a response of the activation of the signalling cascade and has an exclusive transcriptional activator role. The main role of Gli1 and Gli2 is as transcriptional activators. Gli2 and Gli3 can act as activators or repressors depending of the state (on or off) of the Hh signalling pathway. When there is no ligand bound to the receptor PTCH1, Gli2 and Gli3 are processed into their repressor forms: Gli2R and Gli3R respectively. Even though Gli2 and Gli3 have this dual role, Gli3 is considered the main repressor of the pathway and the primary role of Gli2 is transcriptional activator (Dai et al., 1999; Sasaki et al., 1999).

Kinesin member 7 (Kif7) and SUFU the mammalian homologues of *Drosophila* Cos2 and Su(fu) respectively, are located in the primary cilium. Kif7 has two main roles in the Hh pathway: in the absence of Hh proteins, Kif7 and PKA at the base of the primary cilium, are involved in the phosphorylation cascade that is required for the proteolytic processing of the repressor forms Gli3R and Gli2R. However, the proteolytic processing of Gli2 is not as efficient as the process of Gli3 and

while the majority of Gli3 is processed into its truncated amino-terminal repressor form, just some of the Gli2 is processed and is mainly degraded by the proteasome. Gli3R and Gli2R (less abundantly) move out of the primary cilia into the nucleus, repressing the transcription of Hh target genes (Pan et al., 2006; Pan et al., 2009; Tuson et al., 2011).

Mammalian SUFU is an important negative regulator of the pathway, that in the absence of Hh protein, forms a complex with Gli2 and Gli3 to block their activation at the tip of the cilia. SUFU also participates in nuclear-cytosol shuttling of the Gli transcription factors (Humke et al., 2010; Nozawa et al., 2013).

In the presence of the Hh protein, SMO enters the primary cilium and is phosphorylated, which causes the inhibition of the processing of the repressor forms Gli3R and Gli2R. Phosphorylation of SMO stimulates heterotrimeric Gi proteins, reducing PKA activity, this causes the movement of Kif7 and the complex formed by SUFU and full length Gli2 or Gli3 to the tip of the cilia, where the complex accumulates. Kif7 is involved in the dissociation of Gli2 and Gli3 from the complex. Once free from SUFU, these Gli proteins undergo post-translational modifications, not yet fully elucidated, to generate the activator forms: Gli2A and Gli3A, that moved out of the cilia to the cytoplasm and into the nucleus where they activate the transcription of the Hh target genes such as *PTCH1* and *Gli1* (Pan et al., 2006; Pan et al., 2009; Tuson et al., 2011; Nozawa et al., 2013; Yang et al., 2015; Bangs and Anderson, 2017).

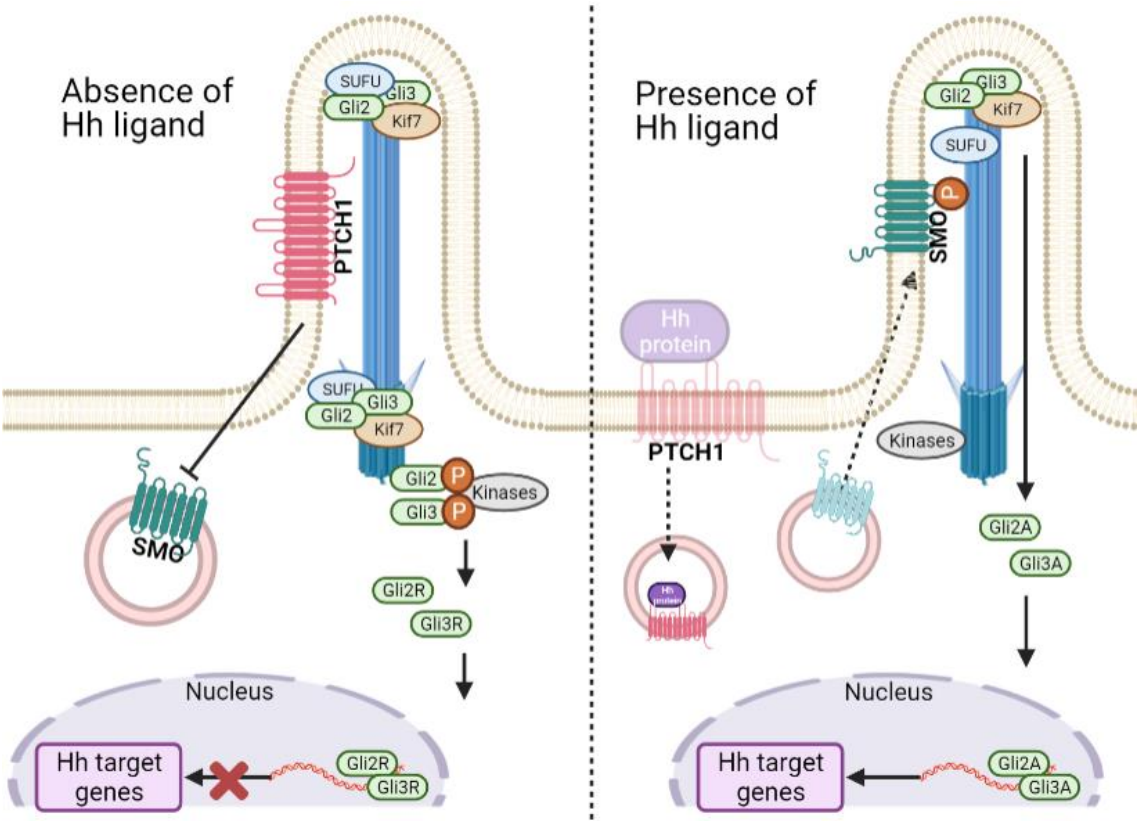

Figure 1.1 Simplified schematic representation of canonical Hh signalling in vertebrates

In the absence of Hh ligand, PTCH1 is located in the primary cilium repressing both, the activity of SMO and its localisation to the cilium. Gli2 and Gli3 are held in the cilium by a complex formed by SUFU and Kif7. Gli2 and Gli3 are phosphorylated and proteolytically processed into their repressor forms which move to the nucleus, where they repress the transcription of Hh target genes.

In the presence of Hh ligand, PTCH1 (along with the Hh ligand) is internalised and degraded. Free of PTCH1 repression, SMO translocates to the primary cilium where its activation regulates the dissociation of Gli2 and Gli3 from SUFU. Activator forms Gli2A and Gli3A move to the nucleus, where they activate the transcription of Hh target genes. Created with BioRender.com.

Is important to highlight that *PTCH1* is a target gene of the Hh signalling. Therefore, the activation of the pathway generates a negative feedback loop. The machinery and mechanisms required to activate the Gli-mediated expression of Hh target genes through this route of signalling and trafficking of components is known as the Hh canonical pathway. However, when the activity of Hh signalling does not depend on the activation of the Gli family, the signalling cascade is referred as the non-canonical Hh pathway (Ingham et al.,1991; Ruiz i Altaba, 1999; Sasaki et al., 1999; Jenkins D. 2009; Brennan et al., 2012).

1.1.4 Non-canonical Hh signalling pathway

The non-canonical signalling pathway diverges from the canonical paradigm as it does not result in the Gli-dependent activation of the transcription of Hh target genes. Non-canonical signalling pathway is involved in the regulation of essential processes required for mammalian development and for maintenance of adult structures. Two different subcategories of the non-canonical Gli-independent Hh pathway have been described. Type I is SMO-independent while type II occurs downstream of SMO. Examples of the responses observed in a non-canonical type I Hh signalling include cell survival and cellular proliferation. While non-canonical type II participates in the regulation of Ca^{2+} flux, cell migration and rearrangement of the actin cytoskeleton **(Figure 1.2)** (Jenkins D. 2009; Chinchilla et al., 2010; Brennan et al., 2012; Riobo, 2012; Robbins et al., 2012; Carballo et al., 2018; Chen et al., 2018).

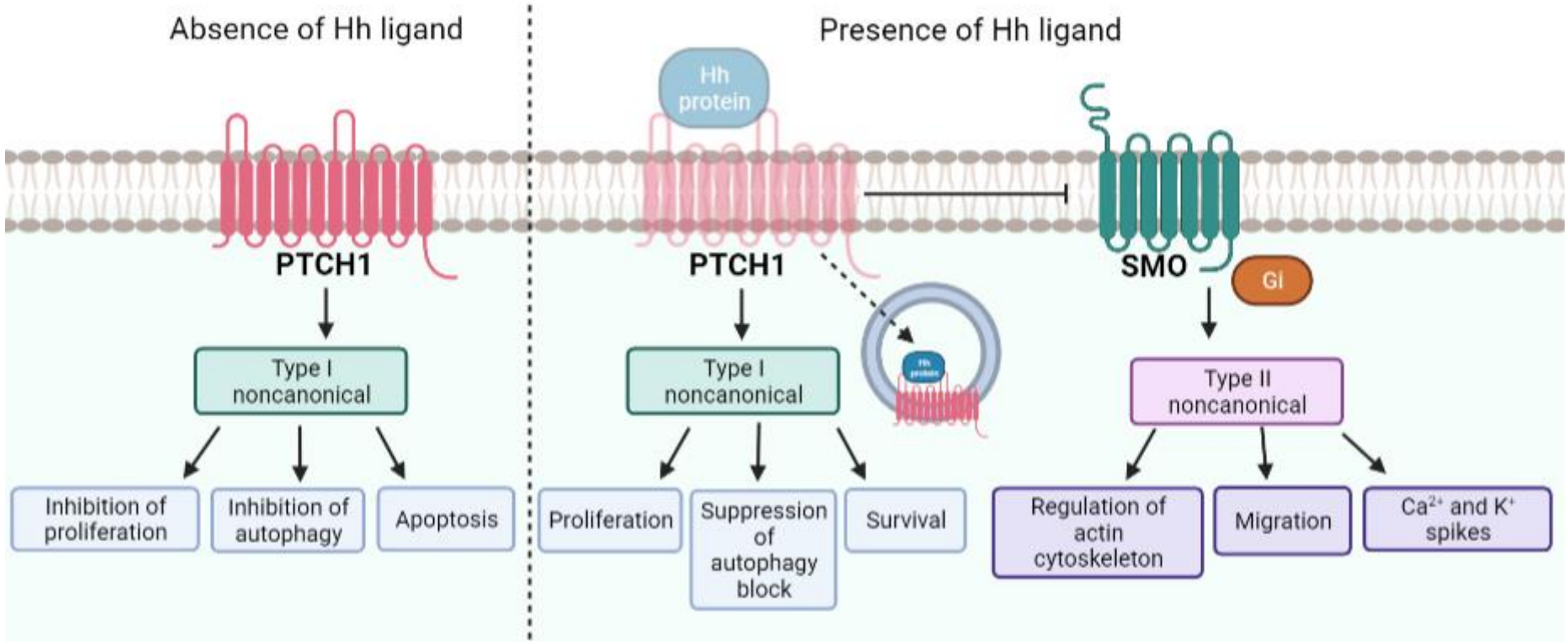

Figure 1.2 Simplified schematic representation of type I and type II non-canonical Hh signalling in vertebrates

Non-canonical type I Hh signalling is independent of SMO and regulated by Hh ligands. Non-canonical type II is dependent of SMO activity and, in most cases, mediated by Gi proteins. Examples of specific responses of the different types of non-canonical signalling are summarised in the graphic. Created with BioRender.com.

Type I non-canonical signalling is dependent on the activity of PTCH1 alone. Apoptosis, a form of programmed and controlled cell death, is in part, regulated by non-canonical type I Hh signalling. When PTCH1 is expressed in mammalian cells (HEK293T and neuroblasts), and in the absence of Hh ligand, apoptosis is enhanced following a mechanism that is not inhibited by activation of SMO. The pro-apoptotic activity of PTCH1 requires the cleavage by caspase 9, of a region within the CTD of PTCH1 (D1392). Hence, the pro-apoptotic activity of PTCH1 is mediated by the CTD (Kerr et al., 1972; Thibert et al., 2003; Chinchilla et al., 2010; Brennan et al., 2012). Type I non-canonical Hh signalling is also involved in regulation of cell division. PTCH1 interacts with phosphorylated cyclin B1. This interaction affects the normal cellular localization of cyclin B1 causing its movement to the cytoplasm and out of the nucleus and inhibiting the completion of mitosis. Expression of Shh was shown to prevent the interaction of PTCH1 with phosphorylated cyclin B1. In the presence of Shh, cyclin B1 was found in the nucleus where it promotes cellular proliferation (Barnes et al., 2001; Brennan et al., 2012).

Non-canonical Hh signalling type II is dependent of SMO activity, in the majority of cases shown to be dependent of its function as GPCR and mediated by Gi proteins. The activation of small GTPases by type II non-canonical signalling is required for the regulation of the actin cytoskeleton. The activation of SMO in the presence of the Hh ligands, promotes the activation of the small GTPase RhoA which is necessary for the formation of actin stress fibres and for tubologenesis in endothelial cells. The effect of this mechanisms is fast and is not accompanied by the activation of the Gli family of transcription factors nor the expression of Hh target genes. Also, the activation of RhoA and Rac1 GTPases via non-canonical

type II Hh signaling promotes cell migration of fibroblasts in the presence of Shh. This mechanism depends on the activation of SMO but the expression of Gli3R, that inhibits canonical pathways, does not block cell migration (Chinchilla et al., 2010; Polizio et al., 2011; Robbins et al., 2012). In cardiac myocytes, activation of SMO leads to reduction of repolarising K^+ currents and prolongation of the action potential duration, resulting in development of arrhythmias. This process in mediated by Gi proteins and inhibition of PKA activity (Cheng et al., 2018).

Of relevance, recent studies show that the activation of the Gli family of transcription factors can also occur independently of SMO following a non-canonical signalling. This non-canonical activation has been linked to cross-talk with different signalling pathways, among them RAS, transforming growth factor β (TGF-β) and the PI3K-AKT-mTOR Signalling. These non-canonical process can lead to the activation of Gli transcription factors and also to post-translational modification of the Gli proteins. Non-canonical activation of the Gli family is involved in the development of different cancer types, and as such its study is key for the development of new therapeutic strategies to treat cancer (Lauth and Toftgård, 2007; Pietrobono et al., 2019).

The mechanisms that regulate the decision to activate canonical or non-canonical Hh signalling pathway have not been elucidated. However, the absence of primary cilium does not prevent most forms of non-canonical Hh signalling, as opposed to causing a complete inhibition of canonical Gli-dependent signalling. Nevertheless, the variety of signalling mechanisms of the Hh pathway clearly show that this signalling cascade should not be viewed as linear. On the contrary, it should be studied as a network that modulates independent and sometimes

overlapping events through different signalling routes (Robbins et al., 2012; Carballo et al., 2018).

1.2 Autophagy

1.2.1 Overview of autophagy

The word autophagy derives from the Greek words “auto” and “phagy” which means self-eating (De Duve and Wattiaux, 1966; Klionsky, 2008). This term is used to describe the evolutionary conserved mechanism by which cytoplasmic substrates are engulfed by a membrane and delivered to the lysosomes (in mammals) or vacuole (in yeast) for degradation (De Duve and Wattiaux, 1966; Marzella et al., 1981). In eukaryotic cells, autophagy regulates the degradation and recycling of different cytoplasmic components, which include, among others, defective organelles, protein aggregates and misfolded proteins (Cuervo and Dice, 1998; Kim and Klionsky, 2000). The breakdown products obtained after autophagic degradation are used to fulfil the metabolic requirements of the cell and to synthesize new components (Rabinowitz and White, 2010). Autophagy is important for the maintenance of cellular homeostasis. In normal conditions, basal autophagy functions as a quality control mechanism that regulates the degradation of components that can be detrimental for cell survival. It also plays a role in the cell’s response to stress conditions such as amino acid starvation, hypoxia, and pathogenic infections. Thus, upregulation of autophagy helps the cell to adapt to changes in the environment (Munafó and Colombo, 2001; Wang and Klionsky, 2003; Rabinowitz and White, 2010; Denton et al., 2015; Yoshii and Mizushima, 2017).

1.2.2 Types of autophagy

Depending on the particular way of enclosing and delivering the sequestered cargo, autophagy is classified as follows: microautophagy, chaperone-mediated autophagy (CMA) and macroautophagy **(Figure 1.3)**. Microautophagy and macroautophagy occur in mammals and yeast, while CMA has only been identified in mammals (Mortimore et al., 1983; Cuervo and Dice, 1998; Mizushima et al., 2002; Mizushima and Komatsu, 2011; Wen and Kliionsky, 2016). Microautophagy, mainly studied in yeast, occurs when the lysosome or vacuole itself engulfs cytosolic components by invagination or protrusion of its membrane (Ahlberg and Glaumann, 1985; Li et al., 2012). In CMA the proteins to be degraded are transported directly to the lysosomes. These proteins contain a KFERQ-like pentapeptide motif which is recognised by chaperones and co-chaperones (chaperone complex) found in the cytosol, among which, the most abundant is the heat shock cognate of 70 kDa (HSC70). Chaperones target the proteins to the lysosome membrane where they interact with the Lysosome-associated membrane protein type 2A (LAMP2A) receptor and the lysosomal HSC70 (Lys-HSC70) for the translocation of the unfolded protein into the lysosomes (Chiang and Dice, 1988; Massey et al., 2004; Massey et al., 2006; Orenstein and Cuervo, 2010, Yoshii and Mizushima, 2017). Macroautophagy (henceforth referred as autophagy), the most widely studied type of autophagy, is highly conserved among higher eukaryotes and, in normal conditions, occurs constitutively at low basal levels (Mizushima, 2005). The morphological characteristic of autophagy is the formation of the autophagosomal vesicle (Arstila and Trump, 1968; Axe et al., 2008).

Autophagy can be further categorised depending on the type of engulfed material for degradation. Under this classification, autophagy is divided in two types, selective and non-selective or bulk autophagy. These two types of autophagy can take place simultaneously. In non-selective autophagy the cargo is not specifically selected. The cytoplasmic components are commonly degraded as a response of nutrient or energy deprivation, therefore, its activation is important in a context of cell adaptation and survival to changes in nutrient availability. On the other hand, selective autophagy refers to the degradation of specific sequestered cargo such as specific organelles, and commonly occurs to maintain homeostasis in nutrient-rich conditions. Whole organelles can be degraded by selective autophagy, for example mitochondria (mitophagy), peroxisomes (pexophagy), protein aggregates (aggrephagy), lipid droplets (lipophagy) and pathogens (xenophagy). Depending of which organelle is selectively degraded, specific adaptor factors play a role apart from the autophagy core machinery (Yorimitsu and Klionsky, 2005; Wen and Kliionsky, 2016; Yoshii and Mizushima, 2017). Microautophagy and macroautophagy can occur in both, selective and non-selective manner. CMA is activated purely by the selective mechanism (Klionsky et al., 2008).

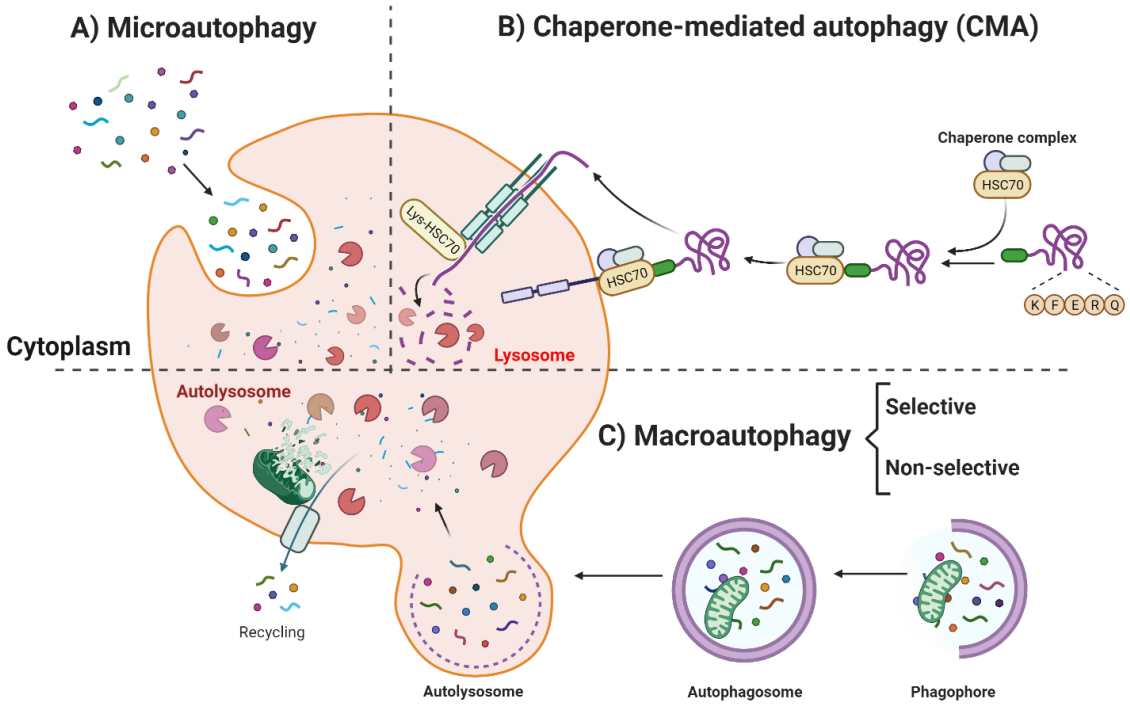

Figure 1.3 Overview of the different types of autophagy

Autophagy can be classified in 3 different types: microautophagy, chaperone-mediated autophagy (CMA) and macroautophagy. **A.** In microautophagy the lysosome engulfs directly the cytosolic components to be degraded. **B.** During CMA, proteins containing a KFERQ motif are targeted by chaperones, such as HSC70, and transported to the lysosome for internalisation and degradation. **C.** Macroautophagy is characterised by the formation of the autophagosome, a double-membrane transient organelle, that engulfs the cytoplasmic contents to be degraded and transport them to the lysosome; the autophagosome fuse with the lysosome to form the autolysosome, where the degradation of the engulfed contents takes place. Adapted from “Three Main Types of Autophagy”, by BioRender.com (2021). Retrieved from https://app.biorender.com/biorender-templates.

1.2.3 Autophagosomes

Autophagosomes are double-membrane vacuoles that isolate the organelle or the portion of the cytoplasm that contains the materials to be degraded, however they do not contain degradative enzymes. Therefore, they transport the sequestered contents to the lysosomes for degradation and recycling **(Figure 1.4)** (Arstila and Trump, 1968; Axe et al., 2008). The biogenesis of the autophagosome involves different process of membrane remodelling carried out at multiple stages: induction, nucleation of the phagophore, expansion of the phagophore and completion of the autophagosome (maturation) (Wen and Kliionsky, 2016; Zhang et al., 2016). Upon autophagy induction, the signalling and recruitment of the autophagy initiation complexes takes place at the membrane sites where nucleation occurs. During nucleation, the formation of a specialized isolation membrane known as the phagophore is carried out. Expansion, occurs while the phagophore elongates by the addition of lipids that come from different membrane sources. The phagophore surrounds the cytoplasmic components in a cup-shaped structure until its edges fuse together to form the autophagosome. No lysosomal proteins are found in this structure (Klionsky, 2005; Axe et al., 2008; Hamasaki et al., 2013; Lamb et al., 2013; Yoshii and Mizushima, 2017). Because the phagophore surrounds the cytoplasmic content, there is a big range in the capacity that the autophagosome can hold. The size of an autophagosome varies depending on the organism and on the engulfed material, in mammals their diameter ranges from 0.5 to 1.5 μm (Mizushima et al., 2002; Wen and Kliionsky, 2016). The formation of the autophagosome occurs in an average of 10 minutes. Once the autophagosome has been conjugated with protein microtubule-associated protein 1 light chain 3

(LC3), this transient organelle has a half-life of around 10 to 20 minutes before fusing with the lysosomes (Pfeifer et al., 1978; Schworer et al., 1981; Köchl et al., 2006; Xie et al., 2008; Mijaljica et al., 2012; Melia et al., 2020). Several autophagosomes are formed simultaneously and, depending on the cue for the initiation of autophagy and on the origin of the cytoplasmic cargo, the site of the autophagosome formation can vary, however the basic machinery for the formation of new autophagosomes is conserved (Jahreiss et al., 2008; Yu et al., 2018). The expansion of the phagophore has been linked to multiple membrane origins (Blommaart et al., 1997; Axe et al., 2008). The most accepted hypothesis about the formation of the autophagosome in mammalian cells suggests that the phagophore is synthesised from existing membranes such as the Endoplasmic reticulum (ER), Golgi and mitochondria, with the ER being the most likely origin (Dunn, 1990a; Dunn, 1990b; Yamamoto et al., 1990; Jahreiss et al., 2008; Lamb et al., 2013; Melia et al., 2020).

The fusion of the autophagosome with the lysosome is tightly regulated, if there is premature fusion between the phagophore and the lysosome, the surrounded substrates will not be delivered (Wen and Kliionsky, 2016). When the outer membrane of the autophagosome fuses with the single membrane lysosome, the autolysosome is formed. At the final step of autophagy, the low pH inside the autolysosome activates the lysosomal hydrolases, these enzymes will degrade the engulfed contents along with the inner membrane of the autophagosome. Once proteins, lipids and carbohydrates have been broken down, they are delivered back to the cytoplasm (Deretic, 2008; Suzuki and Ohsumi, 2010; Devereaux et al., 2013; Peppard et al., 2014; Mauvezin et al., 2015).

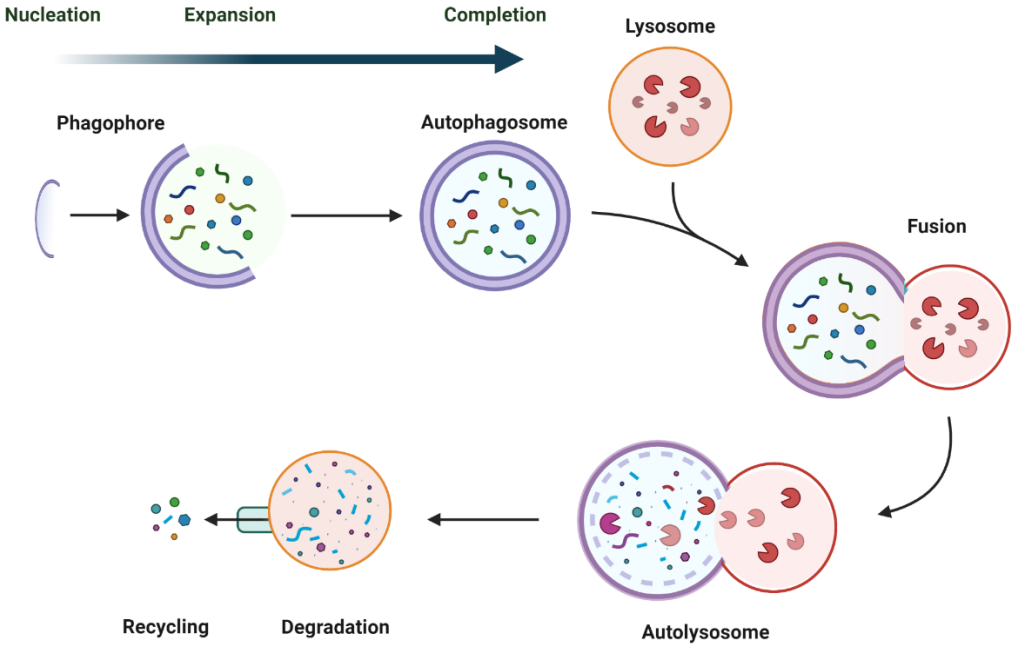

Figure 1.4 Schematic representation of autophagy

The signature structure of autophagy is the autophagosome. During nucleation, complexes are recruited to form the phagophore, which expands to surround the cytoplasmic contents to be degraded. Finally a mature autophagosome is formed when the phagophore closes. The autophagosome fuses with the lysosome to form the autolysosome. Within the autolysosome, the lysosomal hydrolases degrade the enclosed cargo to simpler components which are finally released back to the cytoplasm and recycled. Adapted from “Autophagy Process”, by BioRender.com (2021). Retrieved from https://app.biorender.com/biorender-templates.

1.2.4 Autophagy related proteins

The study of the molecular mechanisms involved in autophagy has been greatly achieved by the discovery and study of autophagy related (*ATG*) genes, firstly found in *Saccharomyces cerevisiae* (Yorimitsu and Klionsky, 2005; Zhao and Zhang, 2019; Melia et al., 2020). In *Saccharomyces cerevisiae*, more than 40 ATG proteins have been identified **(Table 1.1)** and although there is no mammalian homologue for all of the yeast ATG proteins, many of them have their

equivalent in mammals, suggesting that the autophagic machinery is highly conserved between these species. However, autophagy is more complex in mammals (Axe et al., 2008; Delorme- Axford and Klionsky, 2019; Zhao and Zhang, 2019).

Saccharomyces cerevisiae	**Mammals**
Atg1	ULK1, ULK2
Atg2	ATG2A, ATG2B
Atg3	ATG3
Atg4	ATG4A, ATG4B, ATG4C, ATG4D
Atg5	ATG5
Atg6	BECN1
Atg7	ATG7
Atg8	LC3A, LAC3B, LC3C, GABARAP
Atg9	ATG9A, ATG9B
Atg10	ATG10
Atg11	FIP200
Atg12	ATG12
Atg13	ATG13
Atg14	ATG14
Atg15	-
Atg16	ATG16L1
Atg17	FIP2000
Atg18	WIPI1, WIPI2
Atg19	-
Atg20	-
Atg21	WIPI1, WIPI2
Atg22	-
Atg23	-
Atg24	-
Atg25*	-
Atg26	-
Atg27	-
Atg28**	-
Atg29	-
Atg30	-
Atg31	-
Atg32	-
Atg33	-
Atg34	-
Atg35**	-
Atg36	-
Atg37	ABCD5

Atg38	NRBF2
Atg39	-
Atg40	FAM134B
Atg41	-
Atg42	-
Atg43***	-
-	ATG101

Table 1.1 Main autophagy related proteins in yeast and mammals

* Found in *Hansenula polymorpha*. **Found in *Komagataella phaffii* and *Pichia Pastoris*. *** Found in *Schizosaccharomyces pombe* (Adapted from Galluzzi et al, 2017; Delorme-Axford and Klionsky, 2019; Klionsky et al., 2021)

The ATG proteins work in complexes at specific moments to regulate the different steps of autophagosome formation **(Figure 1.5)**. In mammals, the uncoordinated-51-like kinase (ULK) complex initiates the formation of autophagosomes. Upon induction of autophagy in mammalian cells, this serine/threonine kinase complex is formed by the assembly of ULK1/2, ATG13, ATG101 and focal adhesion kinase family interacting protein of 200 kDa (FIP200) (Hara et al., 2008; Hosokawa et al., 2009a; Hosokawa et al., 2009b; Mercer et al., 2009). All components are conserved in *Saccharomyces cerevisiae*, except for ATG101. In mammalian cells, the function of ATG13 is to stabilize ULK1 and to target the entire ULK complex to the cellular region where the formation of the autophagosome occurs (Ganley et al., 2009; Hosokawa et al., 2009a). ATG13 and ATG101 directly interact with each other within the ULK1 complex, where the function of ATG101 is the stabilization of ATG13 and ULK1 (Hosokawa, et al., 2009b). FIP200 is considered a scaffolding protein. Its function in the ULK complex is similar to the ATG13, as it is necessary to localize the complex to the autophagosome

formation site and it also contributes to ULK1/2 stability and kinase activity (Ganley et al., 2009; Hara and Mizushima, 2009).

Once the ULK complex is re-located to the autophagosome formation site, characterised by the presence of ATG9, it triggers the formation of class III phosphatidylinositol 3-kinase (PI3KC3) complex, integrated by the vacuolar protein sorting 34 (VPS34), BECLIN-1, VPS15 and ATG14. The activation of this complex is involved in the generation of phosphatidylinositol 3-phosphate (PI3P), a phospholipid required at the site of the biosynthesis of the autophagosome. PI3P drives the recruitment of additional proteins required for the formation of complexes involved in the completion of the autophagosome (Zeng et al., 2006; Russell et al., 2013; Kaur and Debnath, 2015).

The first ubiquitin-like conjugation complex is formed by ATG16L1, ATG5 and ATG12, it drives the formation of the second ubiquitin-like conjugation system. This second system involves the activity of ATG4, ATG7 and ATG3. These systems work together to later conjugate LC3 or GABA type A receptor-associated protein (GARABAP) to phosphatidylethanolamine (PE) into the expanding membrane of the phagophore (Yang and Klionsky, 2010; Cicchini et al., 2015; Kaur and Debnath, 2015; Bento et al., 2016; Zachari and Ganley, 2017; Yu et al., 2018).

ATG9 protein plays an important role in autophagosome formation. Up to date, it is the only transmembrane ATG protein that has been identified. Studies show that mammalian ATG9 supports the autophagosome formation by supplying membrane to the forming autophagosome from different sources without being incorporated into the autophagosome membrane (Young et al., 2006; Orsi et al., 2012; Levine and Kroemer, 2019).

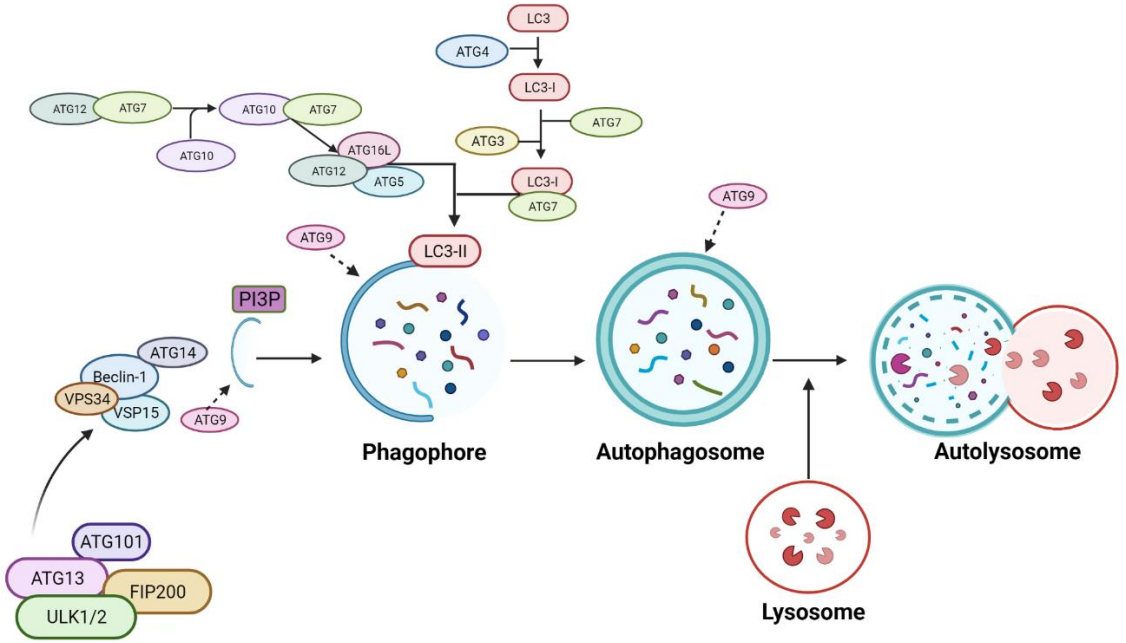

Figure 1.5 Schematic representation of the main components of the autophagy pathway in mammals

The core autophagy proteins involved in the autophagosome biogenesis are illustrated with their respective membrane. Activation of the ULK complex triggers the formation of the VPS34 complex at the site of the phagophore formation, which mediates the production of PI3P. PI3P recruits the components of the ubiquitin-like conjugation systems that are involved in the conjugation of LC3-II to PE and its further integration into the phagophore membrane. ATG9 participates in autophagosome biogenesis by aiding in the incorporation of membrane from different sources into the growing phagophore. The autolysosome is formed by the fusion of the mature autophagosome with the lysosome to degrade the enclosed contents. Created with BioRender.com.

1.2.5 Autophagy regulation

The study of the mechanisms that control autophagy was greatly propelled by the discovery of the target of rapamycin (TOR) in yeast (Heitman et al., 1991). This serine/threonine kinase senses and integrates the signals corresponding to the energy, growth and nutrient levels of the cell, and in this way is involved in the regulation of different cellular processes, among them autophagy (Sarbassov et al., 2005).

Rapamycin, a compound produced naturally by *Streptomyces hygroscopicus*, inhibits the activity of TOR, and by doing so, it stimulates autophagy (Vézina et al., 1975; Sabatini et al., 1994; Brown et al., 1994). The inhibition of TOR by different mechanisms results in the induction of autophagy as a mechanism that allows the cell to respond and adapt to the changing conditions of the cellular environment (Neufeld, 2010).

The mammalian homologue of the yeast TOR was later identified and is currently referred to as the mechanistic target of rapamycin (mTOR) (Brown et al., 1994; Sabatini et al., 1994; Kennedy and Lamming, 2016). mTOR is one of the components of 2 functional complexes: mTOR complex 1 (mTORC1) and mTOR complex 2 (mTORC2). mTORC1 is highly sensitive to rapamycin while mTORC2 is insensitive to rapamycin. Thus, the presence of rapamycin affects mTORC1 capacity to phosphorylate downstream substrates while having no effect in the kinase function of mTORC2. mTORC1 is formed by the association of mTOR, rapamycin-associated protein of TOR (Raptor) and mLST8. mTORC2 consists of mTOR, mLST8, rapamycin insensitive companion of TOR (Rictor), SIN1 and Protor. mTORC1 is the most broadly studied of these two complexes (Kim et al.,

2002; Loewith at al., 2002; Kim et al., 2003; Guertin and Sabatini, 2007; Dunlop and Tee, 2014).

Active mTORC1 is found in energy-rich and nutrient-rich conditions, this active state inhibits autophagy. Nevertheless, basal levels of autophagy are maintained. Inactivation of mTORC1 occurs under amino acid starvation conditions and results in the upregulation of autophagy (Dunlop and Tee, 2014). mTOR phosphorylates ATG13 and ULK1/2 in nutrient-rich conditions, preventing ULK1/2 activation (Wong et al., 2013).

1.2.6 Study of autophagy

Autophagy is frequently studied using two methodologies: the observation of the autophagy-specific structures and their dynamic evolution and/or the measurement of levels of autophagosome marker proteins and organelles as a function of time. Measurement of autophagy has proven to be a challenge as autophagy is not a static mechanism. To overcome this problem and to avoid the misinterpretation accompanied when analysing autophagy as a static process, the analysis of changes in time, representing the “autophagic flux” is preferably used (Yoshii and Mizushima, 2017).

The most commonly used method to study autophagy is the analysis of the expression of the proteins microtubule-associated protein 1 light chain 3 (LC3) and p62/SQSMT1 by western blot (Bonam et al., 2020).

LC3 was identified as a subunit of the neuronal microtubule-associated proteins (MAPs) MAP1A and MAP1B. The role of LC3 in the assembly and disassembly of microtubules was firstly thought to be its only role (Mann and Hammarback, 1994). Subsequently, the association of LC3 to the autophagosome membrane

was described, and its specific role on mammalian autophagy was established (Noda et al., 2000). LC3 is a mammalian homologue of the yeast Atg8. There are 3 LC3 isoforms: LC3A, LC3B and LC3C. LC3B is the most commonly used for the study of autophagy (Noda et al., 2000; Barth et al., 2010; Mizushima et al., 2010). Cleavage of the LC3B precursor at the C-terminal region by ATG4 after LC3B synthesis results in the formation of LC3B-I, which is a soluble cytosolic protein. Upon induction of autophagy, LC3B-I is conjugated to PE to form LC3B-II, which mediates association of LC3B-II to the growing autophagosome membrane. Thus, LC3B-II has been used as a marker for the detection of autophagosomes (Noda et al., 2000; Tanida et al., 2005). LC3B-II is bound to both, the inner and outer membrane of the autophagosomes. After the formation of autolysosomes, the LC3B-II associated to the inner membrane is degraded along with the enclosed cargo while the LC3B-II bound to the outer membrane is delipidated and recycled (Tanida et al., 2005; Mizushima et al., 2010).

The analysis of the levels of LC3B-I and LC3B-II is crucial for the study of autophagy, particularly the levels of LC3B-II turnover. The identification of these two different LC3B forms by Western blotting technique is based on their different migration pattern on SDS-PAGE. Even though the molecular weight of the lipidated form LC3B-II is higher than the soluble LC3B-I form, LC3B-II migrates faster than LC3B-I. The faster mobility of LC3B-II is due to the increased hydrophobicity given by its conjugation to PE. Thus, in SDS-PAGE the apparent molecular weight of LC3B-I is 16 kDa and the apparent molecular weight of LC3B-II is 14 kDa (Barth et al., 2010; Mizushima et al., 2010).

Nevertheless, the levels of LC3B-I and LC3B-II by themselves cannot be used to describe autophagic flux at a specific time point. An increase in LC3B-II levels

could be caused by two different scenarios. In scenario one, the increase in the levels of LC3B-II reflects an increase in autophagosome number as a result of an increase in autophagic activity. In scenario two, the increase of LC3B-II occurs because of the accumulation of autophagosomes that cannot be degraded. To be able to distinguish between these two (and opposing) alternatives, the measurement of LC3B-II levels must be carried out in the presence and absence of lysosomal inhibitors, such as Bafilomycin A1 (BafA1), that prevents downstream clearance of autophagosomes (**Figure 1.6**) (Yoshii and Mizushima, 2017).

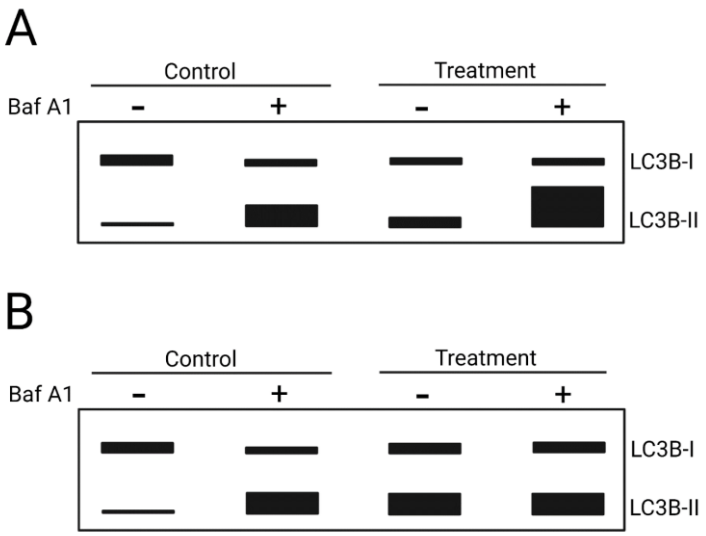

Figure 1.6 Diagram of Western blot showing changes in LC3B marker in the presence and absence of lysosomal inhibitor under control and treatment conditions

Presence of Baf A1 in the control condition results in an increase in the protein levels of LC3B-II, while the presence of Baf A1 in the treatment condition results in: **A.** further increase in LC3B-II levels indicating an autophagic flux increase, or **B.** does not result in changes of LC3B-II levels indicating inhibition of the autophagic flux. Created with BioRender.com.

The ratio of LC3B-II/LC3B-I is no longer commonly used as a measurement for autophagic flux, as most of the antibodies available commercially have more affinity to LC3B-II, masking the amount of LC3B-I present. Secondly, because LC3B-I expression in Western blotting varies depending of the cell line, and in some cell lines the LC3B-I band is very faint or cannot be detected (Yoshii and Mizushima, 2017).

p62, also known as sequestosome 1 (SQSTM1) in humans, is an adaptor protein that targets polyubiquitinated substrates for degradation via autophagy and/or via the proteasomal pathway (Seibenhener et al., 2004; Kirkin et al., 2009). p62 binds to ubiquitin in a non-covalent manner (Vadlamudi et al., 1996), its C-terminal region contains an ubiquitin-associated (UBA) domain that is required for its interaction with the polyubiquitinated substrates. On its N-terminal region, p62 has a Phox and Bem1p (PB1) domain that functions as an ubiquitin-like (UBL) domain. The PB1 domain is required for its interaction with the proteasome and thus, for the delivery of the ubiquitinated substrates for proteasomal degradation (Seibenhener et al., 2004; Bjørkøy et al., 2005; Isogai et al., 2011; Cohen-Kaplan et al., 2016). p62 also contains an LC3 interaction region (LIR) that mediates the interaction with LC3 (Pankiv et al., 2007). The direct interaction between p62 and LC3B in the autophagic vesicles is responsible for the trapping and degradation of p62 alongside the engulfed cargo during autophagy (Bjørkøy et al., 2005; Pankiv et al., T. 2007). Therefore, accumulation of p62 typically indicates the inhibition of autophagy and as such, the analysis of p62 levels is widely used to study autophagic flux (Pankiv et al., 2007).

It is important to emphasise that p62 plays a role in the two major pathways of protein degradation (autophagy and proteasomal degradation), and therefore cannot be used by itself to describe autophagic flux (Mizushima et al., 2010). The ubiquitin-proteasome mechanism is used for the degradation of misfolded, non-functioning proteins as well as short lived proteins. Before proteasomal degradation occurs, these type of proteins are tagged with Lys-48 polyubiquitin chains and transported by Ub-binding receptors, including p62, to the proteasome for degradation (Glickman and Ciechanover, 2002; Pankiv et al., 2007; Kirkin et al., 2009). The second degradation machinery in which p62 plays a role is autophagy. Autophagy is activated to degrade protein aggregates, long-lived proteins and defective organelles, among other substrates. p62 sequesters polyubiquitinated protein aggregates too large to fit into the proteasomal cavity and delivers them to the autophagic vesicles for selective degradation (Bjørkøy et al., 2005; Pankiv et al., 2007; Cohen-Kaplan et al., 2016).

1.2.7 Regulation of autophagic flux by interaction between ATG101 and the C-terminal domain of PTCH1.

With the objective of identifying specific CTD-interacting proteins, a yeast-two-hybrid screening was carried out by past members of the Dr. Riobo Del-Galdo team. One of the retrieved cDNA clones encoded for ATG101, an autophagy related protein that is essential for the initiation of autophagy in mammalian cells. As previously mentioned, ATG101 is one of the members of the ULK complex, that has a nutrient sensing activity and is known as the autophagy initiation complex (Hosokawa et al., 2009a; Hosokawa et al., 2009b; Ganley et al., 2009). By interacting with ATG101, the CTD of PTCH1 mediates a blockade of the basal

and amino acid starvation-induced (via mTORC1) autophagic flux at a step downstream of the action of the ULK complex (Chen et al., 2018).

1.3 ITM2A

The Integral Membrane protein 2A (*ITM2A*) gene was identified for the first time using a cDNA library of in-vitro cultivated condyles from mouse mandible in a study designed to find new markers for chondro-osteogenic differentiation (Deleersnijder et al., 1996). ITM2A is part of the type II Integral Membrane protein (ITM2) family and the BRICHOS superfamily. The ITM2 family does not share structural characteristic associated with other known protein families and it comprises three members: ITM2A, ITM2B and ITM2C (Deleersnijder et al., 1996; Van den Plas and Merregaert, 2004a; Kihara et al., 2014). ITM2A is a 263 amino acids protein and contains a single putative transmembrane domain at 54-74 amino acids (UniProtKB ID: O43736). ITM2A is classified as a type II integral membrane protein as it has an extracellular C-terminus and an intracellular N-terminus. This topology is congruent with its only N-glycosylation site at Asn-166 (Deleersnijder et al., 1996; Kirchner and Bevan, 1999). ITM2A contains a BRICHOS domain in the extracellular region at amino acids 133-227 (Kihara et al., 2014; Tai et al., 2014). The BRICHOS domain is found in some proteins that have been linked to dementia, respiratory problems or different types of cancer. The BRICHOS domain, of approximately 100 amino acids-long, is believed to have an intramolecular chaperone function (Sánchez-Pulido et al., 2002).

The protein sequence of ITM2A, ITM2B and ITM2C is highly conserved between human and mouse. The percentage of homology between these species is, for ITM2A: 94.7%, for ITM2B: 95.5%, and for ITM2C: 92.9%. However, the homology

among the three members in the same species is only around 40%. Human ITM2A is only 38% identical to human ITM2B and 42.1% identical to human ITM2C, while human ITM2C shares 49.5% identity with human ITM2B. Among the different members of the ITM2 family, the N-terminus is the most variable region and the extracellular C-terminal part is the most conserved one (Deleersnijder et al., 1996; Choi et al., 2001). ITM2 family protein members are expressed in different tissues, and only few tissues, such as the brain, co-express all three members (Deleersnijder et al., 1996). ITM2A is highly expressed in skeletal muscle, in the growth plate of long bones and in the thymus, in all of which the Hh pathway plays an important development role. ITM2A expression has also been detected in mature osteoblasts, mature odontoblasts, chondrocytes and T cells (Kirchner and Bevan, 1999; Tuckermann et al., 2000; Kihara et al., 2014). ITM2A is expressed in endochondral bone-derived structures such as ribs and vertebra (Van den Plas and Merregaert, 2004b), and in the foetal heart, brain and skin. In situ hybridization showed the presence of ITM2A in adult brain, renal cortex and small intestine (Choi et al., 2001). Lower expression levels of ITM2A are found in the lymph nodes, spleen, heart, lungs, stomach and uterus (Kirchner and Bevan, 1999). ITM2B is ubiquitously expressed in adult tissues and in several neonatal tissues and ITM2C was found in higher levels in brain tissue (Choi et al., 2001).

The EL4 murine thymoma cell line was used to study the subcellular localisation of Itm2a. Results showed that Itm2a is located at the plasma membrane as well as in intracellular vesicles, and potentially in endosomes and the Golgi apparatus. (Kirchner and Bevan, 1999). Using the EL4 cell line, it was also shown that the endogenous expression levels of Itm2a are highly variable in single cells, ranging

from no expression to high expression. More studies are required to fully understand its cellular localisation and patterns of expression at an mRNA and protein level (Kirchner and Bevan, 1999).

Studies carried out by different groups show that the PKA-CREB (protein kinase A-cAMP responsive element binding protein), PAX3 and GATA-3 play key roles in the regulation of ITM2A expression (Namkoong et al., 2015; Nguyen et al., 2016).

Although ITM2A plays a role in cell differentiation, its effects are cell type specific. There are reports of its involvement in chrondrogenesis, odontogenesis and myogenesis as well as in autoimmune disorders. However, its molecular function has not been fully elucidated (Kihara et al., 2014; Nguyen et al., 2016; Zhou et al., 2019). A recent article suggested that ITM2A plays a negative role in autophagy through an inhibitory interaction with V-ATPase, which acidifies the autolysosomes. Overexpression of ITM2A in HEK293 and HeLa cells resulted in a block of the autophagic flux which generated an accumulation of autophagosomes that could not be degraded. This study suggests that the interaction of ITM2A with V-ATPase inhibits the acidification of the autophagic vesicles and also that this interaction is involved in the suppression of the formation of autolysosomes (Namkoong et al., 2015).

Recent studies show that changes in the expression of ITM2A are linked to breast and ovarian cancer (Nguyen et al., 2016; Zhou et al., 2019). Expression of ITM2A is downregulated in different breast cancer cell lines, while overexpression of ITM2A inhibited the proliferation of breast cancer cells. Published results show that there is a correlation between low levels of ITM2A expression and poor outcomes for breast cancer patients, as well as lower survival rate in specific

types of breast cancer ($HER2^+$). The study of the role of ITM2A in breast cancer supports a different role of ITM2A in autophagy. The study showed that ITM2A stimulates autophagy by inhibiting the activation of mTOR in breast cancer cell lines (SKBR-3 and MDA-MB-231), as opposed to the inhibitory effect in HEK293 and HeLa cells described earlier (Namkoong et al., 2015). Overexpression of ITM2A inhibited 4EBP1 phosphorylation (a readout of mTOR activity), which resulted in decreased cell proliferation, decreased growth and reduced colony formation in breast cancer cells. Interestingly, the study shows the requirement of T35 phosphorylation in ITM2A by the protein kinase HUNK for this effect, suggesting that differential HUNK expression or activity in different cell types could account for the opposite findings (Zhou et al., 2019).

A different study showed that ITM2A acts as a tumour suppressor also in epithelial ovarian cancer. ITM2A is downregulated in ovarian cancer cell lines and in ovarian cancer tissues, particularly in invasive ovarian carcinomas. Loss of ITM2A expression was linked to an increase in resistance to chemotherapy treatment and cancer recurrence. Furthermore, ITM2A overexpression produced a decrease in cell growth in ovarian cells by promoting cell cycle arrest in the G2/M phase. Studies in animal models showed that the expression of ITM2A contributed to the reduction of tumour growth. This study suggests that downregulation of ITM2A expression hinders the G2 checkpoint, which causes an increase in cell proliferation (Nguyen et al., 2016).

1.4 Cell cycle

The cell cycle is a complex process that orchestrates DNA replication and cell division following upstream cues that are involved in the monitoring and

regulation of cell growth, and also signals from different proteins that assess DNA damage (Otto and Sicinski, 2017). Cellular proliferation is the result of the completion of the different phases of the cell cycle. The cell cycle is divided in four phases: Gap 1 (G1), DNA synthesis (S), Gap 2 (G2) and mitosis (M) (Gautier et al., 1988). During the gap phases G1 and G2, cells undergo control checks to evaluate if the cells are ready to progress into the next step of the cell cycle and to prepare for the following phase, S phase or M phase, respectively. During S phase, nuclear DNA is duplicated and during the M phase mitosis occurs to generate two daughter cells (Norbury and Nurse, 1992; Schafer, 1998). The G0 phase, often referred to as “quiescence”, is a resting state that can be permanent or transitory. Most of the cells that are not dividing in adult tissues are found in G0 phase in one of two different ways: they can be quiescent, which is a transient state, meaning that cells can be induced to return to the cell cycle given the right stimulation, for example exposure to mitogens. G0 phase also includes senescent and terminally differentiated cells, which are permanent states (Otto and Sicinski, 2017). The check-points in the cell cycle are crucial for the maintenance of cellular integrity as they function to avoid uncontrolled proliferation and duplication of damaged or mutated DNA (Thu et al., 2018). In mammalian cells, there is also a point known as the restriction point, it occurs in late G1 phase. In this point, the cells integrate external signals before irreversible committing to DNA replication (Hunter and Pines, 1994).

1.4.1 Cyclin dependent kinases and cyclins

The eukaryotic cell cycle is regulated by a family of threonine/serine proteins known collectively as cyclin-dependent kinases (CDKs). The activation and

inactivation of the CDKs is regulated by the formation of different complexes with proteins that are expressed specifically during certain phases of the cell cycle, called cyclins. Cyclins function as the regulatory subunits of the CDKs and the interaction between these two proteins is essential for the activity of the CDKs (Luedde et al., 2003; Otto and Sicinski, 2017;). In a similar manner, the inactivation of CDKs is mediated by their interaction with CDK inhibitors (CDKIs) (Franklin and Xiong, 1996).

Cyclins are the limiting factor for the formation of the CDK-cyclin complexes. While the protein levels of the CDKs are maintained relatively constant during the cell cycle, the level of cyclins changes during the different phases. The activation of the different CDK complexes, as a response of cyclin's presence is what drives the cell cycle progression (Vermeulen et al., 2003; Malumbres, 2014). The CDKs that play key roles in the regulation of the cell cycle are: CDK2, CDK4, CDK6 and CDK1 also known as cell division control protein 2 (CDC2). The cyclins involved in cell cycle progression include: A-type, B-type, D-type and E-type cyclins (Malumbres and Barbacid, 2009).

CDK4 and CDK6 share a high degree of homology and are involved in the process that drives the re-entering of G0 arrested cells into the G1 phase of the cell cycle and also in the cell progression through the early G1 phase. Studies have shown that these two kinases share the same function in many tissues, having some degree of redundancy (Anders et al., 2011; Otto and Sicinski, 2017). CDK4 and CDK6 form complexes with D-type cyclins: cyclin D1, cyclin D2 and cyclin D3. Interaction with D-type cyclins drives the activation of these CDKs (Sherr and Roberts, 1999; Luedde et al., 2003). D-type cyclins are not synthesised and degraded depending on the cell cycle phase, instead they are

expressed in response of the presence of extracellular growth factors (Assoian and Zhu, 1997; Vermeulen et al., 2003). Once these CKDs are activated, they are able to exert their function and phosphorylate their substrate: retinoblastoma tumour suppressor protein (Rb). Phosphorylated (pRb) is inactive (Pines, 1995; Vermeulen et al., 2003). The complex formed by CDK4/6 and a D-type cyclin phosphorylates Rb in mid to late G1 phase, which leads to the synthesis of proteins involved in the following phases of the cell cycle, such as cyclin A and cyclin E (Pines, 1995; Vermeulen et al., 2003). The activation of CDK2 by cyclin E is the next complex to be formed and is required for the progression of the G1 phase and to drive the transition to S phase. This complex plays a role in the maintenance of the hyperphosphorylated state of pRb, which is required until the early M phase. Next in the progression of the cell cycle, the complex CDK2-cyclin A is needed for completion of S phase. The complex formed by CDK1 and cyclin A is required for the transition from G2 to M phase, while the formation of the complex CDK1-cyclin B is required for M phase (Vermeulen et al., 2003).

1.4.2 CDK inhibitors

The regulation of CDKs and CDK-cyclin complexes is mediated by their interaction with CDKIs. Two different families of CDKIs have been described: The INK4 family and the Cip/Kip family (Pines, 1995; Vermeulen et al., 2003). The INK4 family of inhibitors forms complexes with CDK4 and CDK6 exclusively, and is composed of $p16^{INK4A}$, $p15^{INKB}$, $p18^{INK4C}$ and $p19^{INK4D}$. Inhibitors from the INK4 family exert their inhibitory function by binding to the CDKs, blocking in this way the interaction of CDK4 and CDK6 with D-type cyclins. The inactivation of the CDK4/6 by INK4 family of inhibitors prevents the phosphorylation of the target

substrates, such as Rb (Sherr and Roberts, 1999; Luedde et al., 2003). The other family of CDKIs is the Cip/Kip family, that contains three inhibitor proteins: $p21^{CIP1/WAF1}$, $p27^{KIP1}$ and $p57^{KIP2}$, which can interact with most CDKs. The Cip/Kip family of inhibitors exert their activity by interacting with the cyclins in the already formed CDK-cyclin complex (Schafer, 1998; Sherr and Roberts, 1999).

1.4.3 Differentiation

Eukaryotic cells that undergo differentiation are required to exit the cell cycle. Different studies show that the regulation of D-type cyclins expression and of Rb phosphorylation are key for differentiation (Pines, 1995). There is evidence that the decision to stop proliferating and start the differentiation process, occurs during the early G1 phase (Kiyokawa et al., 1994). A study carried out in murine erythroleukemia (MEL) cells that were induced to differentiate, suggests that the commitment to differentiation takes place in G1 phase as a response of a decrease in the levels of CDK4. Downregulation of CDK4 was related to a decrease in the stability of the protein, by a higher rate of degradation. Therefore, there was a decrease in the formation of the complex CDK4-cyclin D, which generated the accumulation of hypophosphorylated Rb, although an amount of phosphorylated pRb remained. In this study, an increase in cyclin D3 was also observed. Cyclin D3 formed a complex directly with hypophosphorylated Rb. These changes potentially induce the withdrawal from the cell cycle and commitment to differentiate in MEL cells (Kiyokawa et al., 1994).

It has been suggested that the downregulation of cyclin D1 is required for the initiation of myogenic differentiation. Overexpression of cyclin D1, blocks myogenic differentiation and promotes the maintenance of the proliferative state.

Different studies show that during myogenic differentiation, the expression pattern of the different D-type cyclins is varied. The levels of cyclin D1 are downregulated and become almost undetectable in myotubes. On the contrary, levels of cyclin D3 are upregulated upon induction of differentiation, and higher levels of cyclin D3 are detected in myotubes. The decrease on cyclin D1 as well as the increase in cyclin D3 is accompanied by the accumulation of hypophosphorylated Rb and most of the Rb detected in myotubes was found in hypophosphorylated state. (Rao et al., 1994; Skapek et al., 1995; Bartkova et al., 1998).

Withdrawal from the cell cycle is an important step for differentiation. Studies suggest that upregulation of p21 is required for myoblasts to exit the cell cycle on G1 phase and enter G0 phase to start myogenic differentiation (Halevy et al., 1995; Parker et al., 1995; Skapek et al., 1995; Duronio and Xiong, 2013).

Alongside cell cycle withdrawal, the induction of myogenic differentiation is accompanied by the expression of muscle specific genes, whose expression is regulated by the activity of the MyoD family of skeletal muscle specific basic helix-loop-helix (bHLH) transcription factors also known as the myogenic regulatory factors (MRFs) family (Lassar et al., 1994; Hernández-Hernández et al., 2017).

The MRF family is composed of 4 members: MyoD, myogenin, Myf-5 and MRF4. Proliferating myoblasts express MyoD and Myf-5, myogenin is expressed in differentiating cells while MRF4 is expressed in terminally differentiated myotubes. MyoD orchestrates different events that induce the expression of myogenin, which also causes the downregulation of Myf-5. The expression of myogenin marks the myoblast commitment to differentiation and is accompanied by withdrawal of the cell cycle. During differentiation, the expression of MyoD and

myogenin is involved in the regulation of the expression of MRF4, among other muscle-specific proteins. Differentiated myotubes are characterised by a decrease in the levels of MyoD and myogenin while the expression of MRF4 is maintained (Skapek et al., 1995; Hernández-Hernández et al., 2017).

Studies suggest that the regulation of the MRF family proteins is linked to the expression of components of the cell cycle. Expression of cyclin D1 inhibits the MRF family. When myoblasts are subjected to reduced mitogen environment, such as the one created *in vitro* by switching to media with 2% horse serum, they undergo cell cycle arrest while the MRF family mediates the transcription of muscle genes (Rao et al., 1994; Skapek et al., 1995).

Therefore, myogenic differentiation of skeletal muscle cells can be separated in four consecutive steps that start, upon differentiation induction, with the expression of myogenin (potentially regulated by the changes in the expression of cell cycle proteins). Next is the cell cycle exit, driven by the upregulation of p21 and cyclin D3 expression, which is followed by the induction of muscle-specific proteins such as Myosin Heavy Chain (MHC), which leads to the final step, cell fusion, that results in differentiated multinucleated myotubes (Walsh and Perlman, 1997; Gurung and Parnaik, 2012).

1.5 Outline of doctoral research

The Hh signalling pathway plays a crucial role during embryonic development, it is also involved in the regeneration of adult tissues. Dysregulation of the Hh signalling pathway has been associated with different diseases including cancer (McMahon et al., 2003; Petrova and Joyner, 2014; Bangs and Anderson, 2017). The Hh receptor PTCH1 is a well-established tumour suppressor that, in an

unbound state, represses the activation of SMO, which results in the generation of Gli2 and Gli3 repressor forms. Binding of any of the Hh ligands to PTCH1 relieves the repression of SMO, which results in the processing of the Gli activator forms that translocate to the nucleus and activate the Hh target genes expression (Yang et al., 2015). The non-canonical Hh signalling have been described in recent years, it does not involve the activation of the Gli family of transcription factors. Type I non-canonical Hh signalling includes the processes that are dependent of PTCH1 and independent of SMO activation. Type II non-canonical Hh signalling is dependent of SMO and independent of the activation of the Gli proteins (Brennan et al., 2012).

Studies show that the CTD of PTCH1 is not involved in the regulation of the canonical Hh signalling pathway, while it is required for PTCH1 localisation and turnover. The CTD is also involved in the pro-apoptotic function of PTCH1 (Thibert et al., 2003; Lu et al., 2006; Fleet et al., 2016). Previous members of our lab carried out a yeast-two-hybrid screening to identify new CTD-interacting proteins. One of the proteins identified was ATG101. Our study showed that the effect of the interaction between PTCH1 and ATG101 occurs at the final step of autophagy and results in the accumulation of autophagosomes that cannot be degraded, causing an inhibition of the autophagic flux (Chen et al., 2018).

Considering that ATG101 is involved in the initiation of autophagy, one of the main aims of my doctoral research was to understand this protein interaction by investigating the functional consequences of three somatic mutations found in the CTD in human cancer databases. We hypothesised that losing the interaction in any of the cancer mutants could have consequences in the autophagic flux blockade induced by PTCH1, which could give cancer cells a growth advantage.

These results are relevant as they strengthen the hypothesis that the tumour suppressor role of PTCH1 is not only given by its function as SMO repressor, but also independently of it following a type I non-canonical Hh signalling (Chen et al., 2018).

Considering that ATG101 is involved in the initiation of autophagy and no role of ATG101 in the final steps of autophagy have been described, we first hypothesised that the autophagic flux blockade induced by PTCH1 might involve the interaction of PTCH1 with other proteins. Therefore, the second part of my research had the aim to validate and characterise the interaction between ITM2A and PTCH1. ITM2A is a type II membrane protein that inhibits autophagic flux at the final step of the process thorough interaction with V-ATPase (Deleersnijder et al., 1996; Namkoong et al., 2015). In addition, ITM2A was also identified by our group in the yeast-two-hybrid screening as a potential CTD interacting protein. Therefore, we first hypothesised that ITM2A was a mediator of the autophagic flux blockade regulated by PTCH1. However, our findings showed that both, ITM2A and PTCH1, inhibit autophagic flux independently of their interaction.

Different studies show that ITM2A is involved in myogenic differentiation of C2C12 cells. ITM2A levels increase during myogenic differentiation of C2C12 cells while higher levels of ITM2A are related to a faster formation of myotubes (Van den Plas and Merregaert, 2004a; Lagha et al., 2013). Of importance, canonical Hh signalling pathway promotes proliferation of C2C12 cells, and in this way prevents myogenic differentiation of C2C12 (Koleva et al., 2005). Therefore, we aimed to investigate the crosstalk of ITM2A with Hh canonical pathway. Considering this, and the results throughout this research we hypothesised that

the function of ITM2A could be involved in the regulation of canonical Hh pathway.

Chapter 2

Materials and Methods

Chapter 2

Materials and Methods

2.1 Cell culture

HEK293, HEK293T, HeLa, NIH3T3 and C2C12 cell lines were obtained from American Type Culture Collection (ATCC). $Ptc1^{+/-}$ and $Ptc1^{-/-}$ mouse embryonic fibroblasts (MEFs) were a gift from Dr. Matthew Scott (Stanford University). **Table 2.1** shows the general information of the used cell lines. All cell lines were maintained in Dulbecco's Modified Eagle's Medium (DMEM, high glucose) (Gibco), supplemented with 10% Foetal Bovine Serum (FBS) (Gibco, D6546) and GlutaMAX™ (Gibco). Cell lines were cultured at 37°C and 5% CO_2 atmosphere in a humidified incubator. For passaging, cell media was removed and cells were washed with 2 ml of 1x PBS and detached with 2 ml of Trypsin-EDTA solution 0.25% (Merk Life Science UK Limited) for approximately 5 minutes. Cells were diluted with 8ml of fresh pre-warmed growth media and then seeded at the desired cell density. HEK293, HEK293T and HeLa cell lines were passaged upon reaching approximately 80-90% confluence at usual dilutions of 1:20, 1:10 and 1:5 as required. C2C12, NIH3T3 and MEFs were subcultured before reaching 80% confluence at usual concentrations of 1:20, 1:10 and 1:5 as required.

shITM2A and shScramble HEK293, HeLa and C2C12 with were generated in-house as described later in this chapter. They were maintained in the same parental growth media with the addition of puromycin at the specified concentration per cell line (described in section 2.7).

Cell line	Organism	Cell type	Tissue	Properties/Disease
HEK293	Human	Epithelial	Embryonic kidney	Adherent
HEK293T	Human	Epithelial	Embryonic kidney	Adherent
HeLa	Human	Epithelial	Cervix	Adherent/ Adenocarcinoma
NIH3T3	Mouse	Fibroblast	Embryo	Adherent
C2C12	Mouse	Myoblast	Skeletal muscle	Adherent
***Ptc1*$^{+/-}$ and *Ptc1*$^{-/-}$ MEFs**	Mouse	Fibroblast	Embryo	Adherent

Table 2.1 Cell lines used for cell biology experiments
Main characteristics of the cell lines used for cell culture.

2.2 Long-term storage and recovery of cell lines

Cryogenic storage in liquid nitrogen was used for long-term storage of cell lines. To prepare the cell stocks, cells were grown to confluence in a 10 cm dish (except NIH3T3, C2C12 and MEFs that were grown to 70% confluence), washed with 2 ml of 1x PBS, detached with 2 ml of trypsin-EDTA and diluted with 8 ml of fresh growth media. Cells were centrifuged for 4 minutes at 4000 RPM, the obtained cell pellet was re-suspended in 3 ml of freezing media (10% DMSO (Sigma) in FBS) and aliquoted into 1 ml cryotubes. Cryotubes were placed in a Mr. Frosty freezing container (Nalgene) filled with isopropanol and frozen overnight at -80°C. Cryotubes were then stored in the liquid nitrogen dewar.

To thaw cells, cryovials were retrieved from the liquid nitrogen dewar and placed immediately into dry ice, and from dry ice, directly into the water bath or bead bath at 37°C. Once thawed, the entire content (1 ml) of the vial was transferred into a culture flask containing 9 ml of pre-warmed growth media. Cells were then incubated at 37°C and 5% CO_2 and monitored for recovery.

2.3 C2C12 myoblast differentiation into myotubes

C2C12 proliferating myoblasts were seeded in 6-well plates (unless otherwise specified) using growth medium at a concentration of 200,000 cells/ml to reach confluence after 24 hours of seeding. Upon reaching 100% confluency, cells were washed twice with 2 ml of 1x PBS and switched to pre-warmed differentiation media: DMEM supplemented with 2% horse serum (Merk Life Science UK Limited) and 1% GlutaMAX™. Cells were maintained in differentiation media for 7 days, fresh media was changed every other day. Morphology of C2C12 during differentiation was monitored and documented using an EVOS® FL Auto Cell Imaging System (Thermo Fisher).

2.4 Cell counting

Cells were quantified manually using a haemocytometer chamber. Briefly, cells were trypsinised and diluted in growth media, 10 µl of the cell mix were placed in the haemocytometer chamber and counted using an inverted microscope. Under the microscope the haemocytometer is divided into 4 quadrants. The cells within those quadrants, as well as the cells in the top and right edge were considered in the quantification. The total number obtained was divided by 4 and multiplied by 10,000 to obtain the number of cells per ml. Cells were then diluted and seeded depending on the cell type and the experiment planned.

To obtain the cell doubling rate of the generated cell lines with silenced ITM2A, cell counting was carried out as above at time points 0, 24, 48 and 72 hours. The number of cells seeded (0 hours) varied depending on the cell line. For HEK293, 75,000 cell/ml were seeded. For HeLa and C2C12, the seeding number was 50,000 cells/ml.

2.5 Transient transfection

Unless otherwise specified, transient transfection was carried out using transfection reagent Lipofectamine™ 2000 (Thermo Fisher Scientific). Cells were plated in 6-well plates in antibiotic-free growth medium at the following densities: 3 x 10^5 cells/ml for HEK293, 1.5 x 10^5 cells/ml for HeLa cells, and 7.5 x 10^4 cells/ml for C2C12 cells. The following volumes correspond to a 6-well plate size configuration, while **Table 2.2** shows the volumes for different plate sizes. Briefly, 250 µl of Opti-MEM® (Thermo Fisher Scientific) were mixed with 4 µg (total) of DNA plasmid or combination of plasmids and mixed gently by pipetting up and down. In a second Eppendorf tube, 10 µl of Lipofectamine™ 2000 were added directly into 250 µl of Opti-MEM®, mixed gently and incubated for 5 minutes at room temperature. To obtain a transfection reagent:DNA (µl:µg) ratio of 2.5:1, 250 µl of the mix Opti-MEM®/Lipofectamine™ 2000 were added to the mix of Opti-MEM®/DNA and incubated for 30 minutes at room temperature. The entire mix Opti-MEM®/Lipofectamine™ 2000/DNA was added dropwise to each well. Cells were incubated overnight at 37°C and 5% CO_2 and media was replaced by fresh growth media before any other assay.

Plate type	DNA (µg)	Opti-MEM® (µl)	Lipofectamine™ 2000 (µl)
24-well	1	125	2.5
12-well	2	250	5
6-well	4	500	10

Table 2.2 Total volume of components required for transient transfection

2.6 siRNA transfection

HEK293 and HeLa cells were transfected in 10 cm culture dishes following the reverse transfection protocol using the transfection reagent Lipofectamine™

RNAiMAX (Invitrogen) using human ITM2A siRNA (Santa Cruz Biotechnology) and MISSION siRNA negative control (Sigma). For HEK293 160 pmol of siRNA was used and for Hela cells 80 pmol of siRNA was used. Briefly, for each transfection the ITM2A siRNA was diluted into 2 ml of Opti-MEM® directly in the culture dish and mixed gently. Then Lipofectamine™ RNAiMAX was added to the dish containing the siRNA (20 µl for HEK293 and 16 µl for HeLa), mixed gently and incubated for 10 minutes at room temperature. Per transfection reaction, HEK293 cells were diluted in 10 ml of growth media at a density of 3.5 x 10^5 cells/ml and HeLa cells were diluted in 10 ml of growth media at a density of 1.5 x 10^5 cells/ml. After incubation time, diluted cells were added to the dish containing the combined siRNA and RNAiMAX in Opti-MEM®, mixed gently and incubated overnight at 37°C and 5% CO_2. 24 after reverse transfection, cells were tripsinised and seeded in 12-well plate at the following densities (1 ml/well): HEK293 cells were seeded at 4 x 10^5 cells/ml and HeLa cells were seeded at a density of 2 x 10^5 cells/ml and incubated overnight at 37°C and 5% CO_2. 24 hours after seeding, cells were transiently transfected with PTCH1-HA or pcDNA3.1 using Lipofectamine™ 2000 as described earlier in this chapter and incubated overnight at 37°C and 5% CO_2. 4 hours before lysis and RNA extraction, cells were treated with Bafilomycin A1 as established later in section 2.12, for a total of 72 hours after siRNA transfection and 24 hours of PTCH1-HA transfection.

2.7 Puromycin killing curve

For cell lines HEK293, HeLa and C2C12, a puromycin (Cayman Chemicals) killing curve was performed to obtain the optimal concentration of antibiotic to be used for selection. For a 6-well plate HEK293 cells were seeded at a

concentration of 3 x 10^5 cells/ml, HeLa cells and C2C12 myoblasts were seed at a concentration of 1 x 10^5 cell/ml. 24 hours after seeding, each well was treated with different concentrations of puromycin: 0-2.5 µg/ml (in 0.5 µg/ml increments). Viability of the cells was examined every two days for 2 weeks, changing to puromycin-containing fresh growth media every 3 days. The chosen puromycin concentration corresponds to the lowest concentration that starts causing massive cell death by day 3 and that kills all the cells within 2 weeks. For HEK293 and HeLa cells the concentration was 1.5 µg/ml and for C2C12 the concentration was 2 µg/ml.

2.8 Transfection of shRNA

ITM2A shRNA plasmid human (Santa Cruz Biotechnology, sc-60867-SH) was used for transfection in HeLa cells and HEK293 cells. Itm2a shRNA plasmid mouse (Santa Cruz Biotechnology, sc-60868-SH) was used for transfection of C2C12 cells. Control shRNA Plasmid A (Santa Cruz Biotechnology, sc-108060) was used as negative control. For a 6-well plate, HEK293 cells were seeded at a concentration of 2 x 10^5 cells/ml, HeLa cells were seed at a concentration of 1 x 10^5 cell/ml and C2C12 myoblasts were seed at a concentration of 5 x 10^4 cell/ml. For each transfection reaction, 1 µg of shRNA was mixed with 250 µl of Opti-MEM®. In a second microcentrifuge tube, 250 µl of Opti-MEM® were mixed with 4µl of Lipofectamine™ 2000 and incubated for 5 minutes at room temperature. The solution containing the shRNA-encoding plasmid was added to the solution containing the transfection reagent, gently mixed by pipetting up and down and incubated 30 minutes at room temperature. After incubation, cells were washed with 2 ml of 1x PBS, next 2 ml of pre-warmed Opti-MEM® were added into each

well followed by the addition of the transfection reaction. Cells were incubated at 37°C and 5% CO_2 for 5 hours. Media was removed and cells washed with 1x PBS, 2 ml of pre-warmed Opti-MEM® with 10% FBS were added to each well and cells were incubated for 24 hours before starting selection of stably transfected cells with puromycin.

2.9 Isolation of single cell-derived clones

To isolate single clones from the shRNA stably transfected cell pool, the limiting dilution technique was used. Cells were counted using the haemocytometer as described previously (section 2.4) and seeded in a 96-well plate at a density of 5 cells/ml (100 µl/well), and left undisturbed for 2 weeks. Colonies growing from individual wells containing 1 cell were expanded in 24-well plate, followed by 6-well plate and T75 flasks using selective growth media.

2.10 Lentivirus particle generation

The HEK293T cell line was used for the generation of replication-incompetent lentiviruses. Briefly, cells were seeded in a T25 flask at a confluence of 1.5 x 10^5 cells/ml (5 ml) to reach a confluence of ~60% 24 hours after seeding. For each transfection reaction 2 µg of psPAX2 packing vector, 2 µg of pVSV-G envelope vector and 3.5 µg of shRNA encoding vector were added into a microcentrifuge tube. Next, 500 µl of Opti-MEM® were added to the DNA mix followed by the addition of 22.5 µl of TransIT-LT1 (Mirus) directly into the Opti-MEM®/DNA mix (transfection reagent volume/µg DNA ratio= 3:1). Transfection reaction was mixed gently by flicking the tube, incubated for 15 minutes at room temperature and added dropwise to the culture flask. Cells were incubated at 37°C and 5%

CO_2 for 5 hours. Media was then aspirated and replaced with fresh growth media, cells were incubated at 37°C and 5% CO_2 overnight. Virus-containing supernatant was collected after 24 hours of transfection and stored at 4°C under Standard Operating Conditions for handling lentiviral-containing cultures. 5 ml of fresh growth media were added to the cells and incubated for an additional 24 hours. Supernatant collected at 48 hours after transfection was harvested and mixed with the 24 virus-containing media. Next, the total volume of conditioned media was passed through a 0.45 µm filter and transferred into vials containing 1 ml aliquots. Vials were stored at -80°C.

2.11 Generation of stable knockdown cell lines

For lentiviral transduction, 1 ml of virus-containing media was thawed in water bath or bead bath at 37°C and added to cells in T25 flask containing 4 ml of growth media with 10 µg/ml of polybrene (Alfa Aesar). After 24 hours of incubation at 37°C and 5% CO_2, media with polybrene was replaced with fresh growth media and cells were incubated for an additional 24 hours at 37°C and 5% CO_2. Next, growth media with puromycin was added to the cells to start selection. Cells were monitored daily and considered virus-free after two weeks of culture or after 2 passages. Fresh media with puromycin was changed at least twice a week. **Table 2.3** shows the in-house generated cell lines.

Parental cell line	Species	ITM2A knockdown cells
HEK293	Human	HEK293 shITM2A-A HEK293 shITM2A-B HEK293 shITM2A-C
HeLa	Human	HeLa shITM2A-A HeLa shITM2A-B HeLa shITM2A-C
C2C12	Mouse	C2C12 shItm2a-A C2C12 shItm2a-B C2C12 shItm2a-C

Table 2.3 In-house generated cell lines with silenced expression of ITM2A

2.12 Bafilomycin A1 treatment

Bafilomycin A1 (BafA1) (Tocris) stock solutions at a concentration of 200 µM were prepared by dissolving BafA1 powder in dimethyl sulfoxide (DMSO). To inhibit autophagic flux, cells were treated with 100 nM of BafA1 for 4 hours before cell lysis. BafA1 was pipetted into an Eppendorf tube, containing 1 ml of growth media and mixed by pipetting up and down. Media containing BafA1 was added dropwise directly into the well. Control cells were treated with the same volume of DMSO.

2.13 Preparation of cell lysates for Western blotting

The procedure for lysing the cells was carried out on ice. Cells were washed with ice-cold 1x PBS. 150 µl of 1x Laemmli buffer (Sigma) were added to each well of a 6-well plate. Cell lysates were harvested using a cell scrapper and transferred to a pre-chilled Eppendorf tube and placed on ice. Lysates were sonicated on ice for 20 seconds at 15 amplitude, incubated in a heat block for 5 minutes at 95°C and stored at -80°C. Alternatively, when comparing samples with transfected

PTCH1, after sonication the lysates were incubated for 30 minutes at 45°C in a heat block and stored at -80°C.

2.14 Co-immunoprecipitation

HEK293 were transiently transfected using Lipofectamine™ 2000 as described earlier. Co-immunoprecipitation (Co-IP) assay was carried out in 10 cm culture dish, when two different test plasmids were transfected in the same reaction, the total DNA quantity was composed of 4µg of each plasmid. Controls expressing just one test plasmid (4µg) were brought up to a total of 8 µg total DNA with empty pcDNA3.1 vector. 24 hours after transfection, cells were placed on ice, washed with 2 ml of ice-cold 1x PBS and scrapped into 700µl of Co-IP lysis buffer (50 mM Tris-HCl pH 7.5, 150 mM NaCl, 1% NP-40, 0.05% Sodium deoxycholate, 1 mM EDTA, 2.5 Mm $MgCl_2$) supplemented immediately before use with 1x Expedeon Proteoloc protease inhibitor cocktail (AEBSF, aprotinin, bestatin, E-64, leupeptin and pepstatin A), 0.2 mM PMSF and 1mM DTT. Lysates were transferred to pre-chilled Eppendorf tubes. Lysates were incubated with rotation at 4°C for 30 minutes and then centrifuged at 13000 RPM for 15 minutes at 4°C to remove debris. Supernatant was transferred to a new 1.5 ml Eppendorf tube and kept on ice, 200 µl of collected supernatant were set apart on ice as whole cell lysate (WCL). Supernatant was incubated with primary antibody **(Table 2.4)** at 4°C with rotation for 1.5 hours. Next, 30 µl of Dynabeads Protein G (Invitrogen) were added and incubated for 1 hour at 4°C with rotation. A magnetic rack was used to collect and then wash the beads three times with 1 ml of Co-IP lysis buffer. After removing the last wash, 18 µl of 2x Laemmli buffer (Sigma) were added to the beads and mixed. The previously saved WCLs were mixed with 40 µl of 6x

Laemmli buffer. Both, beads and WCL, were incubated on heat block at 45°C for 25 minutes and stored at -80°C for Western blotting.

Antibody	Species	Quantity	Company	Catalogue number
DYKDDDDK tag (Monoclonal)	Mouse	4 ug	Proteintech	66008-3-Ig
GFP tag (Monoclonal)	Mouse	4 ug	Proteintech	66002-1-g
Ha tag (Monoclonal)	Mouse	4 ug	Proteintech	66006-2-Ig
MYC-tag (Polyclonal)	Rabbit	4 ug	Proteintech	16286-1-AP

Table 2.4 Antibodies used for Co-IP assays
Information of the antibodies used for Co-IP experiments.

2.15 Western Blotting

SDS-PAGE (Sodium Dodecyl Sulfate-PolyAcrylamide Gel Electrophoresis) technique was used to separate proteins based on their molecular weight. Cell lysates and Plus Protein™ Dual Colour Standard Marker (Bio-Rad) were loaded in 8% or 13% hand-cast polyacrylamide gels (acrylamide:bisacrylamide 29:1) or in 4-20% Mini-PROTEAN® TGX™ precast protein gels (Bio-Rad, 4561093). Hand-cast gels were placed in 1x Running Buffer (25 mM Tris, 192 mM glycine, 0.1% SDS, pH 8.3, Alfa Aesar) and separated at 85V for 30 minutes and then at 120V for approximately 90 minutes. Precast gels were run without samples for 10 minutes at 100V, then samples were loaded and run at 140V for approximately 60 minutes. Proteins were transferred from the gel to a PVDF membrane (Bio-Rad) by wet transfer using ice-cold 1x Transfer buffer (25 mM Tris, 192 mM glycine, pH 8.5, Alfa Aesar) + 20% Methanol (Fisher Scientific) at 50V for 2 hours. After transfer, membranes were blocked in 5% nonfat dried milk (PanReac

AppliChem) diluted in Tris-buffered saline (TBS) with 0.1% Tween 20 (TBST) at room temperature for 1 hour. After blocking, membranes were washed for 5 minutes in TBST and, unless otherwise specified, incubated overnight with primary antibody at 4°C at the specified concentration **(Table 2.5)** with gently rocking. After incubation with primary antibody, membranes were washed 3 times with TBST for 10 minutes per wash and incubated with appropriate secondary antibody **(Table 2.6)** in 5% milk in TBST for 1 hour at room temperature. Next, membranes were washed 3 times with TBST for 10 minutes. Detection of the proteins of interest was carried out by adding Clarity™ Western ECL Substrate (Bio-Rad) to the membranes and visualised in ChemiDoc Imaging System (Bio-Rad) using Image Lab software (Bio-Rad). Western blot signals were analysed later using ImageJ software and normalised to loading control (β-actin or GAPDH).

Primary antibody	Species	Dilution for Western Blotting	Company	Catalogue number
β-Actin (Monoclonal)	Mouse	1:10,000, 5% milk	Sigma	A5316
CDK2 (78B2) (Monoclonal)	Rabbit	1:1000, 5% BSA	CST	2546
CDK4 (DCS156) (Monoclonal)	Mouse	1:1000, 5% milk	CST	2906
CDK6 (DCS83) (Monoclonal)	Mouse	1:2000, 5% milk	CST	3136
Cyclin D1 (DCS6) (Monoclonal)	Mouse	1:1000, 5% milk	CST	2926
Cyclin D3 (DCS22) (Monoclonal)	Mouse	1:2000, 5% milk	CST	2936
p21 Cip1/Waf1 (12D1)(Monoclonal)	Rabbit	1:1000, 5% BSA	CST	2947
DYKDDDDK Tag (D6W5B)	Rabbit	1:1000, 5% BSA	CST	14793
DYKDDDDK tag (Monoclonal)	Mouse	1:2000, 5% milk	Proteintech	66008-3-Ig

GFP (4B10) (Monoclonal)	Mouse	1:1000, 5% milk	CST	2955
GFP tag (Monoclonal)	Mouse	1:4000, 5% milk	Proteintech	66002-1-g
HA-Tag (C29F4) (Monoclonal)	Rabbit	1:1000, 5% BSA	CST	3724
Ha tag (Polyclonal)	Rabbit	1:5000, 5% milk	Thermofisher	51064-2-AP
Ha tag (Monoclonal)	Mouse	1:5000, 5% milk	Proteintech	66006-2-Ig
HRP-conjugated GAPDH (Monoclonal)	Mouse	1:4000, 5% milk	Proteintech	HRP-60004
ITM2A*	Rabbit	1:800, 5% milk	Proteintech	18306-1-AP
Myc-Tag (9B11) (Monoclonal)	Mouse	1:1000, 5% milk	CST	2276
MYC-tag (Polyclonal)	Rabbit	1:5000, 5% milk	Proteintech	16286-1-AP
Myosin Heavy Chain (Monoclonal)	Mouse	0.2µg/ml, 5% milk	DSHB	MF20
LC3B (Polyclonal)	Rabbit	1:1000, 5% BSA	CST	2775
SQSTM1/p62 (Polyclonal)	Rabbit	1:1000, 5% BSA	CST	5114

Table 2.5 Primary antibodies

Information of the primary antibodies used for Western blotting. *ITM2A antibody was incubated for 1.5 hours at room temperature. Abbreviations: BSA=Bovine serum albumin (Sigma), DSHB=Developmental Studies Hybridoma Bank, CST=Cell signaling Technology.

Primary antibody	**Dilution**	**Company**	**Catalogue number**
Goat anti-rabbit IgG (H + L)-HRP conjugate	1:4000	Bio-Rad	1706515
Goat anti-mouse IgG (H + L)-HRP conjugate	1:4000	Bio-Rad	1706516

Table 2.6 Secondary antibodies

Information of secondary antibodies used for Western blotting.

2.16 Densitometric analysis of gels

Western blotting results were analysed by densitometry. Each band, at the expected molecular weight was quantified using ImageJ. The obtained values of the target protein, after subtracting the background, were normalised to the values of the loading control (β-actin or GAPDH). For the semi-quantitative measurement approach of the autophagic flux, the mean changes of the densitometric quantification of LC3B-II (normalised to control) of the samples treated with BafA1 over its level with vehicle (DMSO) were obtained. This approach accounts for the variability in control samples.

2.17 Gli-Luciferase reporter assay

NIH3T3 cells and MEFs were used for this assay. Cells were seeded in a 10 cm culture dish and grown to a confluence of ~90%. Cells were washed with PBS, detached using 2 ml of trypsin and diluted in 8 ml of fresh growth media. Cells were then seeded in 24-well plates at a 1:5 dilution, 0.5 ml/well in growth media. 24 hours after seeding, cells were transiently transfected. Different transfection reagents were used for each cell line: TransIT-2020® (Mirus) for NIH3T3 cells, and TransIT-X2® (Mirus) for MEFs.

A master mix consisting of Opti-MEM® (50 µl/well), reporter construct p8xGBS-Luc (135 ng/well) and reporter construct pRL-SV40 (15 ng/well) or pRL-TK (15 ng/well) was prepared in an Eppendorf tube, vortexed briefly and aliquoted (1 tube per well, 50 µl/well). Next, a total of 375 ng of plasmid DNA (containing a single plasmid or a combination of plasmids) was added directly into the Eppendorf tubes containing the aliquoted master mix, followed by the addition of 1.5 µl/well of the transfection reagent, vortexed briefly and incubated for 30

minutes at room temperature. Next, this mix was added drop-wise into the wells and cells were incubated for 24 hours. Transfected cells were washed with 0.5 ml of 1x PBS and incubated with serum starvation media (DMEM, 0.5% FBS, 1% GlutaMAX) for an additional 48 hours. Cells were washed with 0.5 ml of 1x PBS and lysed with 100 µl of 1x passive lysis buffer (Promega) with vigorous shacking at room temperature for 15 minutes. Dual-luciferase reporter assay system (Promega) was used to measure the activity of Gli-dependent *Firefly* luciferase and normalisation control *Renilla* luciferase using a Promega Glomax 20/20 luminometer. Values of the individual measurements were generated as relative luciferase units (RLUs) and as *Firefly*-luciferase/ *Renilla*-luciferase ratio.

2.18 Bacterial transformation

Escherichia coli (*E. coli*) DH5α competent cells were used for the transformation of previously validated or purchased plasmids. DH5α cells were thawed on ice and 100 µl were transferred into to a pre-chilled Eppendorf tube containing 1 µg of plasmid DNA, mixed gently by flicking the tube and incubated on ice for 10 minutes. Next, cells were heat shocked for 30 seconds at 42°C in a water bath. 1 ml of SOC media (Thermo Fisher Scientific) was added to the Eppendorf tube and cells were incubated at 37°C and 225 RPM for 1 hour.

For transformation of cloning products, the protocol for transformation was as follows. TOP10 competent *E.coli* (Invitrogen) were thawed on ice for 10 minutes, 100 ng of DNA were added directly into the tube containing 50 µl of competent cells, gently mixed by flicking the tube and incubated on ice for 30 minutes. Cells were heat shocked at 42°C for 30 seconds and incubated on ice for an additional

5 minutes. 950 µl of SOC media were added to the cells and incubated for 1 hour at 37°C with shacking at 225 RPM.

After incubation, different volumes (25-100µl) were spread into Luria-Bertani (LB) (Invitrogen) agar plates containing the specific antibiotic corresponding to the plasmid antibiotic resistance, usually ampicillin (100 µg/ml) or kanamycin (50 µg/ml). Plates were incubated overnight at 37°C. Next day, single colonies were picked from the transformation plate and placed into a 10 ml round-bottom tube containing 3 ml of LB broth supplemented with the required antibiotic and incubated at 37°C with and 225 RPM. Colonies containing previously validated DNA plasmids (1 colony per plasmid), were incubated ~8 hours to continue with maxiprep protocol. When part of a cloning procedure, multiple colonies were incubated overnight for miniprep protocol followed by sequencing.

2.19 DNA extraction by Miniprep and sequencing

EZ-10 Spin Column Plasmid DNA Miniprep Kit Low Copy Plasmid (Bio Basic) was used to extract and purify plasmid DNA. Briefly, after overnight incubation, 1.5 ml from the overnight bacterial suspension were transferred into a Eppendorf tube and centrifuged at 12,000 RPM for 2 minutes. Bacterial pellet was re-suspended with 100 µl of Solution I, incubated at room temperature for 1 minute, mixed with 200 µl of Solution II and incubated at room temperature for 1 minute; 350 µl of Solution III were added, mixed, incubated for 1 minute at room temperature and centrifuged at 12,000 RPM for 5 minutes. Supernatant was placed on a EZ-10 column and centrifuged for 2 minutes at 10,000 RPM. Column containing DNA was washed twice with 750 µl of wash buffer at 10,000 RPM for 2 minutes. Plasmid DNA was eluted with 50 µl of elution buffer by centrifugation

at 10,000 RPM for 2 minutes. DNA concentration and purity were measured using NanoDrop 8000 spectrophotometer (ThermoScientific). Samples containing the highest yield and purity were sent for Sanger sequencing to validate the plasmid. Samples were sent to Source Bioscience or GENEWIZ and stored at -20°. Validated plasmids were transformed for maxiprep.

2.20 DNA extraction by Maxiprep

After incubation, the 3 ml of starter culture were used to inoculate 250ml of LB broth with the specific antibiotic and incubated at 37°C and 225 RPM overnight. Plasmid Maxi Kit (QIAGEN) was used for extraction and purification of the DNA plasmid. Briefly, inoculated LB broth was centrifuged at 6000 x g for 15 minutes at 4°C. Supernatant was discarded, and bacterial pellet re-suspended in 10 ml of P1 Buffer containing RNAse, 10 ml of buffer P2 were added and mixed gently by inverting the tube, and quickly incubated at room temperature for 5 minutes. 10 ml of pre-chilled buffer P3, were added to the mix and mixed gently by inverting the tube and incubated on ice for 20 minutes. Mix was then centrifuged at 4 °C for 30 minutes at 20,000 x g. Supernatant was poured into a fresh centrifuge tube and centrifuged at 4 °C for an additional 15 minutes at 20,000 x g to remove all genomic DNA. During centrifugation, the QIAGEN-tip 500 column was equilibrated with 10 ml of QBT buffer. After centrifugation, supernatant was poured into the pre-equilibrated column, followed by 30 ml of the QF wash buffer. Column was placed in an sterile centrifuge tube and 15 ml of QC elution buffer were added to elute the plasmid DNA, 10.5 ml of isopropanol were added and mixed to precipitate the plasmid DNA, mixed gently and centrifuged at 4°C at 15,000 x g for 1 hour. Supernatant was quickly discarded after centrifugation and

pellet was washed with 2 ml of 70% ethanol and let to air-dry for around 10 minutes. Purified DNA was dissolved in 500 µl of TE buffer (Sigma) and transferred to clean Eppendorf tube. DNA concentration and purity of each plasmid was measured using NanoDrop 8000 spectrophotometer. Plasmids were aliquoted at 250 ng/µl and stored at -20°C.

2.21 Cloning

PCR-based cloning was used to generate constructs corresponding to different fragments of the CTD of PTCH1. First, forward and reverse primers were manually designed to: 1) amplify fragments of the CTD of PTCH1, 2) add and N-terminal ATG codon and a C-terminal HA-tag followed by a stop codon and 3) add a HindIII and XbaI restriction sites to the ends of the inserts **(Table 2.7)**. Plasmid PTCH1-eGFP (generously provided by Peter Zaphiropoulos, Karolinska Institute), containing the human full length sequence for PTCH1 isoform M (the longest variant) was used as a template. Inserts were amplified with Phusion polymerase (New England Biolabs), using the PCR cycle conditions described in **Table 2.8.**

Insert	Direction	Sequence (5'-3')
CTD(1179-1447)-HA	Forward	ACCACCAAGCTTATGGGACCATATCCTGAG
	Reverse	TTAATTTCTAGATCATGCATAATCCGGAACATCA TACGGATAGGGGGG GTCCCTGCG
CTD(1179-1308)-HA	Forward	ACCACCAAGCTTATGGGACCATATCCTGAG
	Reverse	TTAATTTCTAGATCATGCATAATCCGGAACATCA TACGGATAGTTGGA GCTGCTTCC

Table 2.7 Sequences of primers used to amplify fragments of the CTD of PTCH1

Cycle step	Temperature	Time	Cycles
Initial denaturation	98°C	30 seconds	1
Denaturation	98°C	10 seconds	30
Annealing	54°C	25 seconds	
Extension	72°C	45 seconds	
Final extension	72°C	7 minutes	1
	4°C	Hold	Hold

Table 2.8 PCR Cycling conditions for amplification of CTD inserts

PCR products were run on an agarose gel for their identification based on the expected size and then purified using GenElute™ gel extraction kit (Sigma) according to manufacturer's protocol. Next Zero Blunt™ TOPO® PCR Cloning kit (Life technologies) was used to clone the PCR products (blunt-end) into the pCRII-Blunt-TOPO® vector (linearized and activated with topoisomerase I). The cloning reaction was set up as described in **Table 2.9**, mixed gently and incubated for 5 minutes at room temperature, followed by transformation into One Shot® *E. coli* competent cells following manufacturer's protocol.

Reagent	Volume
PCR product	3 µl
Salt solution	1 µl
Sterile water	1 µl
pCRII-Blunt-TOPO®	1 µl

Table 2.9 Setup for TOPO cloning reaction

Single colonies from the TOPO cloning transformation were selected and grown overnight in selective media (kanamycin). Next, plasmid DNA was purified using miniprep as described earlier (section 2.19). Plasmid DNA from minipreps and pcDNA3.1 vector were subjected to double enzyme digestion with HindIII-HF

(New England Biolabs) and XbaI (New England Biolabs) as specified by the manufacturer. Double digested products were separated on a 1.5% agarose gel and purified, their concentration was measured using NanoDrop 8000 spectrophotometer. T4 ligase (New England Biolabs) reaction was set up as recommended by manufacturer using an insert:vector ratio of 3:1 and with overnight incubation at 16°C. Ligation products were heat-inactivated and transformed into TOP10 competent cells, followed by Sanger sequencing of single colony minipreps to verify the sequence as described in section 2.19.

2.22 RNA extraction

RNA extraction from cultured cells was performed using the RNeasy® Mini Kit. Media was aspirated from each well and cells washed with 1x PBS, 350 µl of buffer RLT (containing freshly added 10 µl β-mercaptoethanol/ml) were added directly to each well and cell lysate was harvested using a cell scrapper. Cells were homogenised by vortexing for 1 minute, followed by addition of 350 µl 70% ethanol, mixed by pipetting, transferred to RNeasy Mini spin column and centrifuged at 8000 x g for 15 seconds. The column was then consequently washed with 700 µl of RW1 and centrifuged for 15 seconds, with 500 µl of RPE buffer and centrifuged for 15 seconds, and again with 500 µl RPE buffer and centrifuged for 2 minutes. After discarding the flow-through, the columns containing RNA were centrifuged for an additional minute and transferred to a fresh collection tube. 35 µl of RNAse-free water were added directly onto the column membrane and centrifuged for 1 minute. RNA concentration and RNA quality were measured using NanoDrop 8000 spectrophotometer and RNA samples were stored at -80°C.

2.23 Synthesis of cDNA

iScript™ Select cDNA Synthesis Kit (Bio-Rad) was used to transcribe RNA into complementary DNA (cDNA). Briefly, the reaction was setup on ice using random primers and 1 µg RNA, as specified by manufacturer. Reactions were incubated in a thermocycler using the protocol described on **Table 2.10**. cDNA was stored at -20°C for future use.

Step	Temperature	Time
Priming	25°C	5 minutes
Reverse transcription	42°C	30 minutes
Heat-inactivation	85°C	5 minutes
Hold	4°C	∞

Table 2.10 cDNA synthesis protocol

2.24 Quantitative real-time PCR (qPCR)

Quantitative PCR (qPCR) of the reverse transcribed cDNA was carried out using SsoFast™ EvaGreen® Supermix (Bio-Rad). Primers' sequences are listed in **Table 2.11**. All primers were used at a concentration of 5 µM. The reaction was set up as specified by manufacturer in 96-well qPCR plate. Plate was centrifuged for 1 minute at 1000 RPM. Cycling conditions specified in **Table 2.12**, GAPDH was used as housekeeping gene.

Name	Specie	Direction	Sequence (5'-3')
ITM2A	Human	Forward	ACTGCTATCTGATGCCCCTCAAT
		Reverse	GGTCTTCTCGAACCACATAAGTTTG
	Mouse	Forward	CGCACTGTCCGAGCTCAAAT
		Reverse	CATCTCCCAGATGAGCCATC
Ptc1	Mouse	Forward	ATGGTCCTGGCTCTGATGAC
		Reverse	TAGCCCTGTGGTTCTTGTCC
GAPDH	Human	Forward	TCCCATCACCATCTTCCA
		Reverse	CATCACGCCACAGTTTCC
	Mouse	Forward	AGTATGATGACATCAAGAAGG
		Reverse	ATGGTATTCAAGAGAGTAGGG

Table 2.11 Details of qPCR primers

Cycling step	Temperature	Time	Cycles
Enzyme activation	95°C	30 seconds	1
Denaturation	95°C	5 seconds	40
Annealing/extension	*55-60°C	5 seconds	
Melting curve	65-95°C (increment 0.5°C)	5 seconds/step	1

Table 2.12 Cyclin conditions for qPCR

*Annealing temperatures: ITM2A=57°C, Ptc1=59°C.

Fold changes of target genes were calculated with the 2^ΔΔCt method, where ΔCt is the difference of the Ct value between the target gene minus the Ct value of the control gene (GAPDH), and the second Δ is the difference between the treatment (shRNA or overexpression) and its control (scramble shRNA or empty vector).

2.25 Preparation of immunoprecipitates for mass spectrometry

To prepare the samples for proteomic analysis, HEK293 were seeded in 10 cm culture dishes at a concentration of 3 x10^5 and transiently transfected after 24

hours with either, HA-ITM2A or pcDNA3.1, as stated previously in this chapter, using 8 µg of DNA and 20 µl of LipofectamineTM 2000. 24 hours after transfection, cells were washed with 2 ml of ice-cold 1x PBS and collected with 700 µl of the Co-IP lysis buffer described in section 2.14. Lysates were transferred to pre-chilled Eppendorf tubes and pre-cleared with rotation at 4°C for 30 minutes and then centrifuged at 13000 RPM for 15 minutes at 4°C. Supernatant was transferred to a new 1.5 ml microcentrifuge tube and incubated with 2 µl of normal IgG and 30 µl of Dynabeads Protein G for 30 minutes at 4°C with rotation. Supernatant was separated from Dynabeads using a magnetic rack and later incubated with and anti-HA primary antibody (Proteintech) at 4°C with rotation for 1.5 hours. Next, 30 µl of Dynabeads Protein G were added and incubated for 1 hour at 4°C with rotation. A magnetic rack was used to collect and then wash the beads three times with 1 ml of Co-IP lysis buffer. 18 µl of 1x Laemmli buffer (Sigma) were added to the beads, mixed and incubated on heat block at 45°C for 25 minutes and stored at -80°C before submission for mass spectrometry analysis . Samples were submitted in solution form to the mass spectrometry facility of the University of Leeds for the identification of immunoprecipitation-interacting protein partners and for the detection of protein post-translational modifications. Protein digestion of samples was carried out with trypsin. Data was processed by the facility using the software Peaks.

2.26 Statistical analysis

GraphPad Prism software version 9 was used for the statistical analysis and for the generation of graphs. Unless otherwise specified, three biological replicates were performed. Error bars are shown as standard error of the mean (SEM, n=3).

One-tailed and two-tailed paired Student's t-test were used to analyse the significant difference between two groups. One-way ANOVA analysis was selected to analyse at least three different groups when the samples showed normal distribution and equal variance.

Chapter 3

PTCH1 reduces autophagic flux by interactions of its C-terminal domain with ATG101

Chapter 3

PTCH1 reduces autophagic flux by interactions of its C-terminal domain with ATG101

3.1 Introduction

Different studies have shown that the Hh signalling pathway plays an important role during embryonic development, in the maintenance of homeostasis in adult structures and that dysregulation of the pathway is linked to different cancer types and many other human pathologies (Goodrich et al., 1996; Carballo et al. 2018). PTCH1 is the principal and most studied receptor of the Hh pathway. PTCH1 is expressed in different tissues and its deficiency is embryonic lethal (Goodrich et al., 1997). Secondly, mutations that render PTCH1 non-functional are related to the development of medulloblastoma and basal cell carcinoma in humans (Gailani et al., 1996; Goodrich et al., 1997; Kogerman et al., 2002; Banerjee et al., 2019). PTCH1 is widely known as a tumour suppressor, mainly by the regulatory action that it has on the Hh canonical pathway through inhibition of the oncogene SMO. Repression of SMO results in blocking of the transcriptional activity of the Gli family of proteins and, therefore, prevents activation of Hh target genes (Ingham and McMahon, 2001). While the 12-transmembrane and the extracellular domains of PTCH1 are necessary for the inhibition of SMO, the CTD does not play a role in SMO repression. Nevertheless, it is necessary for PTCH1 turnover (Lu et al., 2006; Kawamura et al., 2008; Fleet et al., 2016).

PTCH1 interacts with an array of proteins, therefore it is possible that some of the interactions could be contributing to its tumour suppressor role independently of SMO activation and, thus, they are not related to its function in canonical Hh

signalling. Previous studies in our lab have shown that the CTD of PTCH1 is involved in the regulation of apoptosis and turnover by interaction with the DRAL/procaspase-9 complex and the ubiquitin E3 ligase ITCH (Thibert et al., 2003; Chen et al., 2014). In order to identify additional interactors of the CTD, a previous postdoc in the Riobo Del-Galdo lab (Dr. Lucy Chen) performed a yeast-two-hybrid screening using the CTD as bait. Identification of an autophagy related protein was followed by validation and functional studies, which are briefly described below to provide context to my direct contribution, which resulted in my first publication (Chen et al., 2018).

3.2 Results

3.2.1 Autophagic flux is regulated by the interaction between ATG101 and the C-terminal domain of PTCH1.

Using the yeast two-hybrid screening system, the Riobo-Del Galdo lab used the C-terminal domain (CTD) of PTCH1 as the bait to identify new interacting proteins. One of the proteins identified using this technique was ATG101. Validation of the physical interaction of ATG101 with PTCH1 was carried out in HEK293 cells. Co-immunoprecipitation experiments with different PTCH1 constructs showed that the CTD is both necessary and sufficient for interaction with ATG101. Confocal microscopy studies showed that PTCH1 co-localises with ATG101 to a high degree, further confirming the interaction of these proteins (Chen et al., 2018). As previously mentioned, ATG101 is part of the mammalian autophagy initiation complex. This complex is formed by FIP200, ULK1/2 and ATG13 (Hara et al., 2008; Hosokawa et al., 2009a; Hosokawa et al., 2009b). The obtained results showed that PTCH1 is capable of interacting with the entire ULK

complex, and that this interaction is mediated by the direct interaction between PTCH1 and ATG101 **(Figure 3.1)**. Considering that PTCH1 interacts with the autophagy initiation complex, different assays were carried out to understand the functional consequences of this interaction on autophagy regulation. Analysis of changes in the level of the autophagy markers LC3B-II and p62 in HEK293 and HeLa cells in the presence and absence of lysosomal inhibitors such as BafA1 and chloroquine, showed that expression of PTCH1 blocks the autophagic flux (Chen et al., 2018). The tandem fusion protein eGFP-RFP-LC3B was used as a complementary approach to validate the effect of PTCH1 on autophagic flux. eGFP-RFP-LC3B displays green and red fluorescence in autophagosomes, but only red fluorescence after formation of autolysosomes due to the low pH, allowing the quantification of “successful” autophagy completion. Overexpression of PTCH1 reduced the formation of autolysosomes, confirming the blocking effect of PTCH1 on the last step of autophagy (Chen et al., 2018).

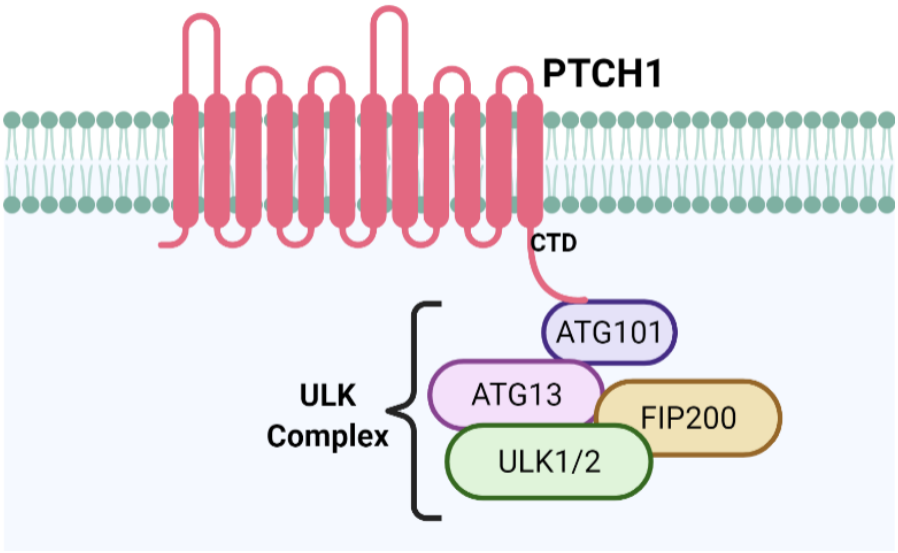

Figure 3.1 Simplified schematic representation of the interaction between the C-terminal domain of PTCH1 and ATG101

The ULK complex is formed by ULK1/2, ATG13, ATG101 and FIP200. PTCH1 interacts with the entire ULK complex through ATG101. The interaction between PTCH1 and ATG101 is mediated by the CTD of PTCH1. Created with BioRender.com.

Experiments using transient silencing of ATG101 showed that the autophagic blockade phenotype observed after expression of PTCH1 is driven mostly by its interaction with ATG101. Considering that the CTD of PTCH1 is not required for the canonical Hh signalling pathway, *Smo*$^{-/-}$ MEFs were used to confirm if the autophagic flux blockade was following a non-canonical Hh signalling pathway. *Smo*$^{-/-}$ MEFs are unable to activate the Hh canonical pathway. *Smo*$^{-/-}$ MEFs were transfected with construct SmoM2, a constitutively active (even in the presence of PTCH1) Smo mutant or empty vector. Overexpression of PTCH1 in the cells deficient of Smo or those expressing the active SmoM2 mutation caused the same inhibition of autophagy like the one observed in HEK293 and HeLa cells while activation of canonical pathway was not affected (Chen et al., 2018). To

further rule out an involvement of the canonical Hh pathway in the autophagic block function by PTCH1, HEK293 cells were transfected with PTCH1 and treated in the absence or presence of SMO inhibitor KAAD-cyclopamine. The analysis of results showed that even in the presence of the KAAD-cyclopamine, PTCH1 expression led to a block in autophagy. These results suggest that the autophagic flux phenotype generated by expression of PTCH1 does not require SMO repression by PTCH1 and, thus, the autophagic flux blockade is independent of SMO activity. Therefore, the autophagic flux blockade exerted by PTCH1 is categorised in the Hh non-canonical signalling pathway. Considering that Shh regulates the proapoptotic activity of PTCH1, which is also mediated by the CTD of PTCH1, HEK293 cells were transfected with PTCH1 and Shh to understand if the Hh ligands could prevent the effect of PTCH1 on autophagy. Analysis of autophagy markers LC3B-II and p62 showed that co-expression of PTCH1 and Shh reverted the autophagic block phenotype observed when PTCH1 is expressed alone. These results indicate that the Hh proteins can inhibit the blocking effect of PTCH1 on autophagy (Chen et al., 2018).

3.2.2 Endogenous Patched1 reduces autophagic flux in mouse embryonic fibroblasts

At the beginning of my PhD, I investigated the effect of endogenous Ptc1 (mouse homolog of PTCH1) on autophagy using mouse embryonic fibroblasts (MEFs) from *Ptc1*$^{-/-}$ mice or *Ptc1*$^{+/-}$ littermates. My results showed that the accumulation of LC3B-II and p62 in response to the inhibitory effect of BafA1 was higher in *Ptc1*$^{-/-}$ than in Ptc1$^{+/-}$ **(Figure 3.2)**. This result is in agreement with the negative regulation of autophagy by PTCH1 and suggests that loss of endogenous

Patched1 increases the basal autophagic flux in a measurable manner (Chen et al., 2018).

Taken together, these results show that a novel function of PTCH1 expression is to restrain autophagic flux, a new type of non-canonical Hh signalling. The decrease in the autophagy rate could be caused by the impairment of the fusion between autophagosome and lysosomes or by inhibiting the acidification of the autolysosomes, since the defect is observed at the last step of autophagy (Chen et al., 2018).

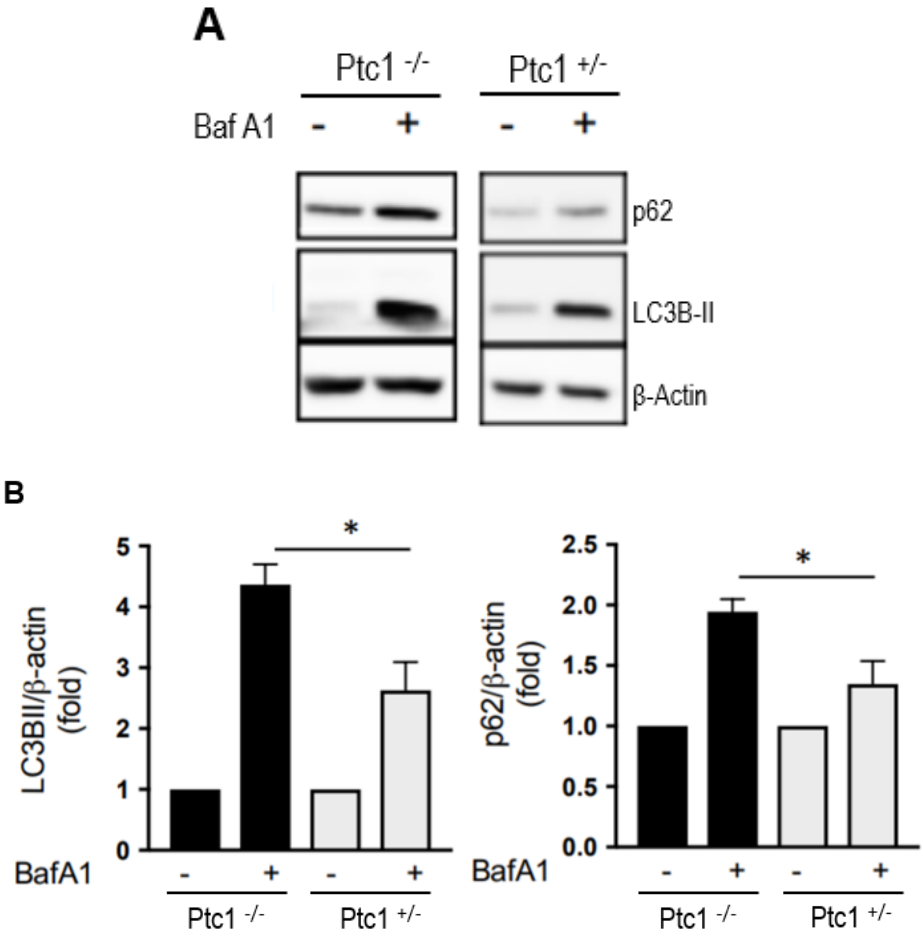

Figure 3.2 Expression of endogenous Patched1 restrains autophagic flux

A. Expression levels of p62 and LC3B-II in *Ptc1*$^{-/-}$ and *Ptc1*$^{+/-}$ MEFs after 4 h in EBSS with or without addition of 100 nM Bafilomycin A1 (BafA1). Representative experiment of n=3. **B.** Densitometric quantification of autophagy markers LC3B-

II and p62 western blot signals normalized to β-Actin in comparison to pcDNA3.1 (n=3; * $P < 0.05$). Adapted from (Chen et al., 2018).

3.3 Discussion

Growing evidence suggest that PTCH1 acts as a tumour suppressor, independently of and in addition to its role as SMO repressor. The CTD of PTCH1, is not involved in its role of SMO repressor. However, is important for PTCH1 turnover and for its pro-apoptotic function (Mille et al, 2009).

We showed that the CTD of PTCH1 interacts with ATG101 causing an inhibition of the autophagic flux through a non-canonical type I Hh signalling. Considering that the effect of the interaction of PTCH1 with ATG101 occurs downstream the formation of the ULK1 complex, and that it leads to an accumulation of autophagosomes that cannot be degraded, further studies are necessary to understand the mechanistic basis of the autophagic flux blockade induced by PTCH1 (Chen et al., 2018).

This novel function of PTCH1 is potentially relevant in the study of specific cancer types, such as colorectal, gastric and endometrial cancers. Mutations in the CTD of PTCH1 could give cancers cells a survival advantage by evasion of the autophagic flux inhibition mechanism. Further studies are required to fully elucidate the functional consequences of the interaction between PTCH1 and ATG101 (Chen et al., 2018).

Chapter 4

Changes in autophagic flux by cancer-associated PTCH1 mutations in its C-terminal domain

Chapter 4
Changes in autophagic flux by cancer-associated PTCH1 mutations in its C-terminal domain

4.1 Introduction

Previous studies in our lab have shown that the CTD of PTCH1 is involved in the regulation of apoptosis and autophagy by interaction with the DRAL/procaspase-9 complex and ATG101 (Chen et al., 2014; Chen et al, 2018). Therefore, it is only logical to hypothesise that mutations in the CTD that could jeopardize the binding of those interacting proteins might have important functional consequences on the processes they regulate.

Autophagy is a homeostatic catabolic process that occurs as a response to an array of biological functions that include, amongst others, adaptation to nutrient depleted conditions, oxidative stress, cellular remodelling during development and differentiation (Yorimitsu and Klionsky, 2005). Dysregulation of autophagy has been linked to different human diseases that include degenerative disorders, inflammatory conditions and cancer. The study of autophagy as well as the proteins involved in the process is becoming more important as it can provide different targets to treat disease (Levine and Kroemer, 2008).

The role of autophagy in cancer is less clear, with controversial evidence supporting a context-dependent positive or negative influence. Activation of autophagy has been frequently observed in growing tumours. Tumours need nutrients to sustain their growth and these nutrients are supplied by autophagy. In this scenario, blocking of autophagy could be used to treat cancer. In addition, a protective role of autophagy by degradation of accumulated damaged organelles and from the potential generation of toxic substrates, such as reactive

oxygen species, was also proposed (White, 2012; Galluzzi et al., 2015). However, autophagy was also shown to contribute to the elimination of early cancer cells before a tumour mass is established, opposing tumour initiation (Bhutia et al., 2013). Considering that our results suggest that tumour suppressor activity of PTCH1 could be partially dependent on its inhibitory function on autophagy mediated by the CTD, we searched for PTCH1 CTD mutations in the Cancer Genome Atlas (TCGA) database (unpublished observations). Remarkably, we found three somatic mutations in the CTD of PTCH1 that are overrepresented in ~5% of colorectal cancers, ~2.7% gastric cancer and ~7.5% of endometrial cancers. Findings in the colorectal cancer cases were further validated by two independent cohorts: the UK 100,000 Genome Project and the Norwegian Series I, where the incidence of the three most common CTD mutations in colorectal cancer cases was also found to be 4.1% and 6% respectively (unpublished observations; Sveen et al., 2017). Two of these mutations are frameshift-causing indels that cause sequence changes after S1203 and R1308 and result in premature truncation of PTCH1. The third one is a substitution in the PPxY motif: Y1316T. Both mutations that cause the truncation have lost the ubiquitylation site (K1426), and the caspase cleavage (D1405), which is required for the pro-apoptotic activity of PTCH1, and all three lack the PPxY motif essential for interaction with ITCH, an E3 ubiquitin ligase that mediates PTCH1 turnover (Lu et al., 2006; Mille et al., 2009; Chen et al., 2014).

4.2 Aims

Given that the interaction of PTCH1 with ATG101 occurs through the CTD and that this region is a hot spot for somatic mutations that have been linked to specific types of cancer, it was decided to investigate what could be the functional consequences of the cancer mutations on the regulation of autophagy and their binding ability to ATG101.

The specific aims of this part of my doctoral investigation were:

- Generation of constructs encoding the three identified PTCH1 CTD cancer mutants.
- Analysis of the interaction of ATG101 with the PTCH1 cancer-associated mutants.
- Investigation of the functional capacity of the CTD cancer mutants to modulate autophagic flux.

4.3 Results

4.3.1 Generation of cancer mutations in the CTD of PTCH1.

There are three specific mutations and truncations in the CTD of PTCH1 that, according to the Cancer Genome Atlas TCGA database, are overrepresented in colorectal cancer, stomach cancer and endometrial cancer **(Figure 4.1)**.

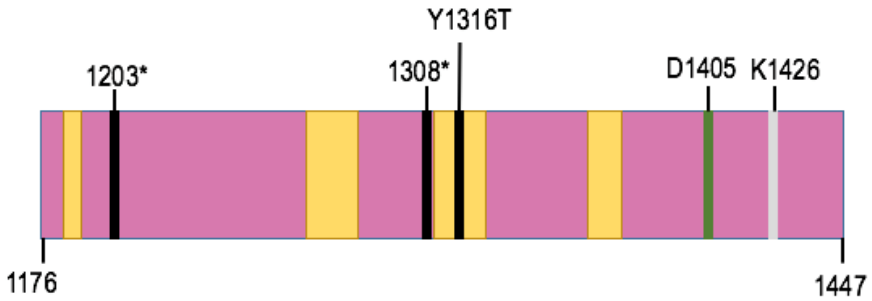

Figure 4.1 Simplified schematic representation of significant structural elements and somatic mutations found in the CTD of PTCH1

Yellow boxes represent the approximate position of Proline-rich motifs. The green line represents the caspase cleavage site. The grey line represents ubiquitylation site. The black lines represent somatic mutations found in the TCGA database.

I supervised MNatSci student G. Jenkins to perform site directed mutagenesis to engineer the three mutants from a plasmid encoding wild type PTCH1 with N-terminal Myc tag: Myc-PTCH1(1-1308), Myc-PTCH1(1-1203) and Myc-PTCH1(Y1316T) **(Figure 4.2A)**. The generation of these mutants was confirmed by Sanger sequencing (data not shown) and subsequently analysed by Western blotting.

Additionally, subcloning of the CTD via PCR amplification and addition to start and stop codons and novel restriction sites was performed to generate two constructs encoding the isolated CTD of PTCH1 with a C-terminal HA-tag: full

length CTD(1179-1447)-HA and the shorter cancer mutant CTD(1179-1308)-HA **(Figure 4.2B)**. Each construct was confirmed by Sanger sequencing. However, expression of the CTD(1179-1308)-HA mutant at the protein level could not be consistently detected by western blotting. It is possible that mutant CTD(1179-1308)-HA was unstable and degraded or that the HA-tag epitope was somehow occluded from the antibody. Another possibility is that the expression levels are below the detection limit by Western blotting.

Two additional CTD constructs of interest with C-terminal HA-tags were designed and synthesised using a commercial source (Agentide): cancer CTD mutant CTD(1179-1203)-HA and CTD fragment CTD(1308-1447)-HA **(Figure 4.2B)**. Expression controls of these CTD fragments showed that only the CTD(1308-1447)-HA construct was readily expressed by Western blotting, while the cancer-associated mutant CTD(1179-1203)-HA could not be detected (data not shown). **Table 4.1** summarises the principal characteristics of the generated constructs. Western blots for the validation of the expression of the generated PTCH1 constructs are shown in **Figure 4.3A&B**.

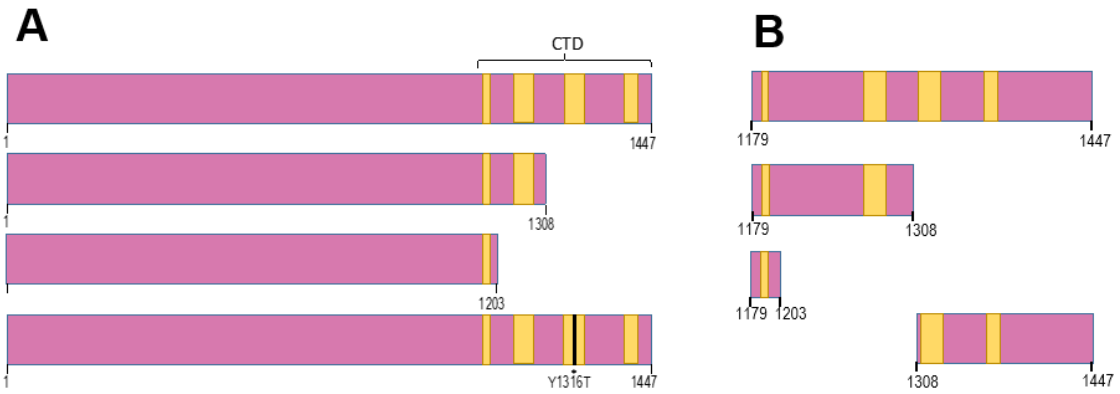

Figure 4.2 Simplified schematic representation of constructs corresponding to the cancer-associated mutations in the CTD of PTCH1 found in the TCGA database

Yellow boxes represents the approximate position of Proline-rich region. **A.** Full length constructs of PTCH1. From top to bottom: Myc-PTCH1(1-1447), Myc-PTCH1(1-1308), Myc-PTCH1(1-1203) and Myc-PTCH1(Y1316T). **B.** CTD constructs of PTCH1. From top to bottom: CTD(1179-1447)-HA, CTD(1179-1308)-HA, CTD(1179-1203)-HA and CTD(1308-1447)-HA.

Plasmid Name	Position Tag	Predicted Molecular weight	Confirmed by Western Blot
CTD(1179-1447)-HA	C-terminal	30 kDa	Yes
CTD(1179-1308)-HA	C-terminal	15 kDa	No
CTD(1179-1203)-HA	C-terminal	4 kDa	No
CTD(1308-1447)-HA	C-terminal	16 kDa	Yes
Myc-PTCH1(1-1203)	N-terminal	135 kDa	Yes
Myc-PTCH1(1-1308)	N-terminal	146 kDa	Yes
Myc-PTCH1(Y1316T)	N-terminal	161 kDa	Yes

Table 4.1 Principal characteristics of generated PTCH1 constructs

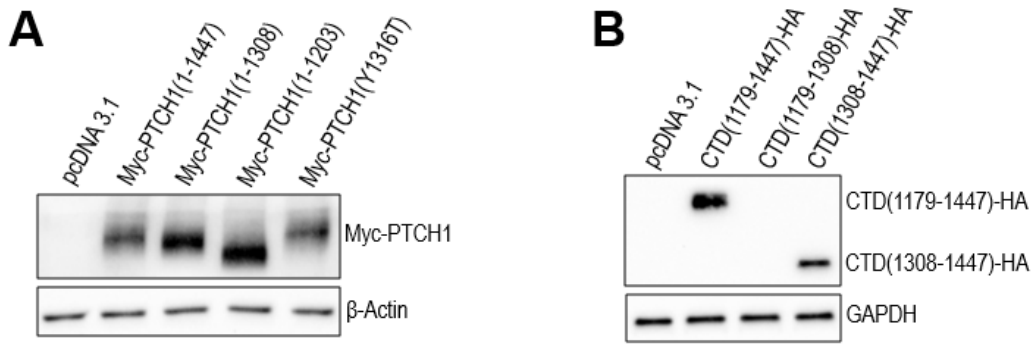

Figure 4.3 Detection of protein expression of generated PTCH1 mutants by Western blotting

Detection of protein expression of generated PTCH1 mutants by Western blotting. **A.** Expression of Myc-PTCH1, Myc-PTCH1(1-1308), Myc-PTCH1(1-1203) or Myc-PTCH1(Y1316T) in HEK293 cells, pcDNA 3.1 was used as control. **B** Expression of CTD(1179-1447)-HA, CTD(1179-1308)-HA or CTD(1308-1447)-HA in HEK293 cells, pcDNA 3.1 was used as control.

4.3.2 Loss of the CTD after R1308 abolishes interaction with ATG101

To investigate the effect of the three CTD cancer mutations on their interaction with ATG101, HEK293 cells were co-transfected with full length Myc-PTCH1(1-1447), Myc-PTCH1(1-1203), Myc-PTCH1(1-1308), Myc-PTCH1(Y1316T) or empty vector along with ATG101-FLAG. Co-immunoprecipitation of Myc-PTCH1 showed that the interaction with ATG101 was only maintained with the Myc-PTCH1(Y1316T) mutant **(Figure 4.4A)**. Our previous study suggests that membrane localization of PTCH1 is not a pre-requisite for its interaction with ATG101 (Chen et al., 2018), therefore HEK293 cells were co-transfected with the soluble CTD constructs: full length CTD(1179-1447)-HA, N-terminal half CTD(1179-1308)-HA and C-terminal half CTD(1308-1447)-HA or empty vector

along with ATG101-FLAG. Co-immunoprecipitation of CTD-HA fragments showed that the interaction with ATG101 was detectable in two of the CTD constructs: full length CTD(1179-1447)-HA and C-terminal half CTD(1308-1447)-HA.

However, it is important to highlight that there was no detectable protein expression of the fragment CTD(1179-1308)-HA **(Figure 4.4B)**. Altogether, co-immunoprecipitation studies using full length PTCH1 or the isolated CTD confirm that the 1308-1447 region mediates its interaction with ATG101 and that the two truncated mutants observed in epithelial cancers cannot interact with ATG101.

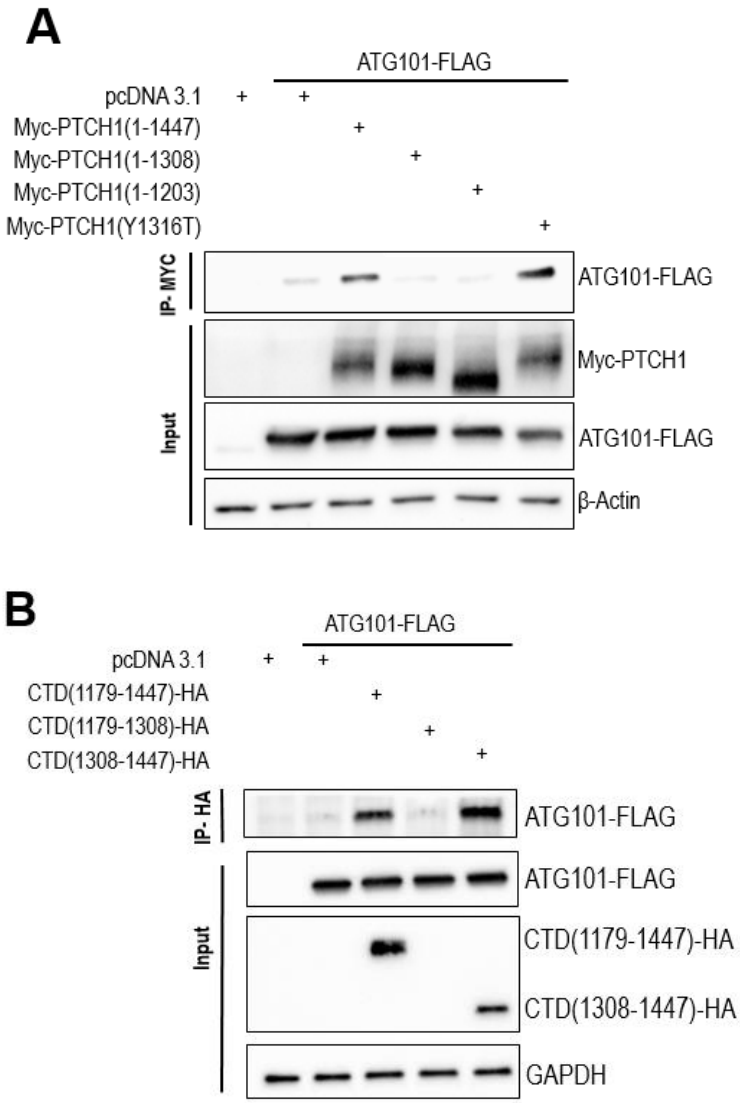

Figure 4.4 The 1308-1447 region of the CTD of PTCH1, absent in two of the cancer-associated mutants, is necessary for interaction with ATG101

A. HEK293 cells were transfected with ATG101-FLAG and full length Myc-PTCH1, Myc-PTCH1(1-1308), Myc-PTCH1(1-1203) or Myc-PTCH1(Y1316T), pcDNA3.1 was used as control. 24 hours after transfection, cells were lysed and immunoprecipitated with Myc tag antibody, followed by analysis of ATG101-FLAG in the IP and whole cell lysate (input). **B.** HEK293 cells were transfected with ATG101-FLAG and CTD(1179-1447)-HA, CTD(1179-1308)-HA or CTD(1308-1447)-HA, pcDNA3.1 was used as control. 24 hours after transfection, cells were lysed and immunoprecipitated with anti-HA antibody, followed by analysis of ATG101-FLAG in the IP and whole cell lysate (input).

4.3.3 Cancer mutations on the CTD of PTCH1 that disrupt the interaction with ATG101 affect the autophagy flux blockade induced by PTCH1

As previously described, the methodologies used for the study of autophagy can be categorised into: qualitative (identification of autophagy-related structures and their fate) and semi-quantitative (measurement of the levels of autophagy proteins and cargoes that are selectively degraded during autophagy). Nonetheless, the study of autophagy remains complex, and most of the methods for the analysis of autophagic flux rely on measuring the changes in autophagic cargo degradation over time, a process known as “autophagic flux” (Yoshii and Mizushima, 2017). The most common method used to study autophagic flux involve the measurement of two forms of LC3B (homolog of the yeast Atg8 protein). As previously mentioned, the LC3B precursor is first cleaved by ATG4 generating LC3B-I. During autophagy LC3B-I is conjugated to PE to form LC3B-II, which can be found embedded in the isolation membrane and in both, inner and outer membranes of the autophagosomes. As a result, LC3B-II is widely used as a marker for the identification of autophagy-related structures such as autophagosomes (Barth et al., 2010; Mizushima et al., 2010). p62/SQSMT1 is a second autophagy marker protein. p62 interacts with ubiquitinated cargo and with LC3B-II to bring cargo into the autophagosome, with both p62 and its cargo being degraded through the autophagy process. Therefore, an increase in p62 protein levels in western blotting reflects a blocking in autophagy, as the protein cannot be degraded and is accumulated (Yoshii and Mizushima, 2017).

We used the changes in those autophagy markers to investigate if the loss of the interaction of PTCH1 with ATG101 in the cancer-associated truncation mutants

affects the regulatory function of PTCH1 on the autophagic flux. In addition, it was decided to investigate whether the mutation Y1316T, which maintains the interaction with ATG101, had any impact on the autophagy phenotype. Consequently, to understand the effect of the CTD cancer mutations on the autophagic flux inhibition exerted by PTCH1, HEK293 cells were transfected with Myc-PTCH1(1-14473), Myc-PTCH1(1-1203), Myc-PTCH1(1-1308), Myc-PTCH1(Y1316T) or empty vector, and after 24 hours of transfection, the cells were treated with BafA1 or vehicle to investigate autophagy flux. Analysis of LC3B-II and p62 levels **(Figure 4.5)** showed that the Myc-PTCH1(1-1203) mutant does not inhibit autophagic flux, which was expected as this mutant losses its interaction with ATG101. Treatment with BafA1 on cells expressing the mutant Myc-PTCH1(Y1316T), which maintains the interaction with ATG101, showed similar results to wild type Myc-PTCH1(1-1447), suggesting a normal function. However, the Myc-PTCH1(1-1308) mutant, which like Myc-PTCH1(1-1203) is also unable to interact with ATG101, showed an intermediate autophagy flux phenotype between PTCH1 (1-1203) and wild type PTCH1.

Taken together, these results show that the interaction of ATG101 with the CTD of PTCH1 occurs mainly in the region of the CTD that encompasses amino acids 1308 to 1447, with additional requirements in the 1203-1308 region. These results also indicate that the mutation in the CTD that causes the amino acid substitution Y1316T does not disrupt the interaction with ATG101 and conserves the autophagy phenotype exerted by wild type PTCH1.

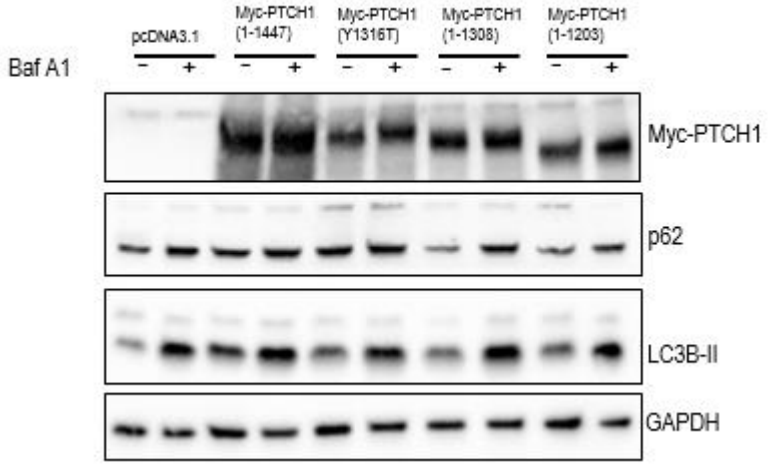

Figure 4.5 Truncation of the CTD of PTCH1 at S1203 or R1308 attenuates autophagic flux blockade by wild type PTCH1

Expression levels of p62 and LC3B-II in HEK293 cells transfected with pcDNA3.1, Myc-PTCH1(1-1447), Myc-PTCH1(Y1316T), Myc-PTCH1(1-1308) and Myc-PTCH1(1-1203), and cultured 24 hours in complete growth medium with or without the addition of 100 nM Bafilomycin (BafA1) during the last 4 h. Representative experiment of n=3.

4.4 Discussion

These results show that the interaction of ATG101 with PTCH1 occurs mainly in the CTD region comprising amino acid 1308 to 1447. However, additional weaker interactions of ATG101 with another region of the CTD of PTCH1 that encompasses amino acids 1179 and 1308 cannot be ruled out given the lack of detection of the protein expression by western blotting of the constructs corresponding to this fragment.

With the help of MBiol student Michael Parkes, an analysis of the predicted secondary structure of the CTD fragments with the epitope tags was carried out. Five different proline regions were found on the CTD based on the following criteria: they contain at least one of the following, a proline motif, arginine residues or lysine residues. The construct CTD(1179-1308)-HA, contains 3 proline rich regions in total, the first one characterised for a PxPxxxP motif and an arginine residue. The second one formed of a PxxP motif and arginine residue, and the third one formed by 3 arginines. The C-terminal HA tag of the CTD(1179-1308)-HA generates an extra proline motif. Proline-rich motifs can form a polyproline II helix (PPII) (Zarrinpar et al., 2003). Therefore, the presence of the HA tag in the CTD(1179-1308)-HA construct could result in a new PPII structure. This PPII structure is important as it could hide the HA epitope (Lopes et al., 2014), and therefore obstruct the detection of the anti-HA antibody in western blotting experiments of the construct CTD(1179-1308)-HA.

Furthermore, it would be interesting to understand if mutations in the caspase cleavage or in the ubiquitylation site, that are contained within the amino acids 1308 and 1447 would disrupt the interaction with ATG101 and/or if they could have an effect on the autophagic flux blockade regulated by PTCH1.

Chapter 5

Interaction of the CTD of PTCH1 with ITM2A: characteristics and effect on autophagy in HEK293 and HeLa cells

Chapter 5

Interaction of the CTD of PTCH1 with ITM2A: characteristics and effect on autophagy in HEK293 and HeLa cells

5.1 Introduction

Recent findings in our lab show that the intracellular CTD of PTCH1 regulates autophagic flux by interacting with ATG101, a protein with a major role in the initiation of autophagy. Paradoxically, the phenotypic consequences of the interaction is observed at the end of the autophagic process, where PTCH1 induces an autophagic flux blockade (Chen et al., 2018). Considering this, it is possible that PTCH1 is interacting with additional proteins to block autophagy completion. Incidentally, another research team published that ITM2A, a type II single pass membrane protein, blocks the autophagic flux at the same step as PTCH1 through an inhibitory interaction with V-ATPase that results in the accumulation of autophagosomes that cannot be degraded (Namkoong et al., 2015). Although the function of ITM2A is not completely elucidated, it has been linked to differentiation of skeletal muscle, cartilage tissue and in T cell development. Nevertheless, its effects are cell type specific (Kirchner and Bevan, 1999; Van den Plas and Merregaert, 2004a). Besides its role in autophagy and differentiation, ITM2A has been shown to be involved in breast and ovarian cancer, although with different consequences on autophagy (Nguyen et al., 2016; Zhou et al., 2019).

It was decided to explore in detail the role of ITM2A since it was also identified in the yeast two-hybrid screen of PTCH1 CTD interactors, suggesting a potential functional interaction.

5.2 Aims

Since ITM2A inhibits autophagy at the same step as PTCH1, and potentially interacts with it in mammalian cells, it was first hypothesised that ITM2A could be a mediator of the autophagic flux blockage by PTCH1. Therefore, the specific aims for this chapter are:

- Validation of the interaction between PTCH1 and ITM2A in mammalian cells.
- Investigation of the role of ITM2A expression on the negative regulation of autophagy by PTCH1.
- Identification of the region of PTCH1 that is involved in the interaction with ITM2A.
- Generation of stable cell lines with ITM2A knockdown to establish if the autophagy flux blockade induced by PTCH1 is mediated by ITM2A.

5.3 Results

5.3.1 PTCH1 physically interacts with ITM2A

Former members of the Hedgehog lab previously identified novel proteins that could interact with the CTD of PTCH1. This was achieved by a yeast-two-hybrid screening in which the GAL4 DNA-binding domain fused to the CTD of PTCH1 was used as the bait to screen the mouse embryo E17cDNA library. The library was fused to the GAL4-activator domain (Chen et al., 2018). The most frequently recovered clone from the yeast-two-hybrid screening encoded for the mouse ITM2A protein, with 21 hits out of the 63 validated interactors (33%) (unpublished data). The involvement of ITM2A in autophagy had been recently published (Namkoong et al., 2015), therefore it was decided to validate ITM2A as an interacting protein of PTCH1 in mammalian cells.

HEK293 cells were co-transfected with HA-tagged full length PTCH1, the isolated CTD (CTD(1179-1447)-HA), the N-terminal half of the CTD (CTD(1179-1308)-HA) or empty vector along with Myc-ITM2A. Co-immunoprecipitation results confirmed the interaction of full length PTCH1 with ITM2A in mammalian cells **(Figure 5.1A&B)**. Interestingly, and despite the fact that the yeast-two-hybrid screening was carried out with the CTD as bait, the results showed no interaction between ITM2A and the full length CTD of PTCH1 in soluble form.

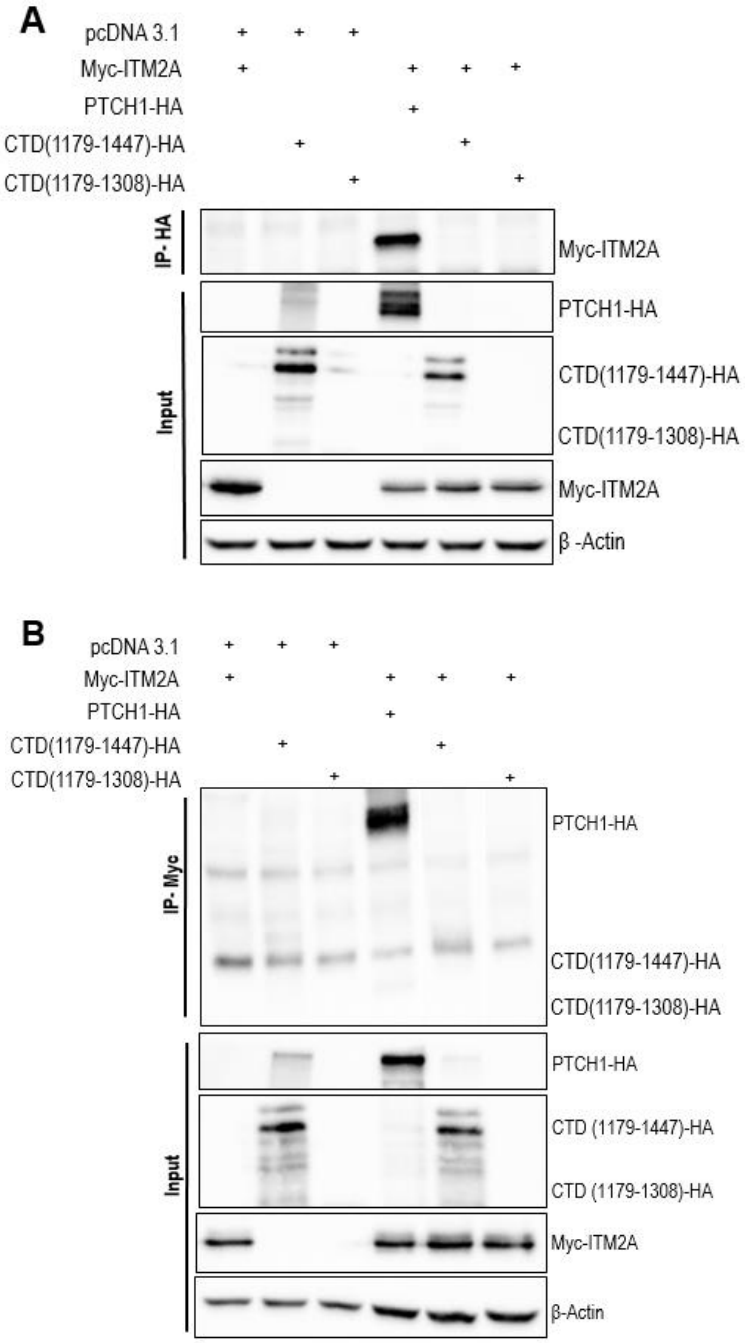

Figure 5.1 PTCH1 physically interacts with ITM2A

HEK293 cells were transfected with Myc-ITM2A and: PTCH1-HA or CTD(1179-1447)-HA or CTD(1179-1308)-HA, pcDNA 3.1 was used as control. 24 hours after transfection, cells were lysed and immunoprecipitated with **A.** Anti-HA antibody, followed by analysis of Myc-ITM2A in the IP and whole cell lysate (input), and **B.** Anti-Myc antibody, followed by analysis of PTCH1-HA or CTD (1179-1447)-HA or CTD (1179-1308)-HA in the IP and the whole cell lysate (input).

Therefore, the next step was to understand if membrane localisation of PTCH1 is a pre-requisite for its interaction with ITM2A. To answer this, the construct myr-eGFP-CTD that localises the CTD of PTCH1 to the membrane through a myristoylation signal, was used. HEK293 cells were co-transfected with full length PTCH-eGFP, myr-eGFP-CTD or empty vector along with Myc-ITM2A. Co-immunoprecipitation analysis showed that ITM2A interacts with the membrane-bound CTD **(Figure 5.2A)**, suggesting that membrane localization of PTCH1 is necessary for the interaction.

To determine if ITM2A interacts with additional intracellular regions of PTCH1, we selected PTCH1 mutants with deletions in the cytoplasmic regions to understand if the removal of the intracellular regions of PTCH1 completely abolished the interaction with ITM2A.

First we selected the mutant PTCH1ΔML-eGFP, with a deletion of the middle cytoplasmic loop (located between TM6 and TM7). In this mutant, all the cytoplasmic middle loop is removed except the first 9 amino acids and the last 18 amino acids of the middle loop. We also selected the double deletion mutant: PTCH1ΔML-ΔCTD-eGFP that, in addition to the previously described deletion of the middle loop, also lacks all the CTD except the first 11 amino acids of this region. The selected mutants were generated by PhD student Alex Timmis.

HEK293 cells were co-transfected with eGFP-PTCH1, eGFP-PTCH1-ΔML, eGFP-PTCH1-ΔML-ΔCTD, or empty vector along with Myc-ITM2A. Surprisingly, co-immunoprecipitation results show that ITM2A interacts with both PTCH1 deletion mutants **(Figure 5.2B)**, suggesting that ITM2A interaction with PTCH1 is not constrained to the intracellular regions of PTCH1. In addition, ITM2A could

potentially be interacting with the transmembrane or extracellular regions of PTCH1.

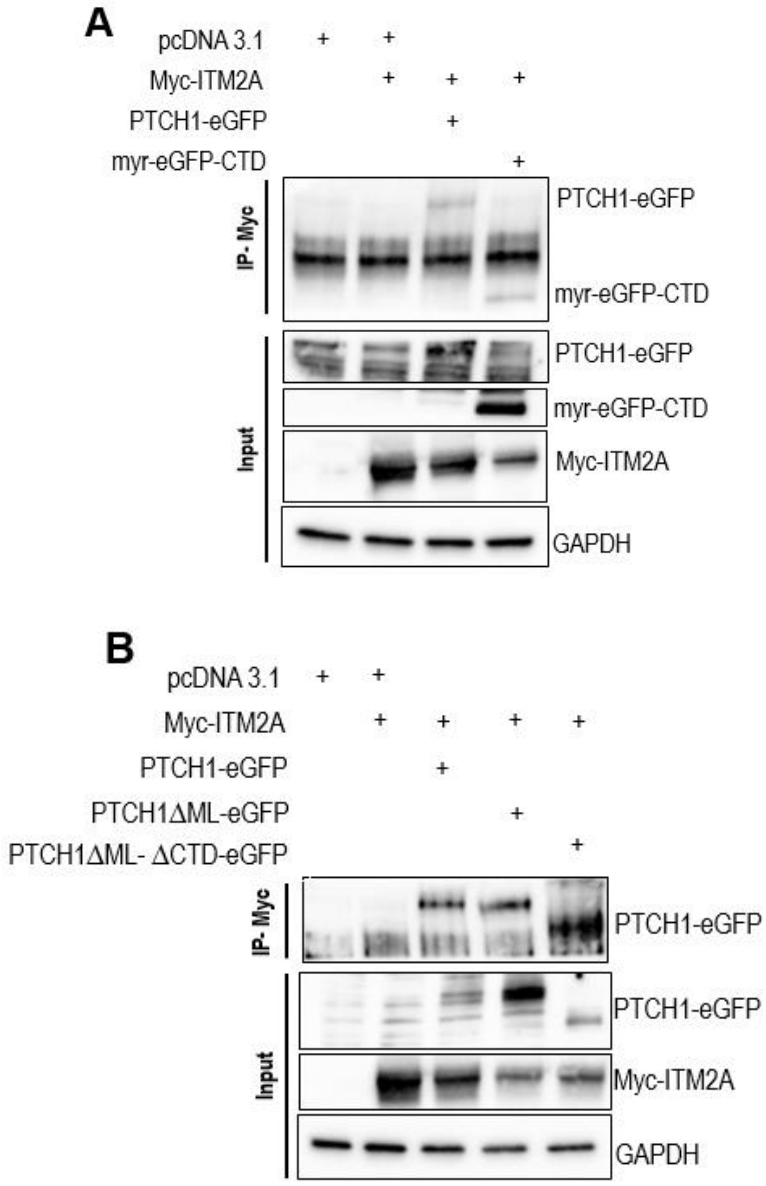

Figure 5.2 ITM2A physically interacts with multiple regions of PTCH1

A. HEK293 cells were transfected with Myc-ITM2A and: PTCH1-eGFP or myr-eGFP-CTD, pcDNA3.1 was used as control. 24 hours after transfection, cells were lysed and immunoprecipitated with anti-Myc antibody, followed by analysis of PTCH1-eGFP and myr-eGFP-CTD in the IP and whole cell lysate (input). **B.** HEK293 cells were transfected with Myc-ITM2A and PTCH1-eGFP or PTCH1ΔML-eGFP or PTCH1ΔML-ΔCTD-eGFP, pcDNA 3.1 was used as control.

24 hours after transfection, cells were lysed and immunoprecipitated with anti-Myc antibody, followed by analysis of PTCH1-eGFP, PTCH1ΔML-eGFP and PTCH1ΔML-ΔCTD-eGFP in the IP and whole cell lysate (input).

5.3.2 ITM2A interacts with itself

There is not much biochemical information available on ITM2A. To understand better this protein's behaviour, it was decided to investigate if ITM2A could interact with itself. This is especially relevant for this study because PTCH1 is known to form functional dimers (Qi et al., 2018). HEK293 cells were co-transfected with Myc-ITM2A, HA-ITM2A and empty vector as a control. Co-immunoprecipitation analysis showed that ITM2A can interact with itself **(Figure 5.3)**. It would be interesting to understand the oligomeric state of ITM2A as this can provide more information about its interaction with other proteins and how this interaction could be manipulated for therapeutic use.

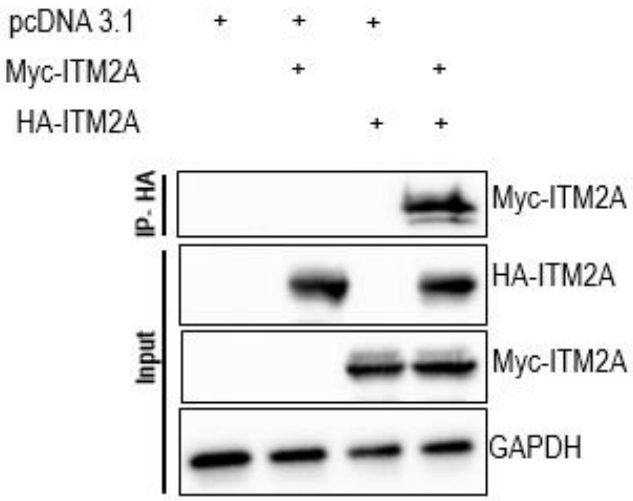

Figure 5.3 ITM2A physically interacts with itself

HEK293 cells were transfected with Myc-ITM2A and HA-ITM2A, pcDNA 3.1 was used as control. 24 hours after transfection, cells were lysed and immunoprecipitated with anti-HA antibody, followed by analysis of Myc-ITM2A in the IP and whole cell lysate (input).

5.3.3 Co-expression of PTCH1 and ITM2A does not change the inhibition of autophagic flux by PTCH1

Once the interaction between PTCH1 and ITM2A had been confirmed in mammalian cells, and considering that our previous work and the work of others shows that both ITM2A and PTCH1 block autophagy at the final step of the process (Chen et al., 2018; Namkoong et al., 2015), it was hypothesised that the interaction of PTCH1 with ITM2A could be necessary for the autophagy inhibition induced by PTCH1. HEK293 cells were transfected with ITM2A or PTCH1 alone or in combination. After 24 hours, cells were treated with BafA1 or DMSO to block autophagy, followed by western blotting of autophagy markers LC3B-II and p62. Results show that both proteins equally inhibit autophagic flux individually and no additive or synergistic effects are observed when both proteins are expressed together **(Figure 5.4A-D)**. Strikingly, western blots showed that when ITM2A was overexpressed alongside PTCH1, the expression of PTCH1 was significantly downregulated **(Figure 5.4E)**, which suggests that ITM2A could be affecting the stability of PTCH1 and promoting its degradation, and in this way ITM2A could be having an indirect effect on the autophagy block induced by PTCH1 by reducing the blocking effect of PTCH1.

It is possible that the effect of PTCH1 on autophagy when co-transfected with ITM2A, is being underappreciated because the system is already saturated by ITM2A. Our results clearly show that ITM2A is causing a reduction on the protein expression of PTCH1. A decrease in PTCH1 expression potentially means a decrease in its autophagy flux blockade function. However, this reduction could be masked if either protein was maximally inhibiting autophagic flux. In addition,

if ITM2A is affecting the stability of PTCH1, this could indicate that ITM2A could be a regulatory factor in canonical Hh signalling pathway.

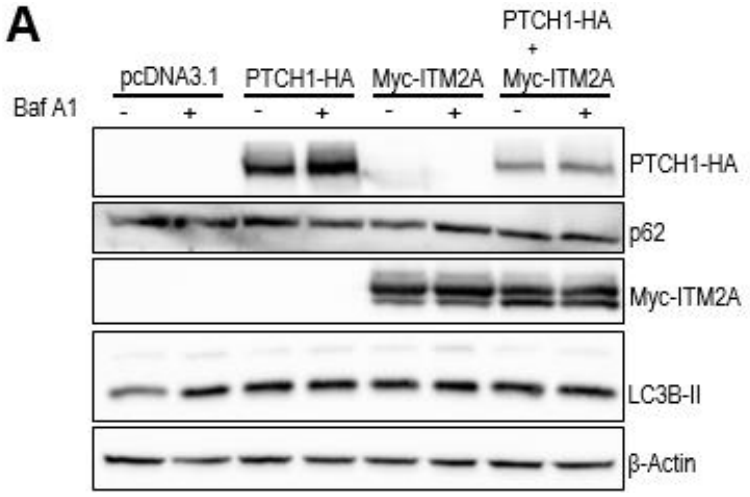

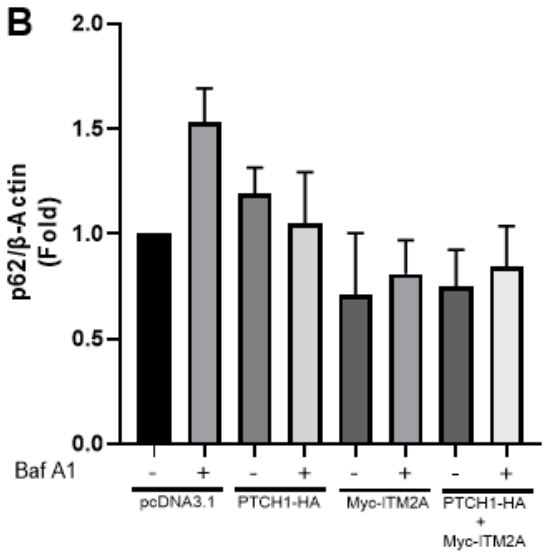

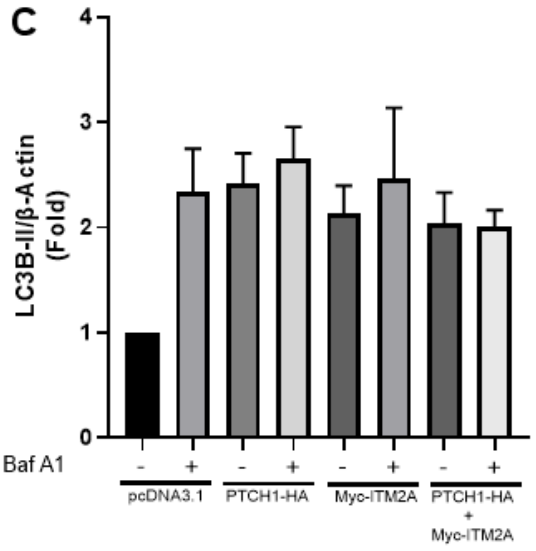

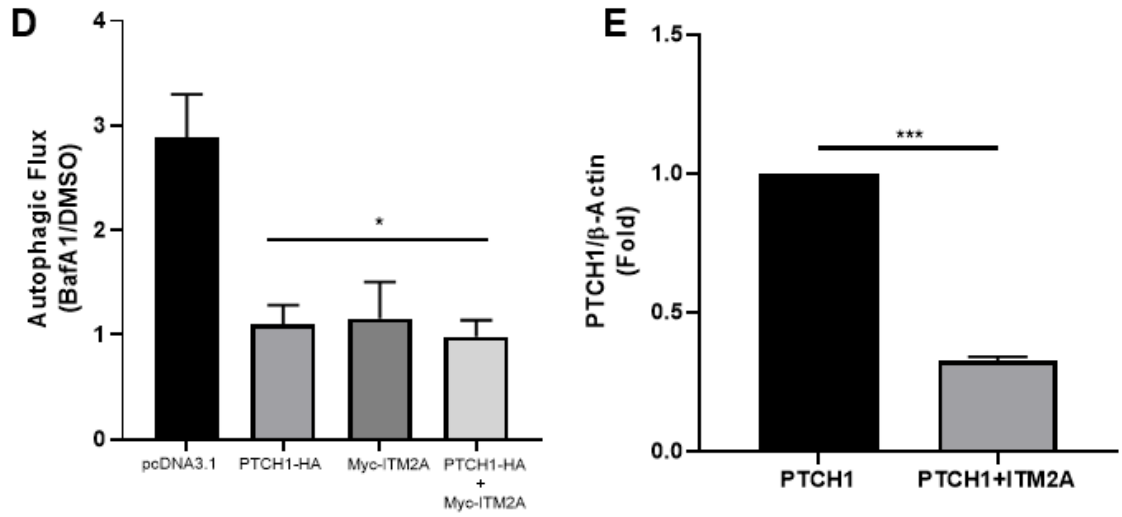

Figure 5.4 . Overexpression of ITM2A does not enhance the autophagic flux block induced by PTCH1

A. Expression levels of p62 and LC3B-II in HEK293 cells transfected with pcDNA3.1, PTCH1-HA, Myc-ITM2A or both and cultured 24 hours in complete growth medium with or without the addition of 100nM Bafilomycin (BafA1) during the last 4 hours. Representative experiment of n=3. **B.** Densitometric quantification of p62 western blot signals normalized to β-actin in comparison to pcDNA3.1 (n=3). **C.** Densitometric quantification of LC3B-II western blot signals normalized to β-Actin in comparison to pcDNA3.1 (n=3). **D.** Calculated values of autophagic flux using mean changes in LC3B-II levels normalised to β-Actin with BafA1 over its level with vehicle (DMSO) for each condition (n=3). **E.** Densitometric quantification of PTCH1-HA western blot signals normalized to β-Actin in comparison to pcDNA3.1 (n=3; * $P < 0.05$, *** $P < 0.001$).

5.3.4 Generation of stable HEK293 and HeLa cell lines with ITM2A knockdown

As a complementary approach to ITM2A overexpression, and to completely understand if the autophagic flux blockade exerted by PTCH1 was mediated through its interaction with ITM2A, it was decided to deplete the cells of endogenous *ITM2A*. First, the mRNA endogenous levels of *ITM2A* in HEK293 and HeLa cells were analysed by qPCR **(Figure 5.5)** because there were no commercial antibodies that can detect the low endogenous expression levels of ITM2A by western blot.

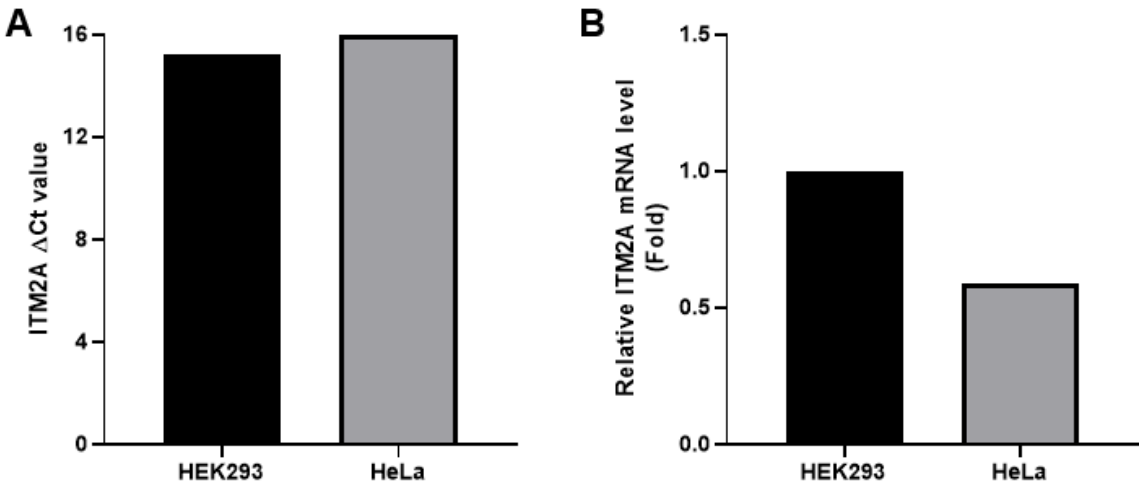

Figure 5.5 Endogenous levels of *ITM2A* in HEK293 and HeLa cells

A. ΔCt values of *ITM2A* in HEK293 cells and HeLa cells, normalised to *GAPDH* (duplicate). **B.** mRNA expression levels of *ITM2A* in HeLa cells relative to HEK293. mRNA levels were normalised to *GAPDH* (duplicate).

The first approach to deplete endogenous levels of *ITM2A* involved transient silencing using siRNAs. For this, HEK293 and HeLa cells were transiently transfected with ITM2A siRNA or control MISSION siRNA to silence the expression of *ITM2A*. Transfection conditions were optimised to achieve the highest *ITM2A* knockdown maintained during 72 hours after transfection. The evaluation of the knockdown efficiency was carried out by RT-qPCR. However, the knockdown efficiency varied significantly among biological repeats. In HEK293 cells, the knockdown efficiency ranged between 0% and 66% **(Figure 5.6A)**. The silencing of *ITM2A* in HeLa cells was more efficient, although similarly variable, with knockdown efficiency between 38% and 97% **(Figure 5.6B).**

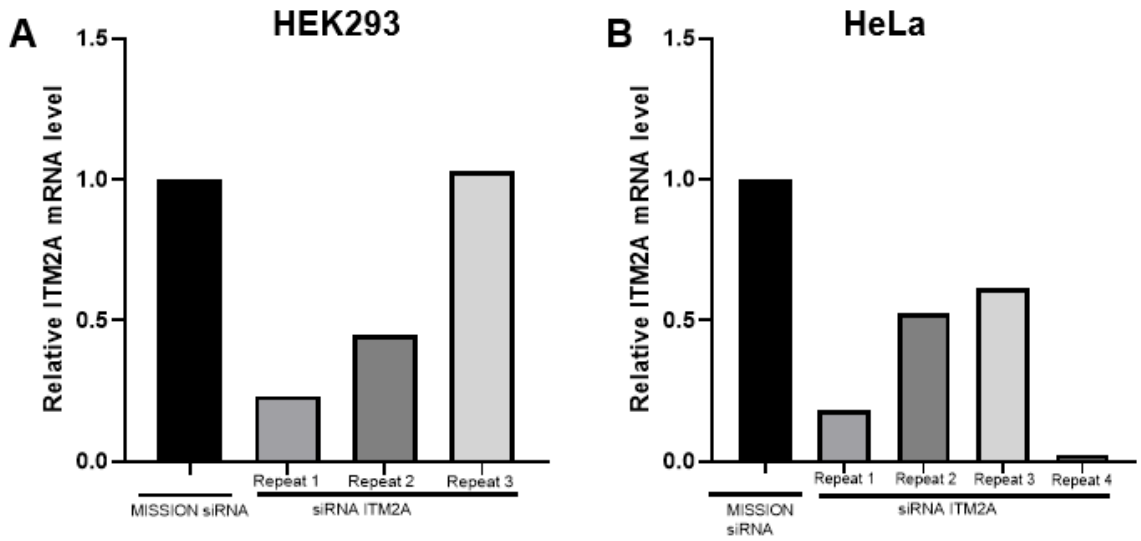

Figure 5.6 *ITM2A* gene transcription after siRNA silencing

A. mRNA expression levels of *ITM2A* in HEK293 cells relative to control MISSION siRNA. mRNA levels were normalised to *GAPDH*. **B.** mRNA expression levels of *ITM2A* in HeLa cells relative to control MISSION siRNA. mRNA levels were normalised to *GAPDH*.

To analyse if ITM2A mediates the autophagic flux blockade regulated by PTCH1, HEK293 cells and HeLa cells with knockdown of endogenous *ITM2A* for 48 hours, were transfected with PTCH1 and empty vector. After 24 hours of transfection with PTCH1 and a total of 72 hours of *ITM2A* knockdown, cells were treated with BafA1 to block autophagy followed by western blotting for PTCH1-HA and autophagy markers LC3B-II and p62 for HEK293 **(Figure 5.7A)** and HeLa **(Figure 5.8A)**. Densitometric analysis of autophagy markers p62 **(Figure 5.7B)** and LC3B-II **(Figure 5.7C)** in HEK293, and for p62 **(Figure 5.8B)** and LC3B-II **(Figure 5.8C)** in HeLa were not conclusive as the biological repeats were highly variable. This could be attributed to the different knockdown efficiency obtained each time the siRNA ITM2A was transfected. However they suggest that *ITM2A* silencing does not affect the autophagic flux blockade exerted by PTCH1. Interestingly, there was a notable increase in the expression of PTCH1 in cells with silenced *ITM2A*, for both HEK293 cells **(Figure 5.9A)** and HeLa cells **(Figure 5.9B)**. The increase in the expression was more marked in HeLa cells, which presented a higher knockdown efficiency when compared to HEK293 cells. These results agree with the observations of the co-expression experiments, further suggesting that even endogenous *ITM2A* could be affecting PTCH1 stability and therefore its ability to block autophagy.

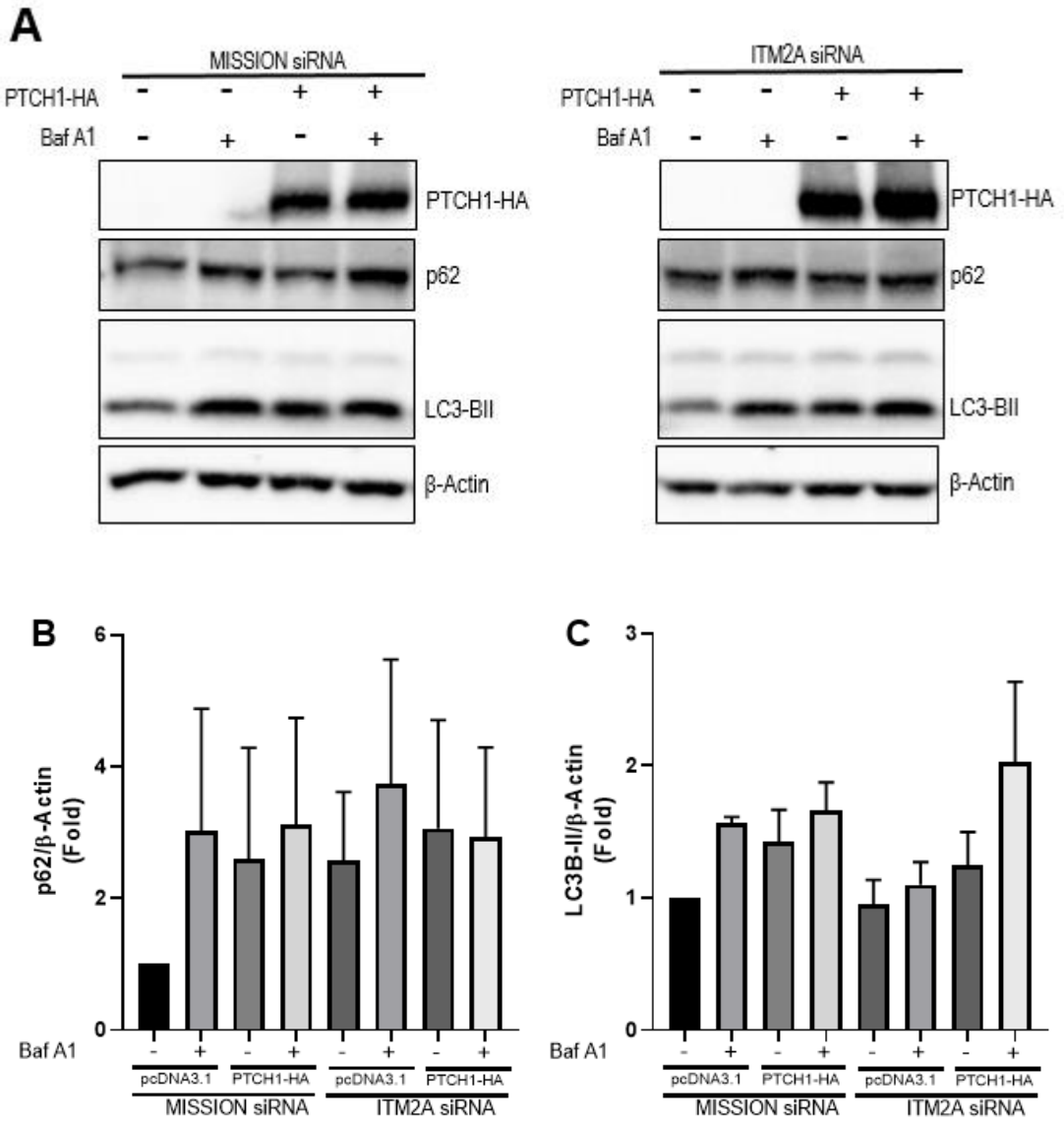

Figure 5.7 Transient *ITM2A* silencing does not change the autophagy phenotype exerted by PTCH1 in HEK293 cells

A. Expression levels of PTCH1-HA, p62 and LC3B-II in HEK293 cells with silenced ITM2A expression and transfected with pcDNA3.1 or PTCH1-HA and cultured 24 hours in complete growth medium with or without the addition of 100 nM Bafilomycin (BafA1) during the last 4 hours. Representative experiment of n=2. **B.** Densitometric quantification of p62 western blot signals normalized to β-Actin in comparison to pcDNA3.1 (n=2). **C.** Densitometric quantification of LC3B-II western blot signals normalized to β-Actin in comparison to pcDNA3.1 (n=2).

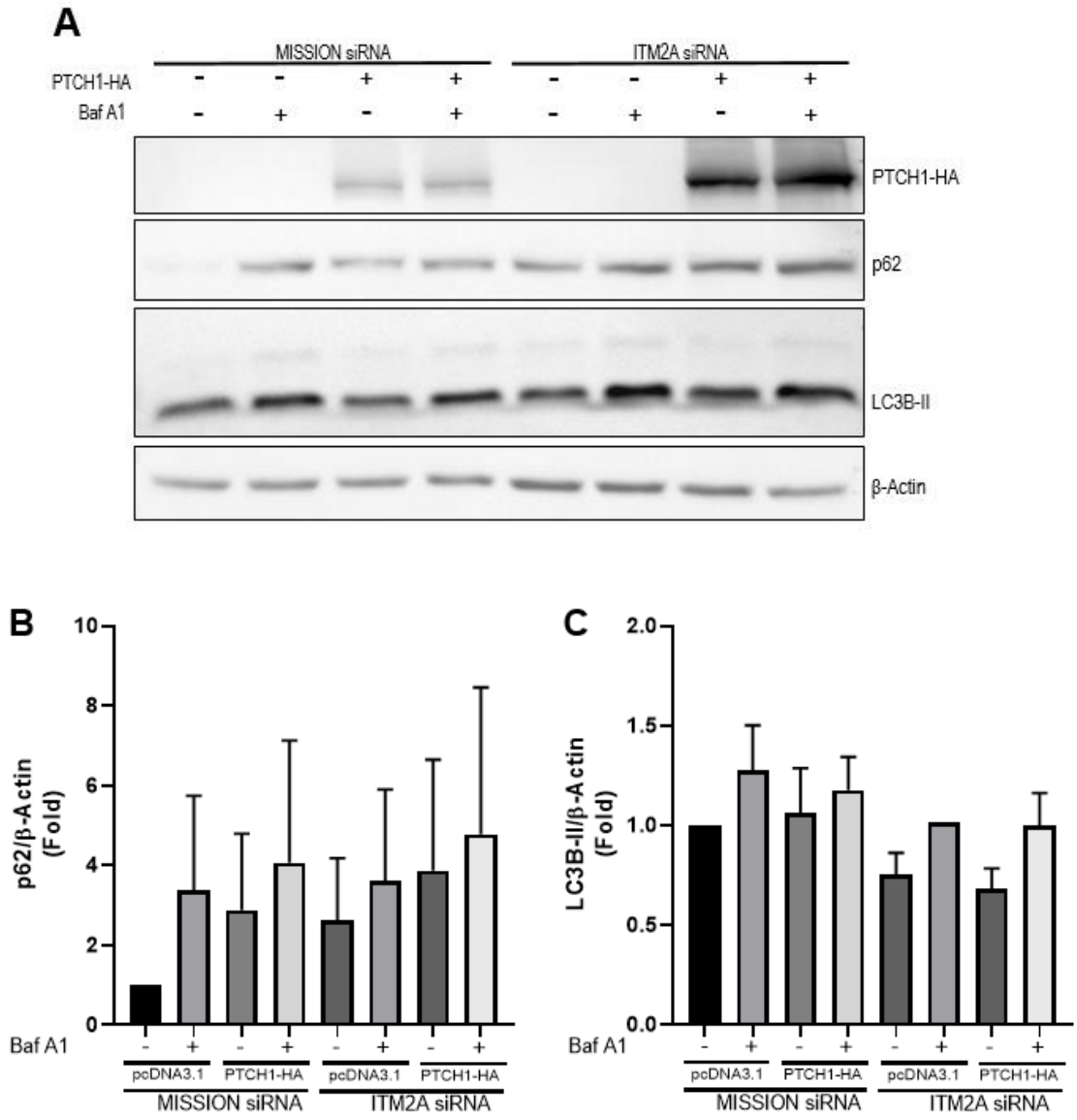

Figure 5.8 Transient *ITM2A* silencing does not change the autophagy phenotype exerted by PTCH1 in HeLa cells

A. Expression levels of PTCH1-HA, p62 and LC3B-II in HeLa cells with silenced ITM2A expression and transfected with pcDNA3.1 or PTCH1-HA and cultured 24 hours in complete growth medium with or without the addition of 100 nM Bafilomycin (BafA1) during the last 4 hours. Representative experiment of n=2. **B.** Densitometric quantification of p62 western blot signals normalized to β-Actin in comparison to pcDNA3.1 (n=2). **C.** Densitometric quantification of LC3B-II western blot signals normalized to β-Actin in comparison to pcDNA3.1 (n=2).

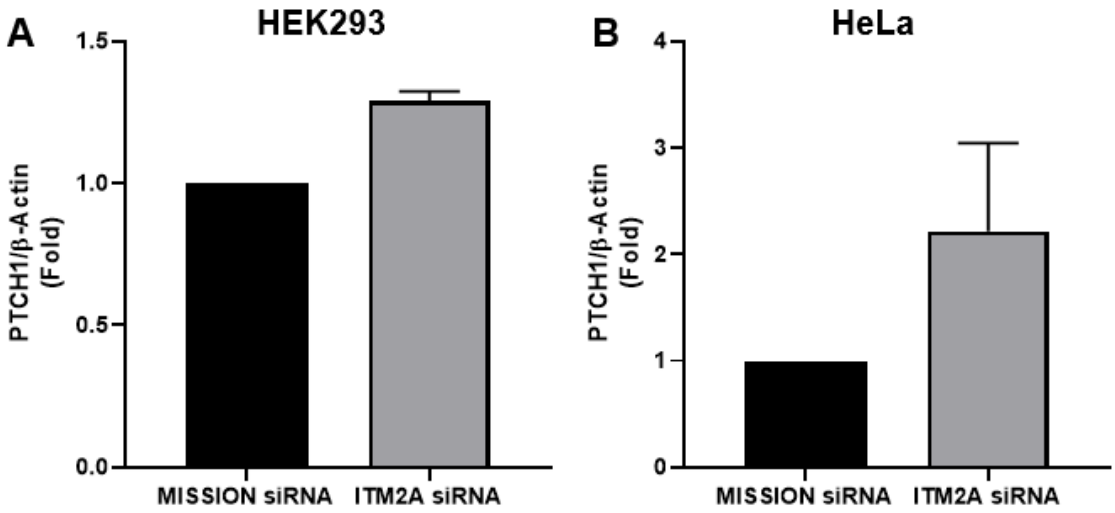

Figure 5.9 Transient *ITM2A* silencing increases the expression of PTCH1 in HEK293 and HeLa cells

HEK293 and HeLa cells with silenced *ITM2A* expression and transfected with pcDNA3.1 or PTCH1-HA and cultured 24 hours in complete growth medium with or without the addition of 100 nM Bafilomycin (BafA1) during the last 4 hours. **A.** Densitometric quantification of PTCH1-HA western blot signals of HEK293 in figure 4.7A normalized to β-Actin in comparison to control (n=2). **B.** Densitometric quantification of PTCH1-HA western blot signals of HeLa in figure 4.8A normalized to β-Actin in comparison to control (n=2).

Considering the unexpected but significant results of the effect of ITM2A on the protein level of PTCH1, and because of the lack of consistent knockdown efficiency, it was decided to generate a stable cell line with shRNA technology. HEK293 and HeLa cells were transfected with a mix of 3 shITM2A duplexes and selected with puromycin, however, as seen in the siRNA knockdowns, the *ITM2A* expression was restored after several passages (data not shown). This might be because as a heterogeneous population, cells expressing higher levels of *ITM2A* had a growth advantage and their proportion increased during passaging. Considering this, it was decided to generate stable single cell derived clones

containing shITM2A. HEK293 and HeLa cells were transfected with shITM2A, selected with puromycin and seeded using the limiting dilution method to obtain multiple clones with different knockdown percentages. However, the silencing was lost after cell passaging (data not shown). Therefore the next approach was to generate stable knockdown cells using lentiviral transduced shRNA ITM2A to successfully integrate the shRNA into the genomic DNA. First, each one of the three shRNAs found in the commercial human shRNA ITM2A was identified by Sanger sequencing and labelled shITM2A-A, shITM2A-B and shITM2A-C. HEK293T cells were transfected with each shITM2A to generate lentiviral particles. Media containing viral particles was used to infect HEK293 and HeLa cells and selected with puromycin to generate a stable cell line for each shITM2A sequence. Samples for different and consecutive passages were collected and the knockdown efficiency was measured by RT-qPCR. The shITM2A with the highest knockdown percentage maintained for at least three passages was identified for each cell line **(Figure 5.10)**. For HEK293 it was the shITM2A-C with a minimum of 65% of knockdown efficiency. For HeLa, it was the shITM2A-B, with a minimum of 75% of knockdown efficiency.

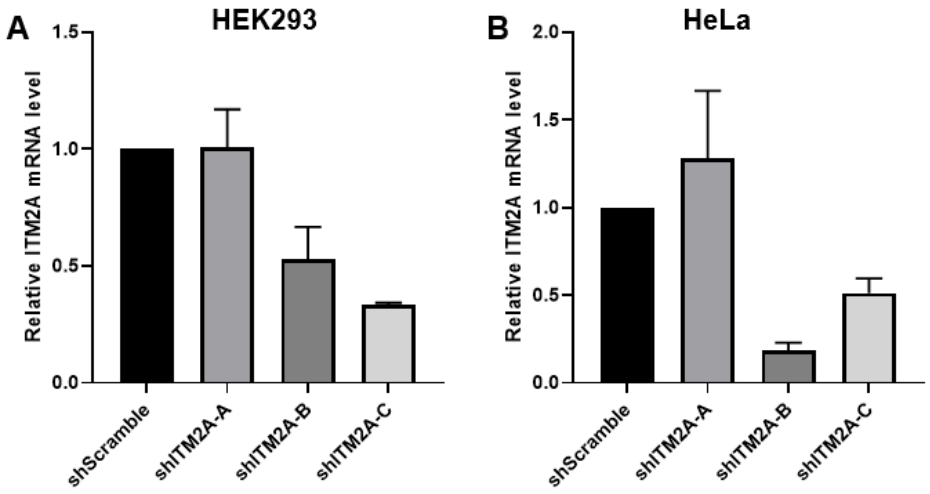

Figure 5.10 . ITM2A gene transcription after shRNA silencing

A. mRNA expression levels of ITM2A in HEK293 cells relative to shScramble. mRNA levels were normalised to GAPDH (n=3). **B.** mRNA expression levels of ITM2A in HeLa cells relative to shScramble. mRNA levels were normalised to GAPDH (n=3).

5.3.5 ITM2A knockdown does not prevent the autophagic flux blockade phenotype induced by PTCH1

Once the *ITM2A* knockdown stable cell lines were confirmed, they were used to study if ITM2A is a necessary mediator of the autophagic flux blockade regulated by PTCH1. HEK293 shITM2A-C and HeLa shITM2A-B were found to present and maintain the highest knockdown efficiency. These cells were transfected with Myc-PTCH1 or empty vector. After 24 hours, cells were treated with BafA1 to block autophagy followed by western blotting of Myc-PTCH1 and autophagy markers LC3B-II and p62.

In HEK293 cells, the *ITM2A* knockdown did not impair the autophagic flux blockade regulated by PTCH1. Western blotting results of autophagy markers

show that the blocking effect of PTCH1 in cells with silenced *ITM2A* expression is similar to the blocking effect of PTCH1 in scramble control **(Figure 5.11A-C)**. Interestingly *ITM2A* silencing generated a slight increase in PTCH1 expression, however this increase was not statistically significant **(Figure 5.11D)**.

In HeLa cells, that have a higher knockdown efficiency, the effect of the knockdown on the autophagic flux blockade exerted by PTCH1 is more pronounced than in HEK293 cells. HeLa cells with silenced *ITM2A* were more susceptible to the effect of PTCH1 on autophagy, and therefore they presented an increased autophagic flux blockade when compared to scramble control **(Figure 5.12A-C)**.

It is possible that the effect of PTCH1 on autophagy increased in the knockdown cells, because, as the previously described results suggest, the expression of ITM2A affects the stability of PTCH1 and could be promoting its degradation. In the cells with silenced *ITM2A*, PTCH1 has increases stability, and therefore its autophagy blocking phenotype is subsequently increased.

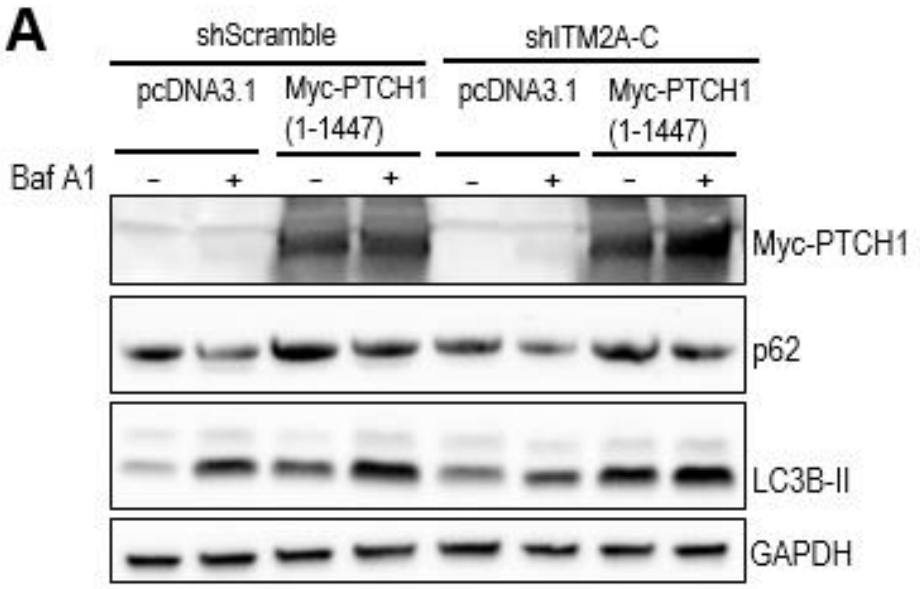

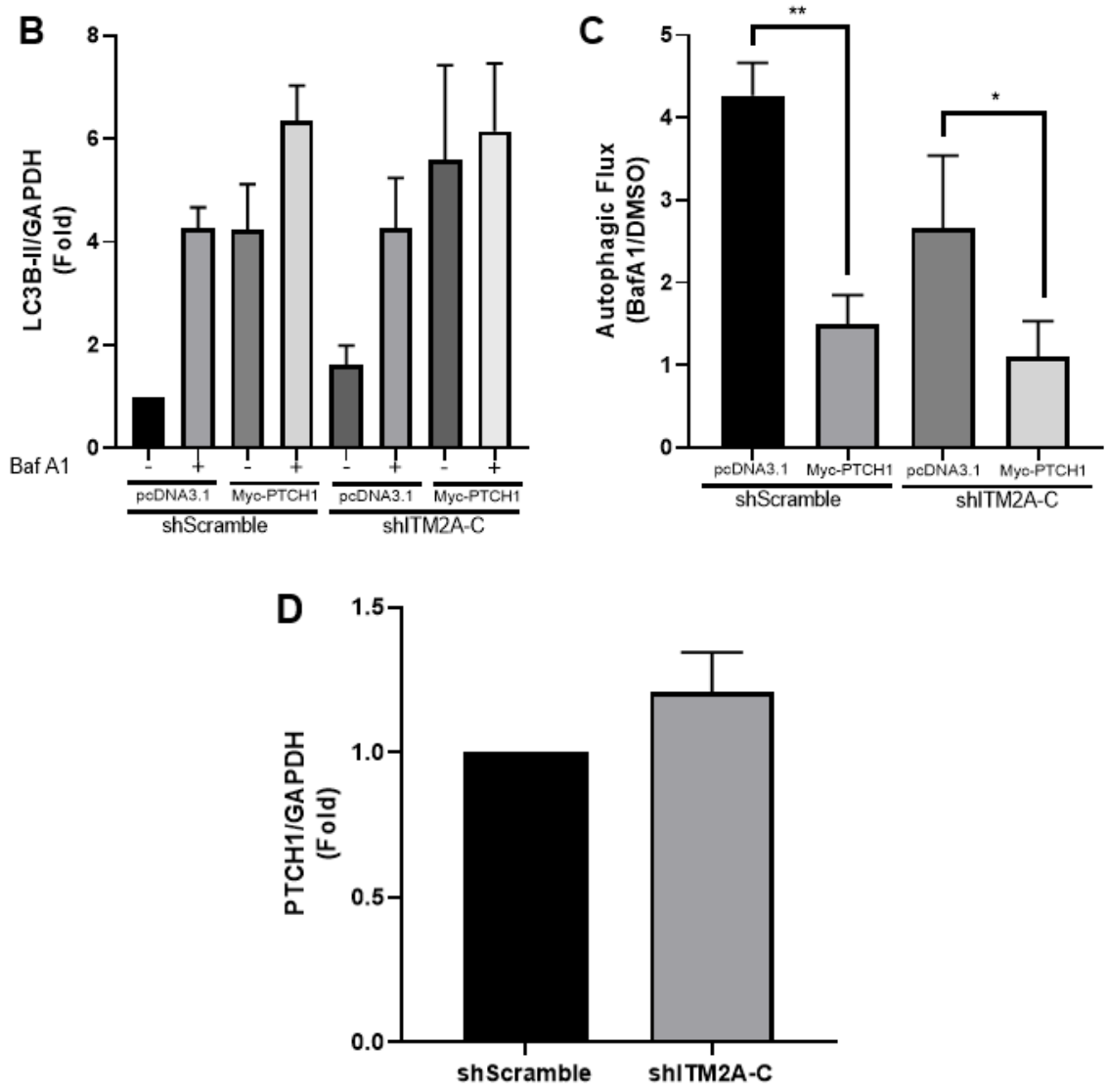

Figure 5.11 *ITM2A* knockdown does not prevent the autophagic flux blockade induced by PTCH1 in HEK293 cells

A. Expression levels LC3B-II in HEK293 shScramble and HEK293 shITM2A-C cells transfected with pcDNA3.1 or Myc-PTCH1 (1-1447), and cultured 24 hours in complete growth medium with or without the addition of 100 nM Bafilomycin (BafA1) during the last 4 hours. Representative experiment of n=3. **B.** Densitometric quantification of LC3B-II western blot signals normalized to GAPDH in comparison to pcDNA3.1 (n=3). **C.** Calculated values of autophagic flux using mean changes in LC3B-II levels normalised to GAPDH with BafA1 over its level with vehicle (DMSO) for each condition (n=3; * $P < 0.1$, ** $P < 0.05$)

D. Densitometric quantification of Myc-PTCH1 western blot signals normalized to GAPDH in comparison to pcDNA3.1 (n = 3).

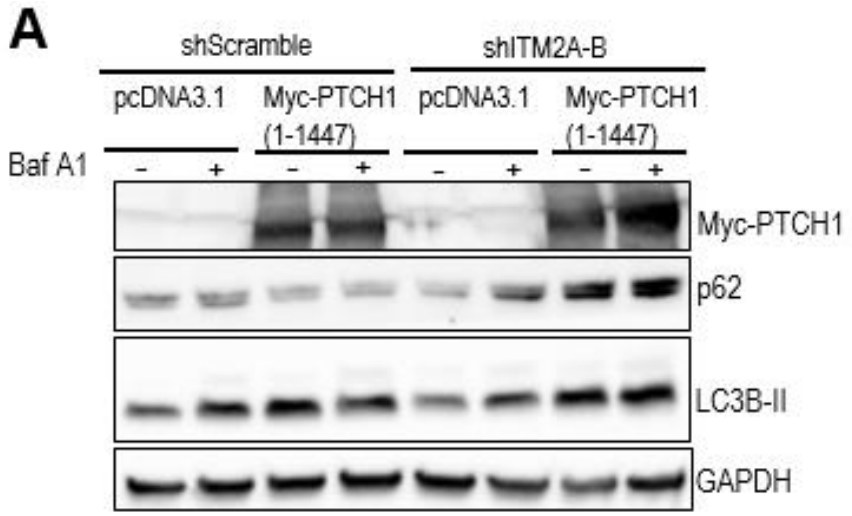
A
shScramble
shITM2A-B
pcDNA3.1
Myc-PTCH1 (1-1447)
pcDNA3.1
Myc-PTCH1 (1-1447)
Baf A1
- + - + - + - +
Myc-PTCH1
p62
LC3B-II
GAPDH

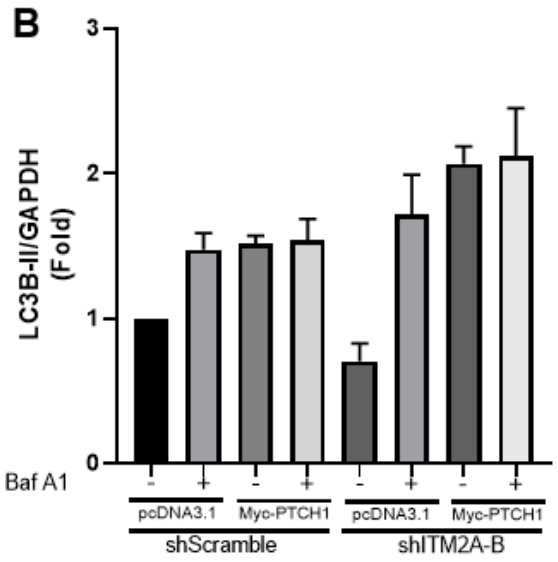
B
LC3B-II/GAPDH (Fold)
0
1
2
3
Baf A1
- + - + - + - +
pcDNA3.1
Myc-PTCH1
pcDNA3.1
Myc-PTCH1
shScramble
shITM2A-B

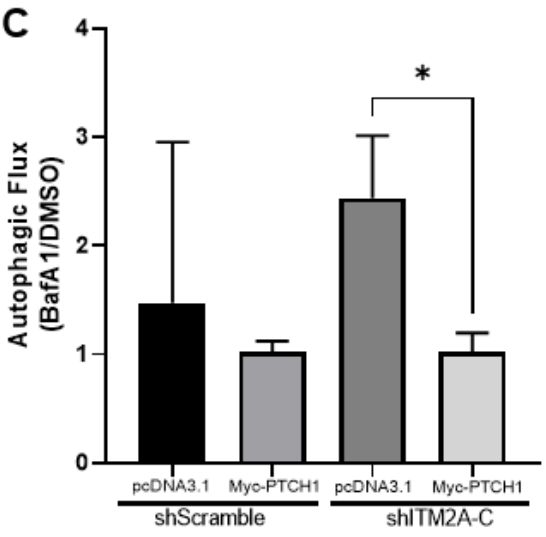
C
Autophagic Flux (BafA1/DMSO)
0
1
2
3
4
*
pcDNA3.1
Myc-PTCH1
pcDNA3.1
Myc-PTCH1
shScramble
shITM2A-C

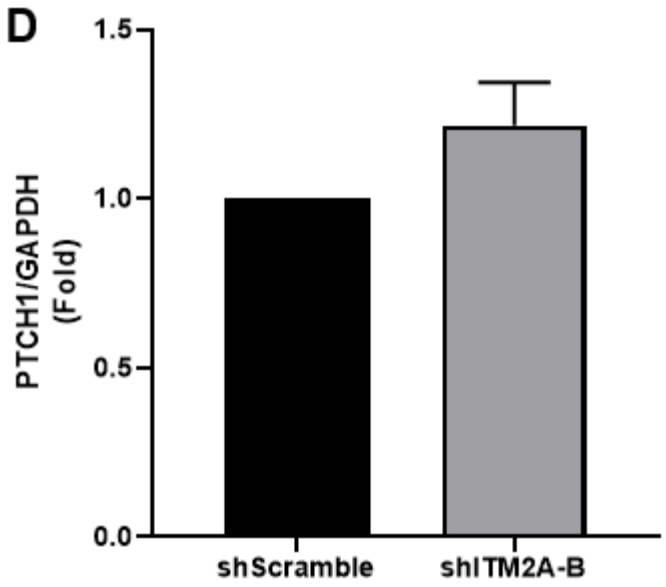

Figure 5.12 *ITM2A* knockdown does not prevent the autophagic flux blockade induced by PTCH1 in HeLa cells

A. Expression levels LC3B-II in HeLa shScramble and HeLa shITM2A-B cells transfected with pcDNA3.1 or Myc-PTCH1 (1-1447), and cultured 24 hours in complete growth medium with or without the addition of 100 nM Bafilomycin (BafA1) during the last 4 hours. Representative experiment of n=3. **B.** Densitometric quantification of LC3B-II western blot signals normalized to GAPDH in comparison to pcDNA3.1 (n=3). **C.** Calculated values of autophagic flux using mean changes in LC3B-II levels normalised to GAPDH with BafA1 over its level with vehicle (DMSO) for each condition (n=3; *P<0.05). **D.** Densitometric quantification of Myc-PTCH1 western blot signals normalized to GAPDH in comparison to pcDNA3.1 (n=3).

Notably, *ITM2A*-depleted HeLa cells displayed an increased basal autophagic flux, that could be the result of the *ITM2A* silencing as ITM2A blocks autophagy. The expression of PTCH1 is slightly higher in *ITM2A* knockdown cells, although not statistically significant **(Figure 5.12D)**.

Finally, to confirm that the phenotype observed is generated by the silencing of *ITM2A* and not due to an off-target effect of the shRNA, it was decided to use the shITM2A with the second highest knockdown efficiency for both cell lines. For HEK293, shITM2A-B produced a knockdown efficiency of at least 21%. For HeLa, shITM2A-C generated a knockdown efficiency of at least 35%.

The selected cells were transfected with Myc-PTCH1 or empty vector. After 24 hours, cells were treated with BafA1 to block autophagy followed by western blotting of Myc-PTCH1 and autophagy markers LC3B-II and p62. On both, HEK293 and Hela cells, the results suggest the same phenotype as the one observed with the shITM2A that gave the highest knockdown efficiency **(Figure 5.13A&B)**. Western blotting results for autophagy markers show a slight increase in the PTCH1 blocking effect of autophagy after *ITM2A* silencing when compared to scramble control, suggesting that the ITM2A knockdown does not impair the autophagic flux blockade regulated by PTCH1. Also, western blotting results show a slight increase in PTCH1 expression in cells with silenced ITM2A. Is important to notice that these results were obtained with a single repeat.

Taken together, these results show that ITM2A is not a mediator of the autophagic flux blockade regulated by PTCH1, in fact results suggest that the expression of ITM2A is causing the degradation of PTCH1 and in this way its expression might be causing a reduction on the autophagic flux blockade induced by PTCH1.

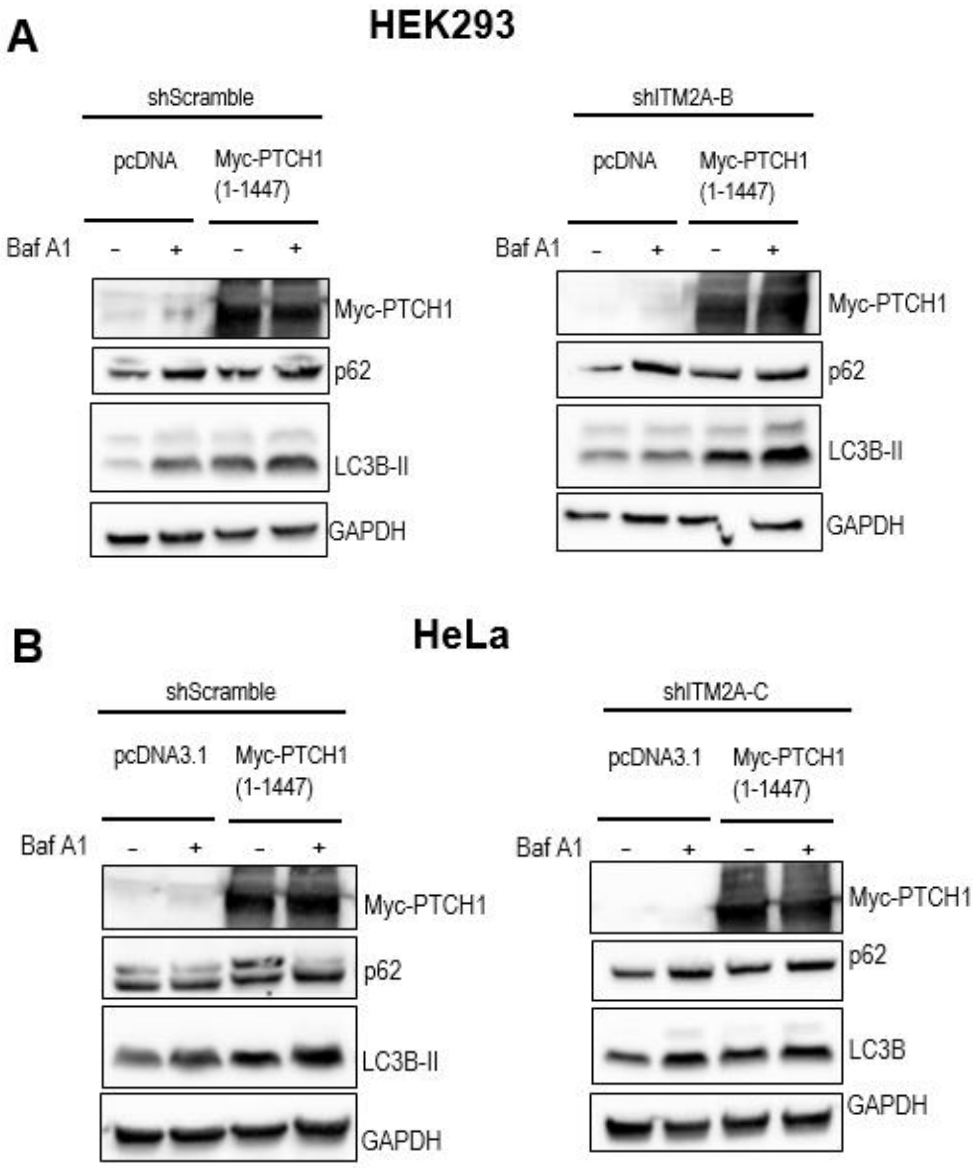

Figure 5.13 *ITM2A* knockdown does not impair the autophagic flux blockade induced by PTCH1 in HEK293 and HeLa cells

Expression levels of p62, LC3B-II and Myc-PTCH1 in **A.** HEK293 shScramble and HEK293 shITM2A-B and **B.** HeLa shScramble and HeLa shITM2A-C transfected with pcDNA3.1 or Myc-PTCH1 (1-1447), and cultured 24 hours in complete growth medium with or without the addition of 100 nM Bafilomycin (BafA1) during the last 4 hours (n=1).

We also investigated if the *ITM2A* knockdown had any effect on HEK293 and HeLa cells doubling time. For each cell line the number of cells was counted at 24, 48 and 72 hours after seeding. Stable shITM2A-expressig cells with the highest and second highest knockdown efficiency were compared to their respective scramble controls. In HEK293 cells, results show that *ITM2A* silencing does not affect the cell doubling rate when compared to control **(Figure 5.14)**. In HeLa cells, results show that ITM2A knockdown caused a statistically significant decrease in the cell doubling rate of shITM2A-B cells from ~18 hours to ~12 hours **(Figure 5.15)**. A potential reason for why the *ITM2A* silencing only affected HeLa cells, is that the knockdown efficiency in HeLa cells was higher than in the HEK293 cells. These results suggest that even low levels of *ITM2A* have a negative regulatory effect on expansion of HeLa cells, probably related to its effect as a negative regulator of the autophagic flux.

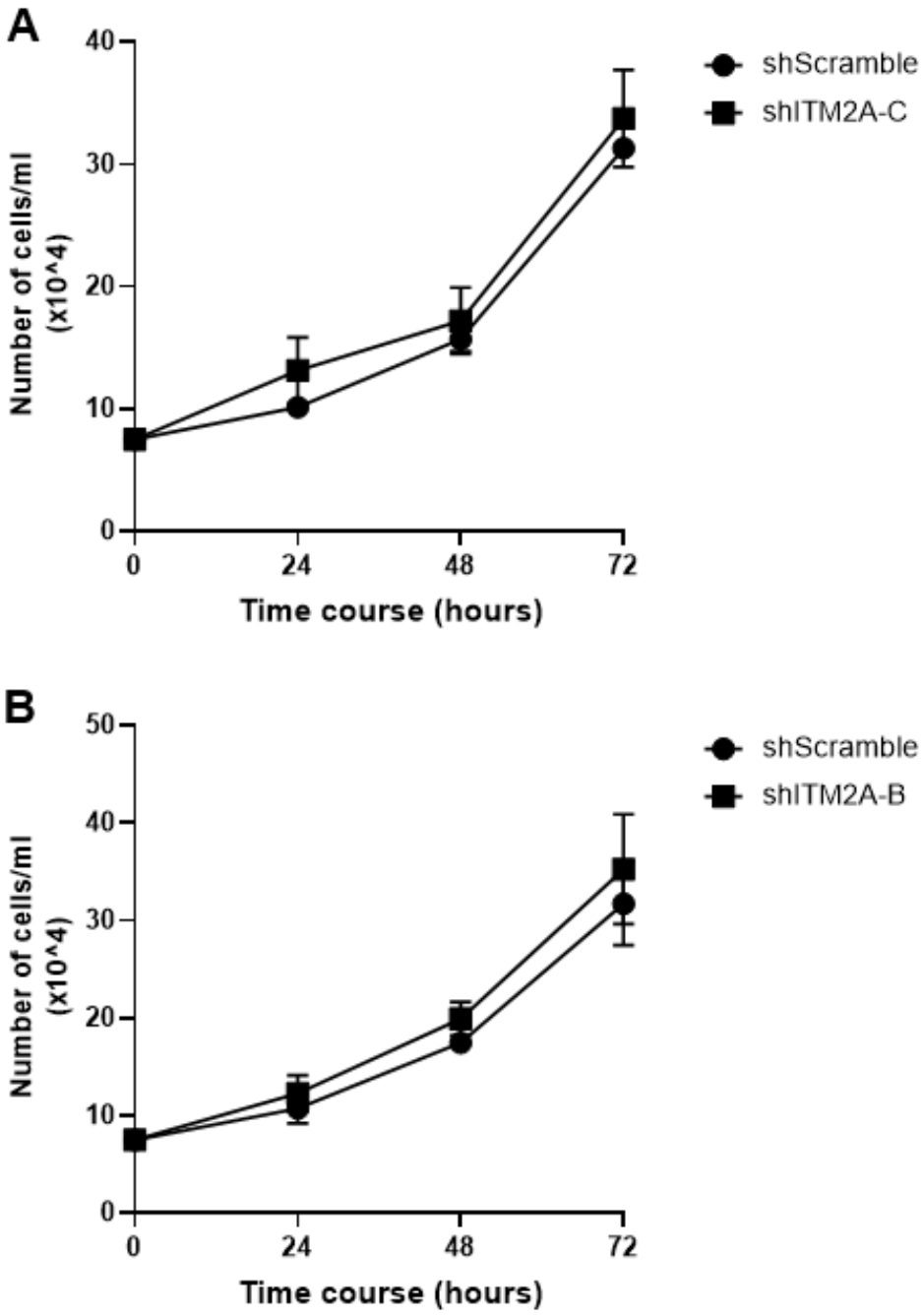

Figure 5.14 *ITM2A* partial silencing does not change the cell doubling rate of HEK293 cells

Cells were cultured in complete growth medium, trypsinised and the number of cells counted using a haemocytometer chamber at 24 hours, 48 hours and 72 hours **A.** HEK293 shScramble and HEK293 shITM2A-C (n=3). **B.** HEK293 shScramble and HEK293 shITM2A-B (n=3).

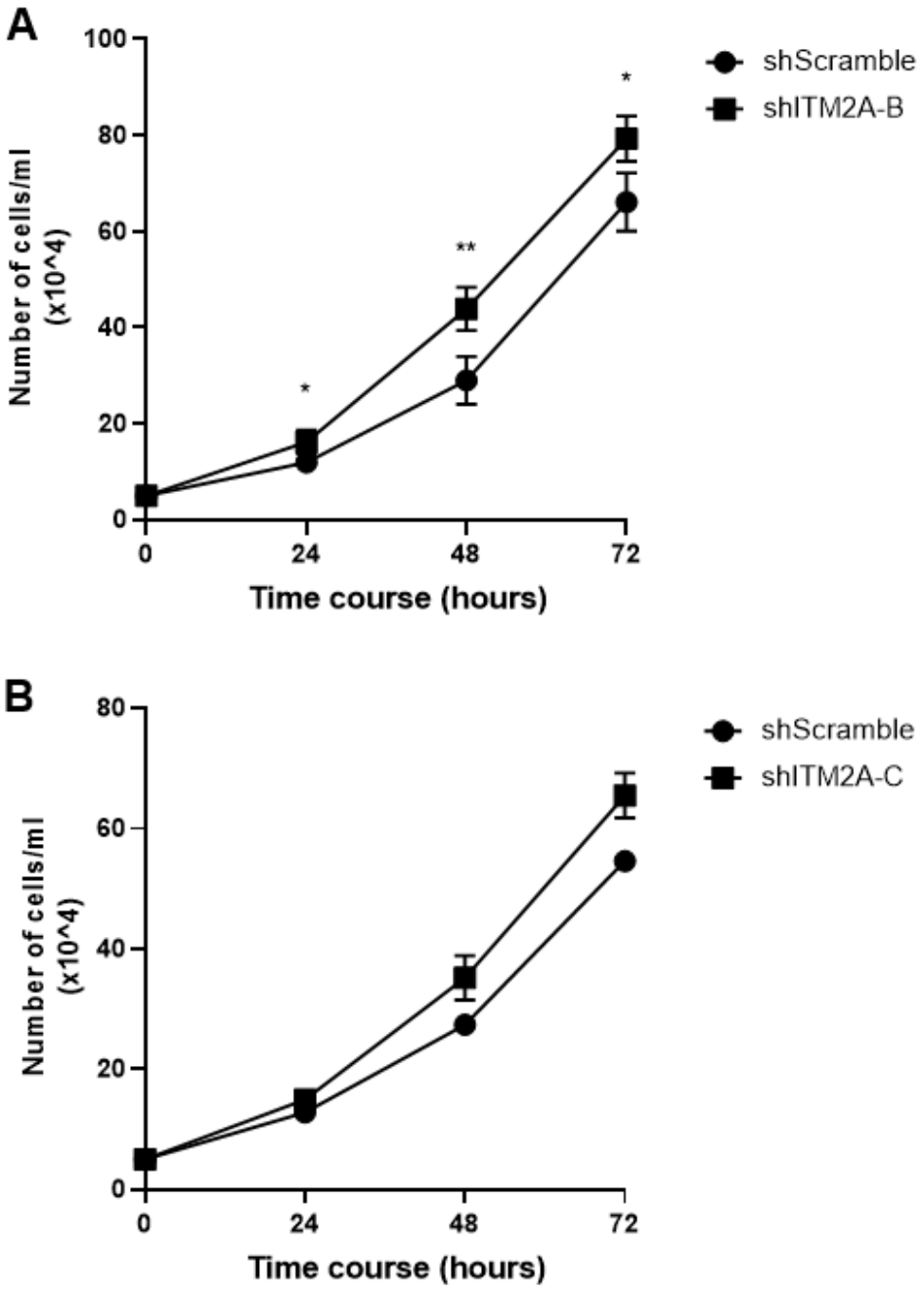

Figure 5.15 *ITM2A* partial silencing decreases the cell doubling rate of HeLa cells

Cells were cultured in complete growth medium, trypsinised and the number of cells counted using a haemocytometer chamber at 24 hours, 48 hours and 72 hours **A.** HeLa shScramble and HeLa shITM2A-B (n=3). **B.** HeLa shScramble and HeLa shITM2A-C (n=3; * $P < 0.05$, ** $P < 0.01$)

5.3.6 ITM2A inhibits the canonical Hh signalling pathway at the level of Gli1 and Gli2

PTCH1 physically interacts with ITM2A. Interestingly, this interaction was first identified through the CTD, which mediates non-canonical Hh signalling, but results in the previous chapter later demonstrated that is not restricted to that domain. The previously presented results show that ITM2A is potentially interacting with the transmembrane regions and/or with the extracellular loops of PTCH1. Given that ITM2A interacts with other regions of PTCH1 involved in SMO regulation, it was hypothesised that ITM2A could be causing an important effect in the canonical Hh signalling. This hypothesis is further supported by the observation that, in the different cell lines used the overexpression of ITM2A appears to cause a downregulation of PTCH1 levels. ITM2A could potentially be reducing PTCH1 stability and promoting its degradation, affecting in this way the overall regulation of the canonical Hh signalling pathway.

To investigate if ITM2A plays a role in canonical Hh signalling, the well-established Gli-luciferase activity assay was used. The assay was performed in NIH3T3 cells, which are the best characterised model to study canonical Hh signalling. Results show that the expression of ITM2A does not affect the activation of Gli-luciferase when the pathway was stimulated by co-expression of Shh or an oncogenic mutant SmoM2 (that is active even in the presence of PTCH1). However, a non-significant increasing trend was present, perhaps reflecting an additive effect over endogenous Ptc1 levels. In addition, ITM2A expression did not ectopically increase basal Gli-luciferase in the absence of a specific stimulus. pSV40-Renilla was used for normalisation purposes **(Figure 5.16A)**. However, when ITM2A was co-expressed with Gli1 and Gli2, it displayed

a strong inhibitory effect. Given the unexpected finding of a “distal” effect of ITM2A, a plasma membrane protein, on soluble cytosolic/nuclear Gli transcript factors, the experiment was repeated again with a different normalisation reporter. The pRL-TK construct expressing *Renilla* luciferase from the promoter, was also used instead of the pRL-SV40 construct, which expresses *Renilla* luciferase under the control of the strong SV40 promoter. Similar results were observed, confirming the validity of our findings **(Figure 5.16B)**.

An additional control was performed to determine if the inhibitory effect of ITM2A on Gli1 and Gli2 was dependent on its interaction with PTCH1. Using *Ptc1*$^{-/-}$ mouse embryonic fibroblast (MEFs) cells, which have a constitutively active canonical Hh signalling as they are deficient in Ptc1, the Gli-luciferase assay showed that ITM2A can inhibit Gli1 and Gli2 transcriptional activity in the absence of Ptc1, indicating that this effect is independent of modulation of PTCH1 levels **(Figure 5.17)**.

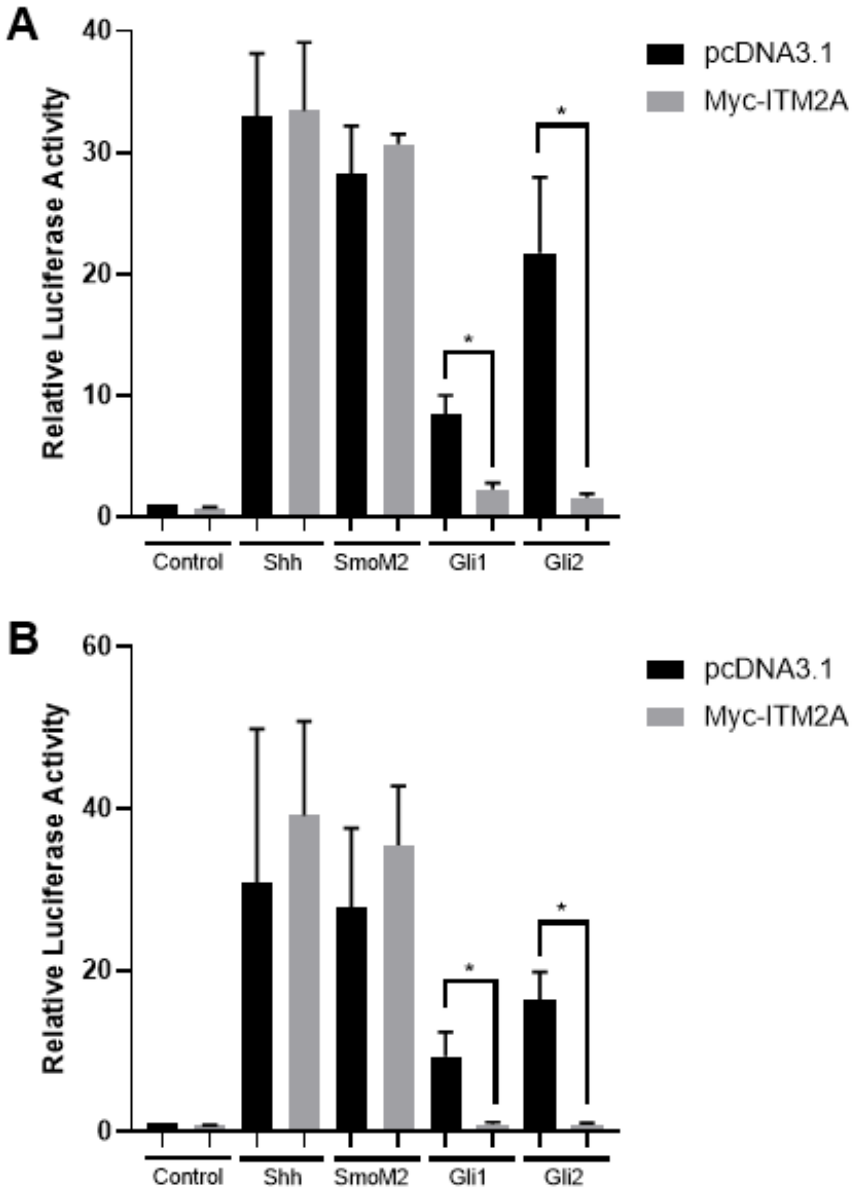

Figure 5.16 Overexpression of ITM2A inhibits Gli1 and Gli2 transcriptional activity in NIH3T3 cells

Gli-luciferase activity was measured in NIH3T3 cells co-transfected with the promoter reporter constructs **A.** pSV40 and **B.** pRL-TK and plasmids pcDNA3.1, Myc-ITM2A, Shh, SmoM2, Gli1 and Gli2 (as specified). After 24 hours, cells were changed to serum starvation media and incubated for 24 additional hours. Cells were harvested and luciferase activity was determined using the Dual-Luciferase Reporter Assay System (Promega) according to manufacturer's instructions (n=3; * $P < 0.05$).

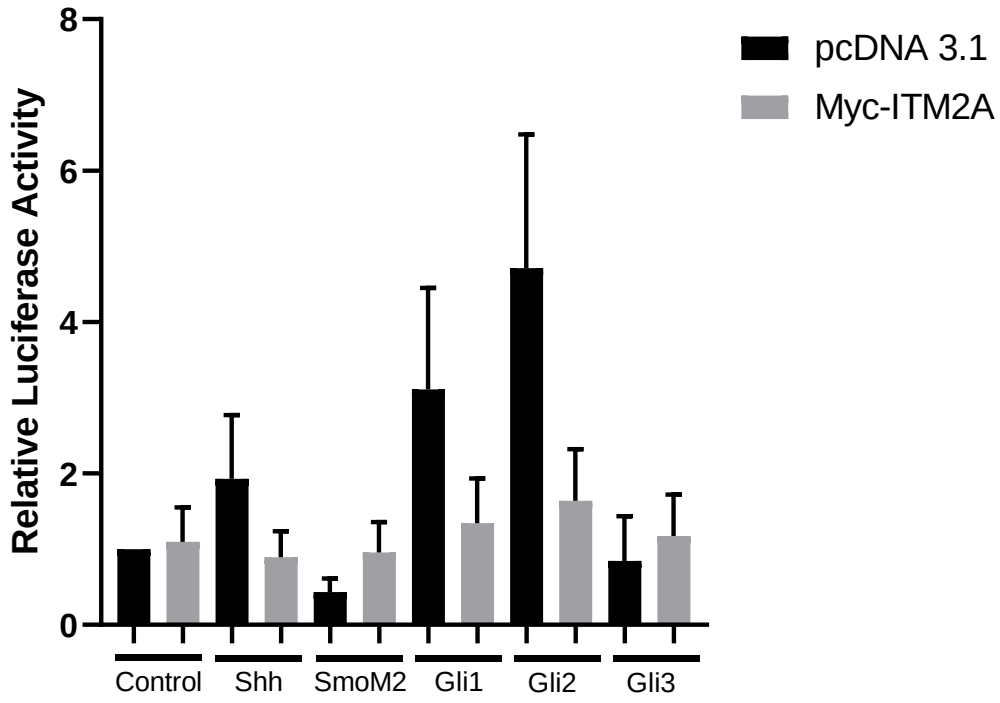

Figure 5.17 Overexpression of ITM2A inhibits Gli1 and Gli2 transcriptional activity in *Ptc1*$^{-/-}$ MEFs cells

Gli-luciferase activity was measured in Ptc1$^{-/-}$ MEFs cells co-transfected with the promoter reporter construct pRL-SV40 and plasmids pcDNA3.1, Myc-ITM2A, Shh, SmoM2, Gli1, Gli2 and Gli3 (as specified). After 24 hours, cells were changed to serum starvation media and incubated for 24 additional hours. Cells were harvested and luciferase activity was determined using the Dual-Luciferase Reporter Assay System (Promega) according to manufacturer's instructions (n=3).

5.4 Discussion

ITM2A and PTCH1 exert the same autophagy blocking phenotype characterised by an accumulation of autophagosomes (Namkoong et al., 2015; Chen et al., 2018). The results presented in this chapter show that ITM2A and PTCH1 physically interact with each other. However, their interaction is not necessary for the autophagic flux blockade induced by PTCH1 in HEK293 and HeLa cells. Results suggest that each protein, individually and through a potentially different mechanism, blocks autophagy at the last step of the process. Furthermore, our results also show that ITM2A indirectly affects the biological function of PTCH1 by reducing its stability. Therefore, ITM2A is not a mediator of the autophagic flux blockade regulated by PTCH1, but instead reduces its activity, while still maintaining its capacity to block autophagy independently of the interaction.

Our results clearly show that ITM2A has an important consequence on the expression of PTCH1. Even when the change in the expression of PTCH1 in the ITM2A knockdown cells was not statistically significant, the slight increase in PTCH1 expression was enough to enhance its inhibitory effect on autophagy. It is possible that the effects on the knockdown are not as marked as the effects of the overexpression because the endogenous levels of ITM2A in HEK293 and HeLa are low, and also because the efficiency of the knockdown was not 100%. This is supported by the observation that, when comparing the effects in the two cells lines, the results are statistically significant in HeLa cells, which presented a higher knockdown efficiency.

Of great importance as well, were the findings that ITM2A not only interacts with the CTD of PTCH1 and that the interaction with this region can only occur when the CTD is membrane bound. As ITM2A is a single pass transmembrane protein,

and we first hypothesised that the interaction occurs with the intracellular N-terminus, which is only 53 amino acids long, close proximity in the plasma membrane could be important for the interaction. Unexpectedly, our results show that ITM2A maintained the interaction with a mutant of PTCH1 without the CTD and with a double mutant without the intracellular middle loop and without the CTD, which suggest that ITM2A could also be interacting with the transmembrane regions or extracellular domains of PTCH1 through ITM2A's BRICHOS domain.

Overall, these results are of great importance as further strengthen the hypothesis that the main effect of ITM2A in the Hh signalling pathway is not as a mediator of the autophagic flux blockaded regulated by PTCH1 categorised in the Hh non-canonical signalling. Instead ITM2A involvement in the Hh signalling could be occurring through regulation of PTCH1 levels and by altering the activity and/or stability of the Gli1 and Gli2 transcriptional activators.

Chapter 6

Role of Itm2a on autophagic flux regulation during myogenic differentiation

Chapter 6
Role of Itm2a on autophagic flux regulation during myogenic differentiation

6.1 Introduction

Different studies have shown that the specific role of ITM2A varies depending on the cell type (Van den Plas and Merregaert, 2004a; Van den Plas and Merregaert, 2004b; Tai et al, 2014). Therefore, it is possible that the impact of its expression would be more relevant in cells with higher endogenous levels of Itm2a, such as skeletal muscle cells. The murine skeletal myoblast C2C12 cell line was established from myoblasts obtained 70 hours after crush injury in the thigh muscle of a 2-month-old C3H mouse (Yaffe and Saxel, 1977). The expression of Itm2a is upregulated during differentiation of C2C12 cells into myotubes. Higher expression levels of Itm2a are related to an earlier appearance of the morphological changes associated with myotube formation and to a faster achievement of terminal differentiation. However, it was reported that the expression of Itm2a does not exert any effect in myoblast proliferation rate (Van den Plas and Merregaert, 2004a; Lagha et al., 2013). The C2C12 cell line is commonly used to study myogenic differentiation as its differentiation is easily induced in a reproducible and time-dependent manner. C2C12 myoblasts proliferate in the presence of high serum (10% FBS) at low medium density and are induced to differentiate into fully mature myotubes by partially withdrawing the serum from the culture medium (2% horse serum) at high confluence (Van den Plas and Merregaert, 2004a) **(Figure 6.1)**.

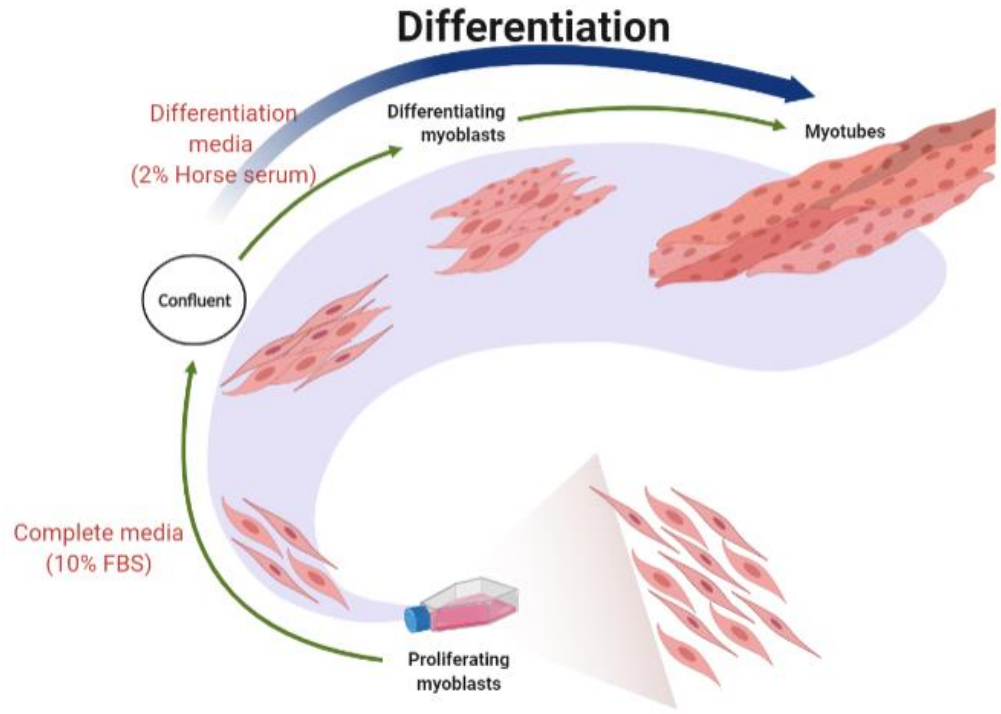

Figure 6.1 Simplified schematic representation of C2C12 myogenic differentiation

C2C12 cells are kept as proliferative myoblasts in complete media supplemented with 10% FBS. The induction of differentiation is carried out once myoblast reach confluence by switching the complete media to differentiation media containing 2% horse serum. Differentiating myoblast fuse with each other to form differentiated myotubes. Created with BioRender.com.

A recent study showed that Itm2a plays a role in the regulation of key myogenic transcription factors, as *Itm2a* knockdown caused a decrease in the expression of MyoD, myogenin and myosin light chain (MYL2) in C2C12 cells during differentiation (Lee et al., 2018). Muscle-specific transcription factors MyoD and Myf5 are expressed in proliferating myoblasts, upon induction of differentiation the expression of Myf5 is downregulated and the upregulation of myogenin is

observed after cell cycle withdrawal (Lee, 2002). Therefore, as exit of the cell cycle is required, skeletal muscle differentiation involves the interaction between myogenic factors and cell cycle regulators (Hwang et al., 2015; Lee, 2002). The progression of the cell cycle, in eukaryotes, relies in the expression (in an orderly fashion) of cyclin-dependent kinases (CDKs), cyclins and CDK inhibitors (CDKIs). CDKs are activated by cyclins and negatively regulated by CDKIs (Franklin and Xiong, 1996). D-type cyclins (D1, D2 and D3), form complexes and activate CDK4 and CDK6 in the G1 phase of the cell cycle to promote cell proliferation (Duronio and Xiong, 2013). The expression of D-type cyclins is regulated by the presence of growth factors and during proliferation they share similar functions in different cell types. However, it has been suggested that upregulation of cyclin D3 is a requisite for myogenic differentiation (Bartkova et al., 1998; Cenciarelli et al., 1999).

The C2C12 cell line is particularly relevant to this study because it has been used to study the role of Hh signalling in skeletal muscle. Shh promotes proliferation of C2C12 myoblasts, inhibiting terminal differentiation and, in this way, opposing the role of Itm2a (Koleva et al., 2005).

6.2 Aims

To study if reported changes of Itm2a expression during skeletal muscle cell differentiation regulate the autophagic flux during the process, the last part of my research was aimed at:

- Investigating the consequences of *Itm2a* knockdown on C2C12 myoblast proliferation and differentiation.
- Understanding the consequences of *Itm2a* knockdown on basal autophagy in C2C12 myoblasts.
- Exploring potential Itm2a interacting partners by mass spectrometry.

6.3 Results

6.3.1 Characterisation of Itm2a expression during C2C12 cells differentiation

Considering that the effects of Itm2a are cell-type specific and that it has been shown that during myogenic differentiation of C2C12 cells an increase in the expression levels of Itm2a is observed (Van den Plas and Merregaert, 2004a: Lee et al., 2018). It was firstly decided to establish the differentiation conditions for the C2C12 cell line. Myogenic differentiation of the C2C12 cell line was examined by their morphological changes. As expected, during the differentiation process the mononucleated and spindle-like shape myoblasts aligned, elongated and fused together to form multinucleated myotubes **(Figure 6.2A-H)**. Maximal differentiation accompanied by spontaneous contractions of myotubes was observed after 7 days of differentiation.

When C2C12 cells differentiate, myoblasts become mature myotubes by undergoing a remodelling process that is accompanied by the expression of muscle-specific proteins and proteins involved in cell fusion. Myosin heavy chain (MHC) is a structural protein highly expressed in myotubes, and therefore a specific marker for myotubes and differentiation (Hwang et al., 2015; Tang et al., 2018). C2C12 cells were induced to differentiate by serum switch, and whole cell lysates were prepared along each day of the process, from day 0 to day 7. Expression of MHC, as a marker for differentiation, was analysed by western blotting **(Figure 6.3)**. The changes in protein and mRNA expression of *Itm2a* were analysed throughout the 7 days of differentiation in C2C12 cells **(Figure 6.4A&B)**. Additionally, the changes in mRNA expression of *Ptc1* during myogenic differentiation were also analysed by qPCR **(Figure 6.5)**.

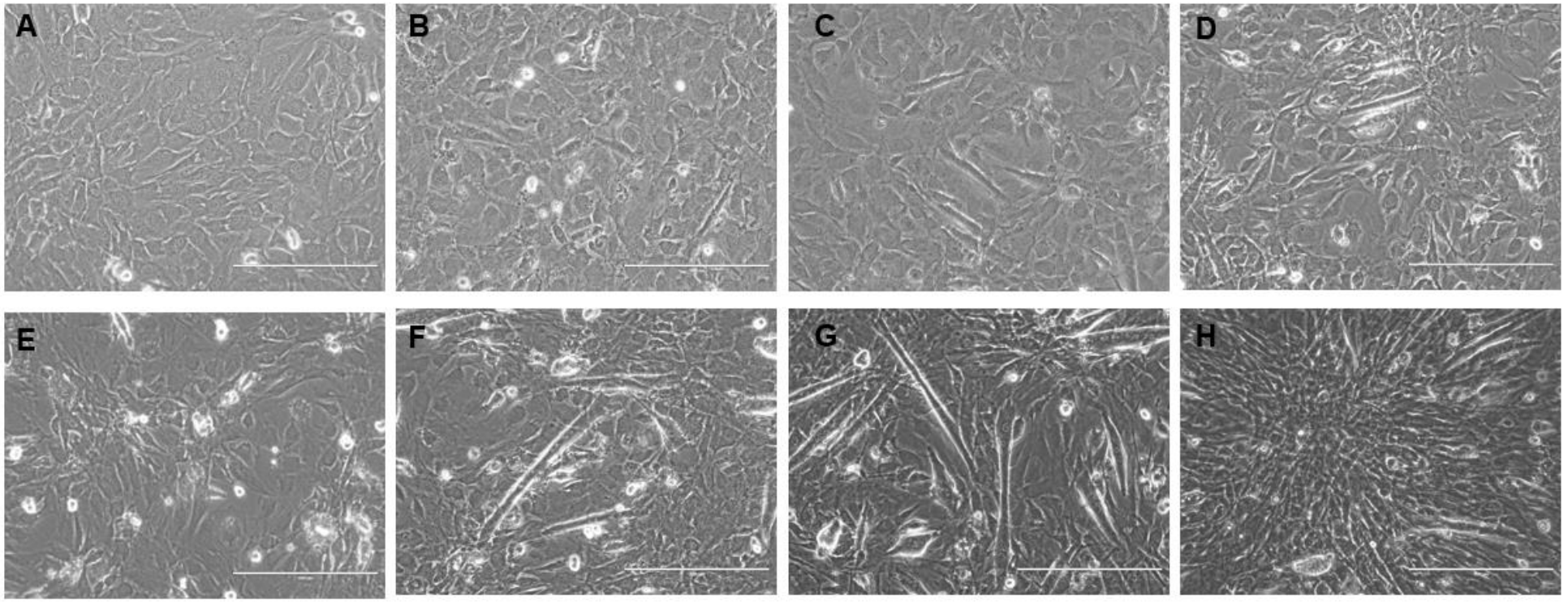

Figure 6.2 Myogenic differentiation of C2C12 cells

C2C12 were cultured in differentiation media for 7 days. Differentiation media was added to cells at day 0 and changed to fresh differentiation media every other day. **A.** Day 0. **B.** Day 1. **C.** Day 2. **D.** Day 3. **E.** Day 4. **F.** Day 5. **G.** Day 6. **H.** Day 7.

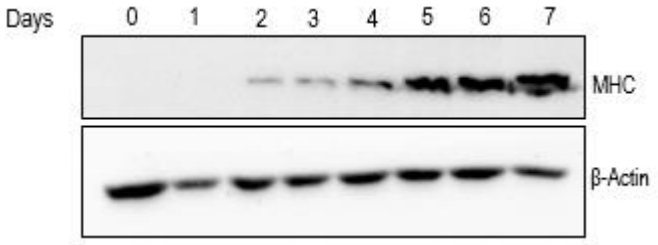

Figure 6.3 Myosin heavy chain expression is upregulated during myogenic C2C12 cells differentiation

Expression levels MHC in C2C12 cells during 7 days of differentiation. Differentiation media was added to cells at day 0 and changed to fresh differentiation media every other day. Representative experiment of n=3.

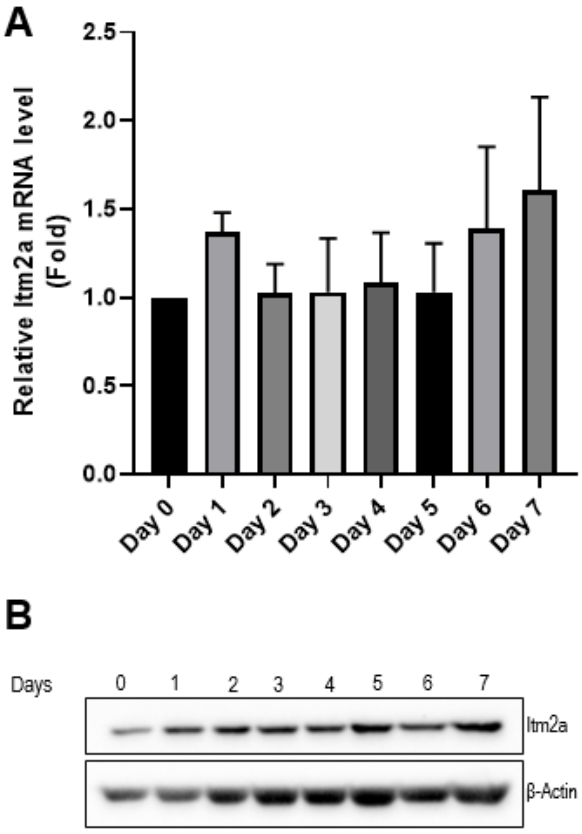

Figure 6.4 Itm2a expression during myogenic differentiation of C2C12 cells

A. mRNA expression levels of *Itm2a* in C2C12 cells during differentiation. mRNA levels were normalised to *GAPDH* (n=3). **B.** Expression levels Itm2a in C2C12 cells during 7 days of differentiation. Representative experiment of n=3. Differentiation media was added to cells at day 0 and changed to fresh differentiation media every other day.

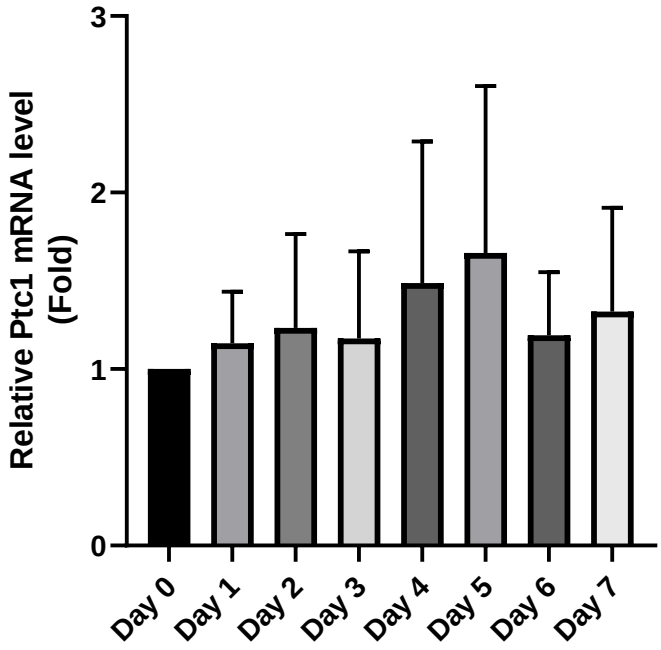

Figure 6.5 *Ptc1* expression during myogenic C2C12 cells differentiation

mRNA expression levels of *Ptc1* in C2C12 cells during differentiation. mRNA levels were normalised to *GAPDH* (n=3). Differentiation media was added to cells at day 0 and changed to fresh differentiation media every other day.

6.3.2 Generation of stable C2C12 cells with shRNA-mediated silencing of Itm2a

To investigate the role of Itm2a in the myogenic differentiation process, it was decided to generate stable itm2a-shRNA C2C12 cells by lentiviral transduction followed by selection of cells resistant to puromycin. A commercial shRNA plasmid mix targeting *itm2a* contained three plasmids with different shRNA sequences. An initial attempt showed insufficient knockdown, which prompt us to isolate and sequence each plasmid (shItm2a-A, shItm2a-B and shItm2a-C) were sequences for individual use. HEK293T cells were transfected with each single shItm2a and additional lentiviral packaging plasmids, as indicated in Materials

and Methods chapter, to generate individual lentiviral particles targeting *Itm2a*. C2C12 cells were infected with HEK293T supernatant containing the viral particles and selected with puromycin to generate a stable cell line for each shItm2a duplex. Control shRNA C2C12 cells were generated in a similar manner using control shRNA Plasmid-A (shScramble). Samples from different passages were collected to establish the knockdown efficiency by qPCR and its stability over time. None of the individual shRNAs achieved a very high knockdown efficiency. shItm2a-C displayed the highest knockdown efficiency (<40%) in undifferentiated cells maintained for at least three passages **(Figure 6.6)** and was, thus, selected for future experiments, under the assumption that we would expect to see relatively minor effects.

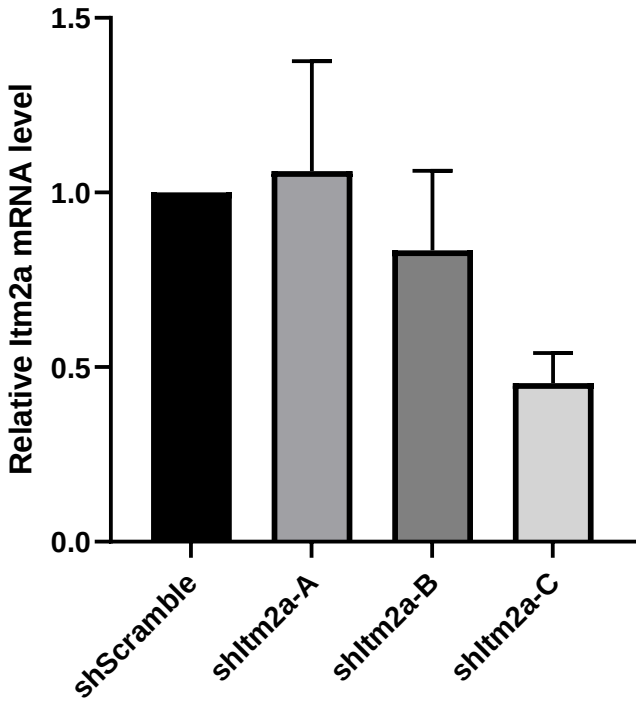

Figure 6.6 *Itm2a* gene transcription after shRNA silencing

mRNA expression levels of *Itm2a* in C2C12 cells relative to shScramble. mRNA levels were normalised to *GAPDH* (n=3).

6.3.3 Autophagy modulation during skeletal muscle differentiation

Given that ITM2A regulates autophagic flux in HEK293 and HeLa cells and it is upregulated during myogenic differentiation, it was decided to investigate changes on basal autophagic flux during C2C12 differentiation. Protein samples were collected from day 0 to day 7 of differentiation. Four hours before protein extraction, BafA1 or DMSO was added to the cells. Lysates were analysed by western blotting for relative levels of autophagy markers LC3B-II and p62 **(Figure 6.7A,C&D)**. The overall levels of p62 and LC3B-II increased during differentiation, although becoming progressively more insensitive to the activity of BafA1. Calculation of autophagy flux showed progressive inhibition of the basal autophagic flux during differentiation of C2C12 cells **(Figure 6.7E)**. This is in agreement with a potential inhibitory function of Itm2a on autophagic flux during myogenic differentiation.

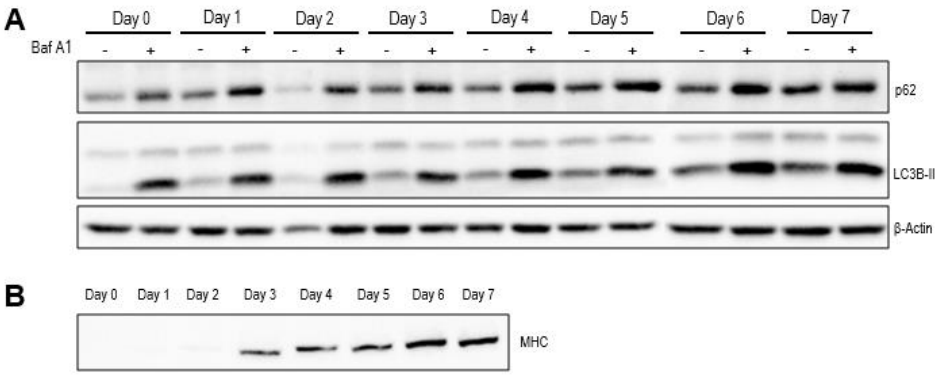

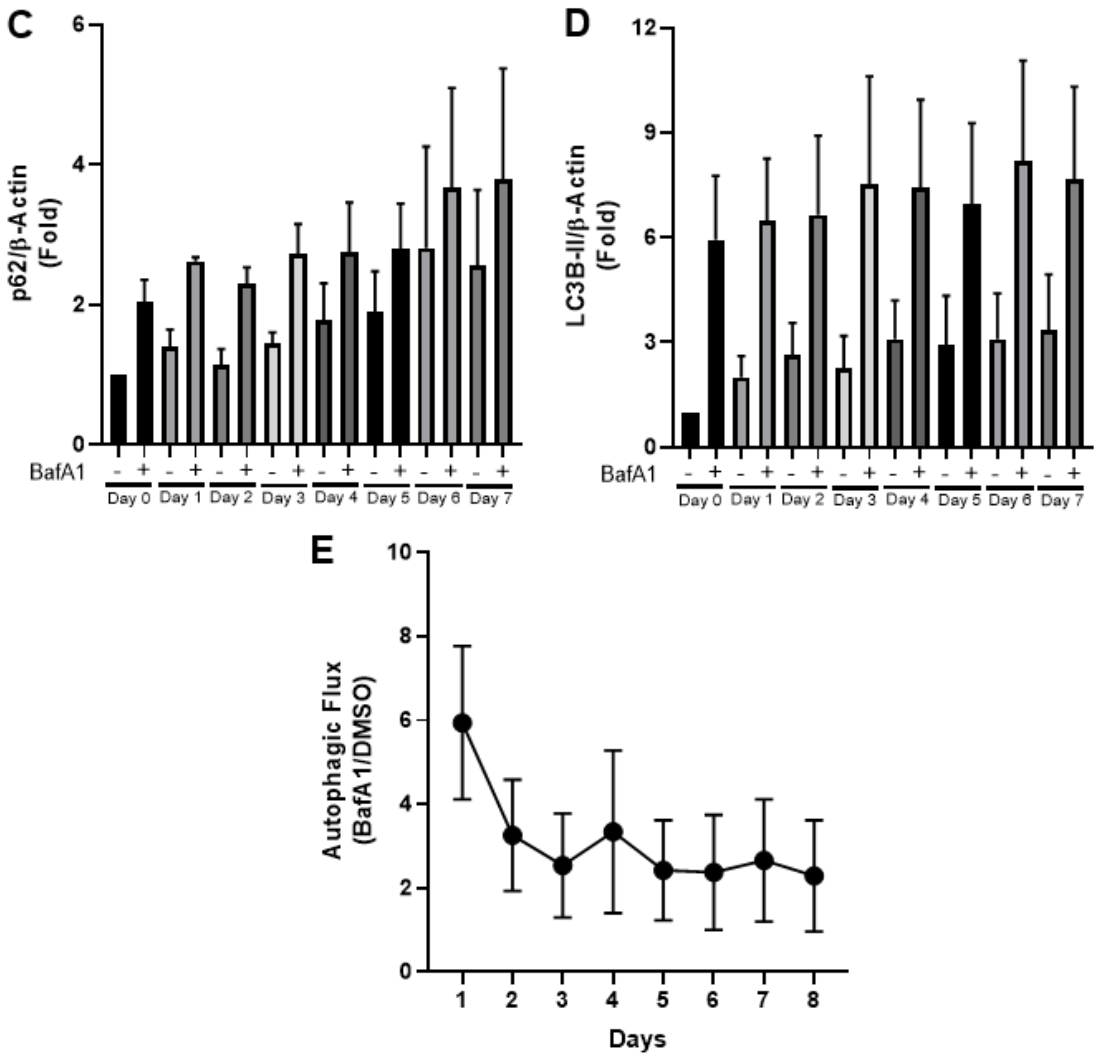

Figure 6.7 Reduction of basal autophagic flux during C2C12 cell differentiation

A. Expression levels of p62 and LC3B-II in C2C12 cells during 7 days of differentiation day with or without the addition of 100 nM Bafilomycin (BafA1) during the last 4 hours. Representative experiment of n = 3. **B.** Expression levels of myosin in C2C12 during 7 days of differentiation. Differentiation media was added to cells at day 0 and changed to fresh differentiation media every other. Representative experiment of n=3. **C.** Densitometric quantification of p62 western blot signals normalized to β-actin in comparison to pcDNA3.1 (n=3). **D.** Densitometric quantification of LC3B-II western blot signals normalized to β-actin in comparison to pcDNA3.1 (n=3).**E.** Calculated values of autophagic flux using mean changes in LC3B-II levels normalised to β-Actin with BafA1 over its level with vehicle (DMSO) for each condition (n=3).

6.3.4 Effect of PTCH1 on autophagic flux in control and *itm2a*-silenced C2C12 cells

Next, C2C12 myoblasts with partially silenced *Itm2a* expression were used to understand the ability of PTCH1 to regulate autophagic flux in undifferentiated cells. C2C12 shItm2a-C cells and C2C12 shScramble control were transfected with Myc-PTCH1 or empty vector for 24 hours and treated with BafA1 or DMSO for 4 hours before protein extraction. Western blotting of autophagy markers LC3B-II and p62 was carried out **(Figure 6.8A)**. Unexpectedly, results show that the overexpression of PTCH1 in the C2C12 shScramble myoblasts did not evoke the autophagic blockade phenotype previously described in HEK293 and HeLa cells (Chen et al., 2018). LC3B-II levels were not changed with PTCH1 overexpression **(Figure 6.8C)** while there was only a moderate accumulation of p62 after overexpression of PTCH1 **(Figure 6.8B)**. Remarkably, the silencing of Itm2a seemed to slightly restored the blocking effect of PTCH1 on autophagy **(Figure 6.8B-D)**, albeit not to the same extent as previously described for HEK293 and HeLa cells (Chen et al., 2018). The same slightly restoring of the phenotype was observed in C2C12 shItm2a-B cell line after PTCH1 overexpression **(Figure 6.8F)**. However, there were technical problems with the p62 antibody and the blot could not be obtained.

Interestingly, the expression of PTCH1 in C2C12 shItm2a-C cells was lower than in the scramble control cells although not significantly different **(Figure 6.8E)**.

These results suggest that Itm2a is negatively regulating the activity of PTCH1 in C2C12 cells or, alternatively, that the presence of high levels of Itm2a makes the effect of PTCH1 on autophagy negligible.

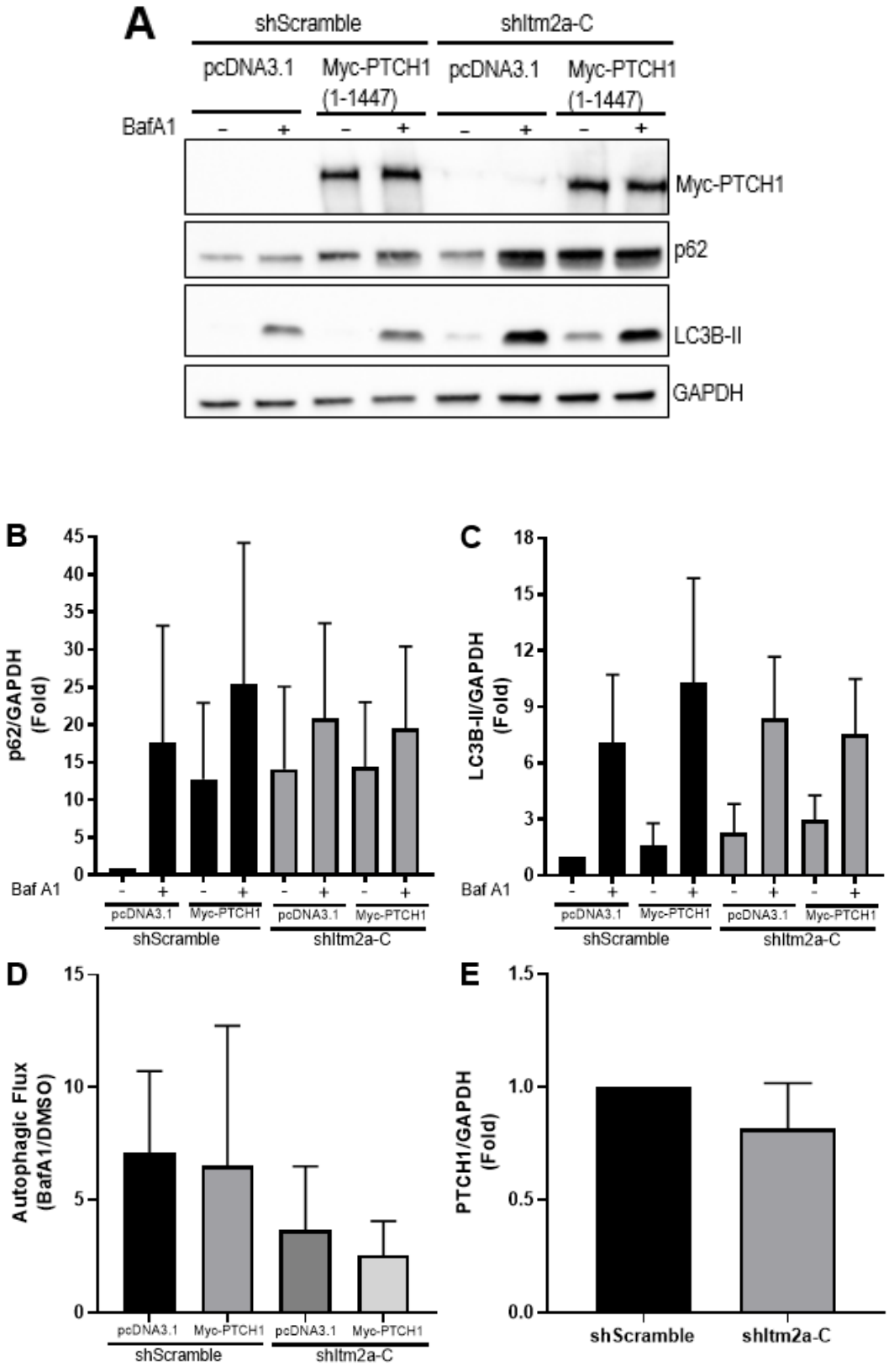
A
shScramble
shItm2a-C
pcDNA3.1
Myc-PTCH1 (1-1447)
pcDNA3.1
Myc-PTCH1 (1-1447)
BafA1
– + – + – + – +
Myc-PTCH1
p62
LC3B-II
GAPDH
B
p62/GAPDH (Fold)
Baf A1
pcDNA3.1
Myc-PTCH1
pcDNA3.1
Myc-PTCH1
shScramble
shItm2a-C
C
LC3B-II/GAPDH (Fold)
Baf A1
pcDNA3.1
Myc-PTCH1
pcDNA3.1
Myc-PTCH1
shScramble
shItm2a-C
D
Autophagic Flux (BafA1/DMSO)
pcDNA3.1
Myc-PTCH1
pcDNA3.1
Myc-PTCH1
shScramble
shItm2a-C
E
PTCH1/GAPDH (Fold)
shScramble
shItm2a-C

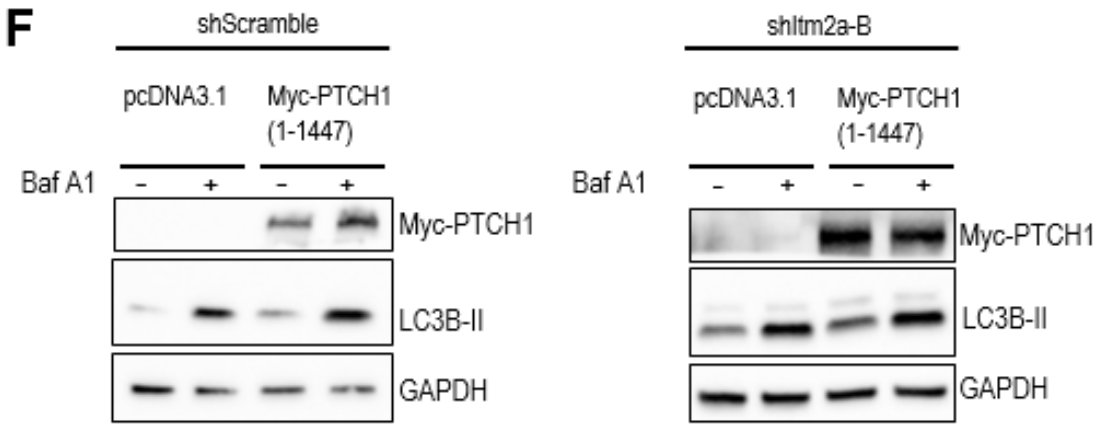

Figure 6.8 *Itm2a* silencing slightly restores the blocking effect of PTCH1 on autophagy in C2C12 myoblasts

A. Expression levels of Myc-PTCH1, p62 and LC3B-II in C2C12 shScramble and C2C12 shITM2A-C cells transfected with pcDNA3.1 or Myc-PTCH1 (1-1447), and cultured 24 hours in complete growth medium with or without the addition of 100 nM Bafilomycin (BafA1) during the last 4 hours. Representative experiment of n=3. **B.** Densitometric quantification of p62 western blot signals normalized to GAPDH in comparison to pcDNA3.1 (n=3). **C.** Densitometric quantification of LC3B-II western blot signals normalized to GAPDH in comparison to pcDNA3.1 (n=3). **D.** Calculated values of autophagic flux using mean changes in LC3B-II levels normalised to GAPDH with BafA1 over its level with vehicle (DMSO) for each condition (n=3). **E.** Densitometric quantification of Myc-PTCH1 western blot signals normalized to GAPDH in comparison to pcDNA3.1 (n=3). **F.** Expression levels of Myc-PTCH1 and LC3B-II in C2C12 shScramble and C2C12 shItm2a-B cells transfected with pcDNA3.1 or Myc-PTCH1 (1-1447), and cultured 24 hours in complete growth medium with or without the addition of 100 nM Bafilomycin (BafA1) during the last 4 hours (n=1).

6.3.5 Reduction of endogenous Itm2a levels delays the myotube differentiation process

To understand the effects of *Itm2a* knockdown in C2C12 cells, stable shItm2a-C and shScramble C2C12 cells were induced to differentiate by switching to differentiation media. The effect of *Itm2a* silencing on the morphology of the cells was evaluated daily throughout the 7 days of the differentiation process **(Figure 6.9)**. Morphologically, differentiation is characterised by the loss of the myoblasts' spindle-like shape and the formation of multinucleated myotubes of elongated shape (Hwang et al., 2015). Results showed that the appearance of morphological changes associated with myogenic differentiation is delayed in the cell line with reduced expression of *Itm2a*. Despite the initial delay in differentiation, after 7 days both, stable shItm2a-C and shScramble C2C12 cells, exhibited mature multinucleated myotubes. Our findings are in agreement with an independent study that reported that overexpression of Itm2a in C2C12 cells accelerated the formation of myotubes (Van den Plas and Merregaert, 2004a).

The results presented in this chapter indicate that high levels of Itm2a are required for timely differentiation, with partial silencing delaying the differentiation process. These results should be observed with caution as the knockdown efficiency obtained during the 3 passages was at least 40% at the mRNA level. Therefore a higher knockdown efficiency would allow to discern if *Itm2a* knockdown could prevent differentiation. Experiments using the CRISPR/Cas9 technology to knockout *Itm2a* would allow the validation of the presented findings.

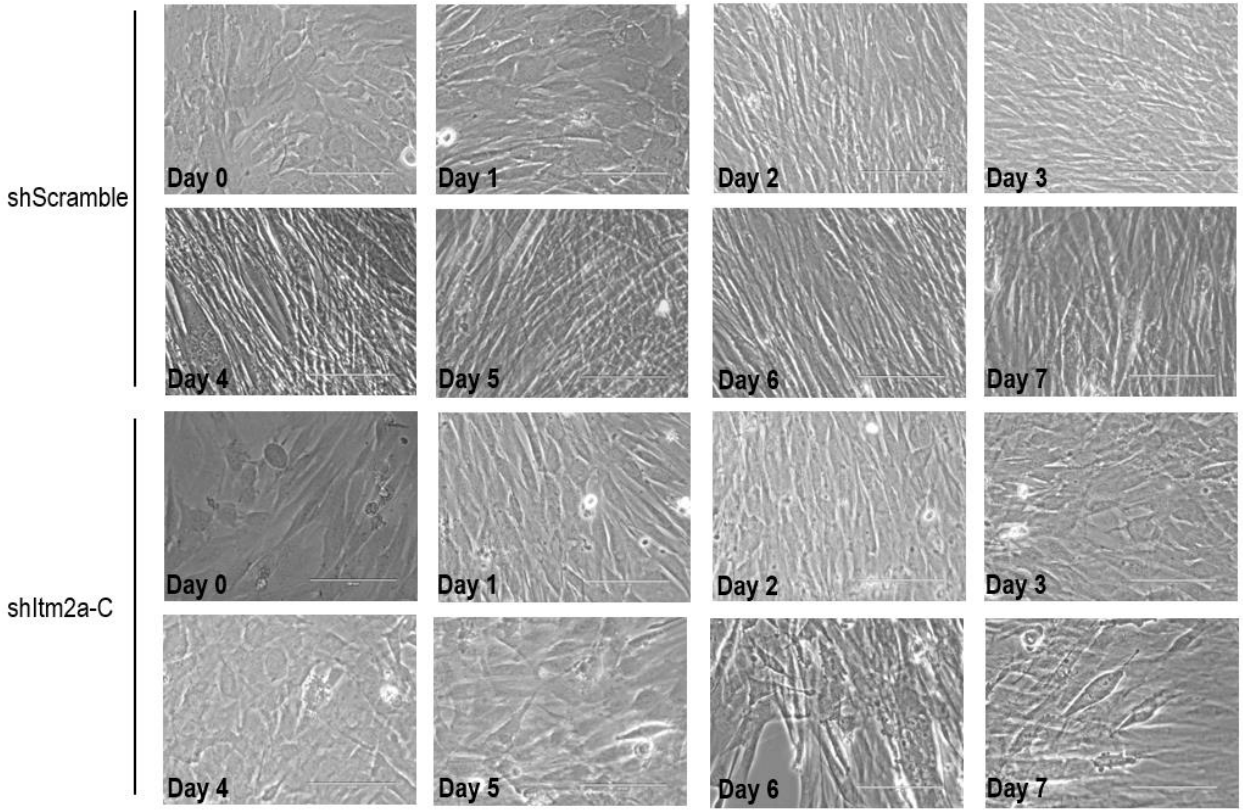

Figure 6.9 Myogenic differentiation of C2C12 cells with stable silencing of *Itm2a*

C2C12 shItm2a-C and C2C12 shScramble control were induced to differentiate by switching complete media to differentiation media. Images were obtained from day 0 to day 7 of differentiation. Media was added to cells at day 0 and changed to fresh differentiation media every other day.

The morphological changes in differentiation were confirmed by analysing the expression of MHC **(Figure 6.10).** Protein samples from C2C12 shItm2a-C and shScramble control were collected from day 0 to day 7 of differentiation and analysed by western blot. shItm2a-C cells expressed lower levels of itm2a, as expected. Results show that there is a delay in the expression of MHC in C2C12 shItm2a-C compared to control cells. MHC expression appears on day 3 of differentiation in the shItm2a-C cells, while the expression of MHC in shScramble control appears on day 2 **(Figure 6.10)**. Delay in the expression of MHC was also observed in the C2C12 shItm2a-B cells when compared to shScramble (data not shown). Even though both shItm2a-C and shItm2a-B presented a delay in the expression of MHC, the downregulation of MHC is more marked in the shItm2a-C cells than in the shItm2a-B cells. This difference could be attributed to the previously indicated differences in knockdown efficiency.

Protein samples were then used to study the changes in the expression of cyclin D3, a key regulator during cell cycle exit during myoblast differentiation (Gurung and Parnaik, 2012). Differentiation of the C2C12 myoblast cell line requires that the proliferative cells exit the cell cycle and remain arrested in the G1 phase, this is regulated by changes in the expression of cyclins, CDKs and CDK inhibitors (CDKIs). Cell cycle withdrawal allows differentiation and fusion of myoblasts to form myotubes (Walsh and Perlman,1997; Perry and Rudnick, 2000). During myogenic differentiation the expression levels of cyclin cyclin D1 are downregulated, while the expression levels of cyclin D3 increases upon differentiation, this upregulation of cyclin D3 is key for the cell cycle arrest required for the differentiation of myoblasts into myotubes (Cenciarelli et al., 1999; Gurung and Parnaik, 2012; Pavlidou et al., 2017). Studies suggest that

higher expression levels of cyclin D3 are related to faster differentiation kinetics through transcription of Pax7, and that differentiated myotubes express higher levels of cyclin D3 when compared to undifferentiated myoblasts. Studies have also shown that overexpression of cyclin D3 is accompanied with an increase in the expression levels of the CDKI p21 (Gurung and Parnaik, 2012). As previously mentioned, CDKIs regulated the progression of the cell cycle by negatively regulating the activity of CDKs. CDKIs exert their function by interacting directly with CDKs (before they interact with cyclins) or by interacting with the CDK-cyclin complexes causing their inactivation. p21 has an important role in regulation of the C2C12 cell cycle progression. Studies suggest that p21 allows the initiation of differentiation. However, its expression is not necessary to maintain the cell cycle arrest. Furthermore, p21 silencing does not disrupt cell cycle exit and does not block the differentiation into myotubes because of its functional redundancy with other inhibitors (Perlman, 1997; Walsh and Perlman, 1997; Cenciarelli et al., 1999; Williamson et al., 2009; Pavlidou et al., 2017).

In accordance to the phenotypic findings that *Itm2a* silencing produces a delay in myogenic differentiation, the expression levels of cyclin D3 did not increase until the final days of differentiation in C2C12 shItm2a-C cells when compared to C2C12 shScramble control cells. The expression levels of cyclin D3 in shItm2a-C cells steadily and moderately increased during differentiation, while the level of cyclin D3 in shScramble cells plateaued after day 3 and then maintained throughout differentiation **(Figure 6.10)**.

Taken together, these results suggest that Itm2a has a role in the kinetics of myogenic differentiation by regulating cell cycle progression and, possibly, autophagy. It is possible that *Itm2a* knockdown in the C2C12 cells causes a

change in the timing of the cell cycle withdrawal which delays, but not abolishes, the formation of fully differentiated myotubes. However, the specific regulatory mechanisms involved in the changes of the cell cycle induced after *Itm2a* silencing need to be further analysed.

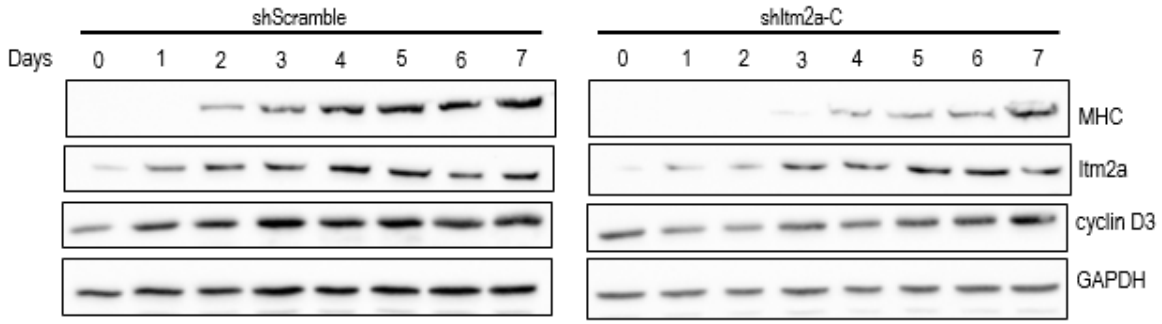

Figure 6.10 Cell cycle marker expression during differentiation of C2C12 cells

Expression levels of MHC, endogenous Itm2a, cyclin D3 and GAPDH in C2C12 shItm2a-C and C2C12 scramble control during 7 days of differentiation.

6.3.6 *Itm2a* silencing does not affect the cell doubling time in C2C12 myoblasts

It has been reported that overexpression of Itm2a in the C2C12 cell line does not change its doubling rate (Van den Plas and Merregaert, 2004a). However, the effect of *Itm2a* silencing in the cell division rates of C2C12 myoblasts has not been studied. Therefore, stable shItm2a-expressig cells with the highest and second highest knockdown efficiency were compared to scramble control to analyse the effect of *Itm2a* knockdown on myoblast expansion rate. Cells were seeded at low confluence on complete media (10% FBS) and trypsinised and counted at 24, 48 and 72 hours after seeding **(Figure 6.11)**. Results show that

Itm2a silencing in C2C12 myoblast does not affect the cell doubling rate when compared to control.

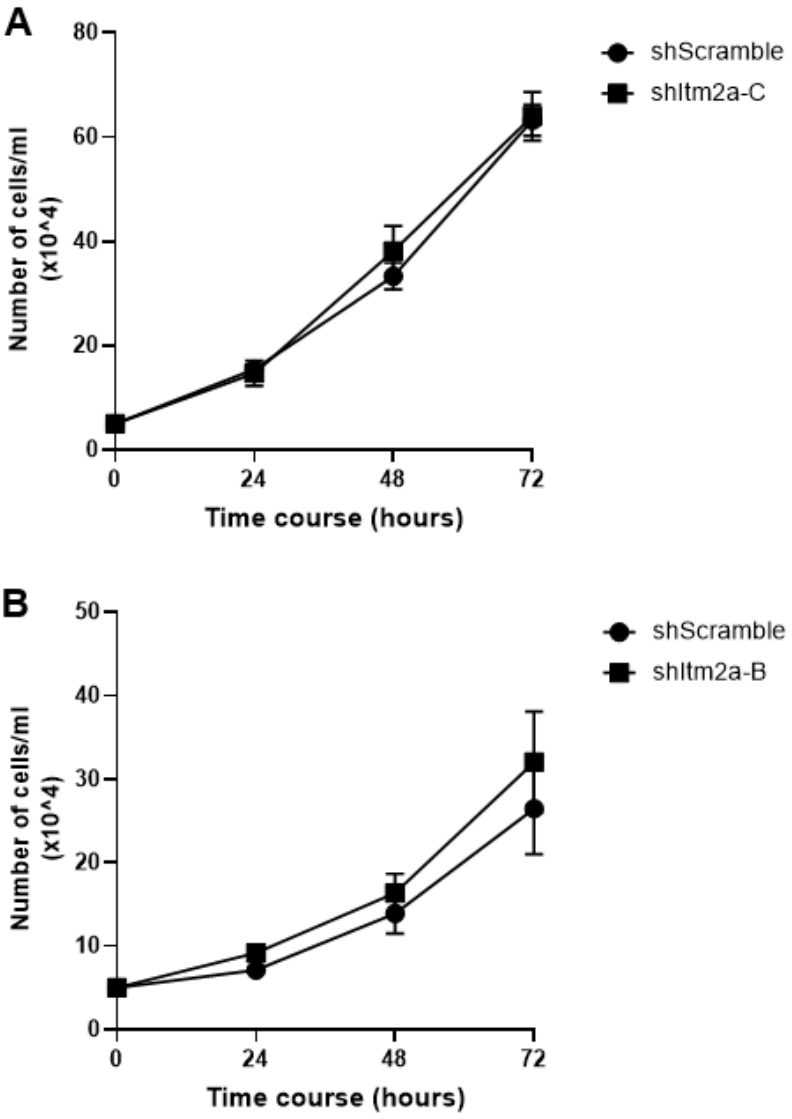

Figure 6.11 *Itm2a* silencing does not affect the doubling time of C2C12 myoblasts

Cells were cultured in complete growth medium, trypsinised and the number of cells counted using a haemocytometer chamber at 24 hours, 48 hours and 72 hours **A.** C2C12 shScramble and C2C12 shItm2a-C (n=3). **B.** C2C12 shScramble and C2C12 shIym2a-B (n=3).

6.3.7 Identification of additional ITM2A-interacting proteins by mass spectrometry

To identify new interacting partners of ITM2A that would help understand its function, HEK293 cells were transfected with HA-ITM2A or empty vector followed by immunoprecipitation after 24 hours using anti-HA. HEK293 cells were used due to their high transfection efficiency, although it is likely that muscle-specific proteins will not be expressed. Immunoprecipitates of ITM2A and a control with empty vector were sent proteomic analysis to the mass spec facility at the University of Leeds. **Table 6.1** lists the proteins identified as present solely in ITM2A immunoprecipitates.

The identification of ITM2A interacting proteins is relevant for this study as it can provide a better understanding of the mechanistic basis of specific process affected by ITM2A, in particular autophagy, cell cycle regulation and Hh signalling. Is important to consider that protein-protein interactions might vary in different cell types and can change as a response to modifications in the cellular environment (Richards et al., 2021). Therefore, the proteomic analysis in HEK293 cannot be directly extrapolated to other cell types, and might not reveal the extent of potential binding partners in C2C12 cells. Nonetheless, this analysis is the first step towards the identification followed by the validation of novel protein interactions, and further along the line would be the analysis of the functional consequences of the validated interactions in more relevant models of study.

The identified proteins show interaction with enrichment in endocytic machinery, DNA repair and ribosomal proteins. Potential nuclear localisation of ITM2A cytosolic domain is suggested by the types of interacting proteins. This could explain the strong effects on Gli1 and Gli2-mediated transcription. In addition,

identification of CDK2 inhibitor 2A (CDKN2A), also known as $p16^{INK4}$ points to potential mechanistic basis for modulation of cell cycle progression.

Mass spectrometry analysis was also used to identify the post-translational modifications of ITM2A **(Figure 6.12)**. The N-terminal domain, composed of the first 53 amino acids of the protein, was of interest of this analysis as we hypothesised that this region is key for ITM2A interaction with the CTD of PTCH1. Post-translational modifications can change the protein structure and in this way the properties of the protein and its biological function. They also play a role in how the protein of study interacts with other proteins (Wang et al., 2014). Therefore, the analysis of the post-translational modifications can be used as a first approach for the identification of the potential regions that could be manipulated. Mutations in specific regions can be used to further study the functions of ITM2A and the functional consequences of its interaction with other proteins to regulate cellular processes, such as proliferation and differentiation, or to study its involvement in signalling pathways, such as the Hh pathway. Results obtained show that a phosphorylation event of interest in the N-terminal region of ITM2A, which could affect its interaction with PTCH1 and modulate its function. Further studies will be necessary to investigate this further.

Protein name	**Function**	**UniProtKB identifier**
ABCF2	ATP-binding cassette sub-family F member 2	Q9UG63
ACTG1	Structural constituent of cytoskeleton	P63261
ADAR	Adenosine deaminase, RNA editing	P55265
ALB	Albumin	P02768
ATAD3A	Mitochondrial network organization	Q9NVI7

ATP2A2	ER-isolation membrane contacts, autophagosome formation	P16615
ATP5F1C	Mitochondrial membrane ATP production	P36542
ATXN2L	Stress granule and P-body formation	Q8WWM7
BAG2	Co-chaperone for HSP70/HSC70	O95816
C1orf57	Nucleotide phosphatase	Q5TDE9
CANX	ER protein folding quality control	P27824
CDK1	Cell cycle progression	P06493
CDKN2A	Negative regulator of proliferation	P42771
CISD2	Regulator of autophagy	Q8N5K1
CSE1L	Nuclear export receptor	P55060
DARS	Aspartate tRNA-ligase	P14868
DNAJA1	Co-chaperone of HSC70, mitochondria protein transport	P25685
DNAJA2	Co-chaperone of HSC70	O60884
EEF1G	Elongation factor	P26641
EIF4A1	Eukaryotic initiation factor	P60842
ERLIN2	Endoplasmic reticulum-associated degradation, cholesterol homeostasis	O94905
FAF2	Endoplasmic reticulum-associated degradation	Q96CS3
FLG	Keratin intermediate filament aggregation	P20930
FLNA	Branching of actin filaments	P21333
FLNC	Muscle-specific filamin	Q14315
G3BP2	Stress granule formation	Q9UN86
GANAB	Neutral alpha-glucosidase	Q14697
GP96	ER-chaperone, ERAD	P14625
HNRNPR	Processing of mRNA precursor in the nucleus	O43390
HSD17B12	ER-localised fatty acid elongation	Q53GQ0
HSPA1B	HSP70 chaperone	P0DMV9
HSPA5	ER chaperone	P11021
LMAN1	ER to Golgi transport	P49257

MARS	Methionine-tRNA ligase	A0A024RBA2
NPM1	Ribosome biogenesis, ribosome nuclear export	P06748
NSUN2	RNA-C5 methyl transferase, tRNA stability, mRNA decay	Q08J23
NUP93	Nuclear pore complex	Q8N1F7
PAI-1	Serine protease inhibitor	P05121
PGAM5	Mitochondrial dynamics	Q96HS1
PHB	Mitochondrial chaperone, mitophagy receptor	P35232
PHB-2	Mitochondrial chaperone, mitophagy receptor	Q99623
PSMD3	Component of the 26S proteasome	O43242
RALY	Transcriptional cofactor for cholesterogenesis	Q9UKM9
RCN	Post-ER calcium regulatory protein	Q15293
SFPQ	Pre-mRNA splicing factor	P23246
SLC25A3	Cytosol-mitochondria phosphate transport	Q00325

Table 6.1 Proteins identified by mass spectrometry in ITM2A immunoprecipitates

This table shows the proteins identified by mass spectrometry, with details of their relevant functions and their UniProtKB ID.

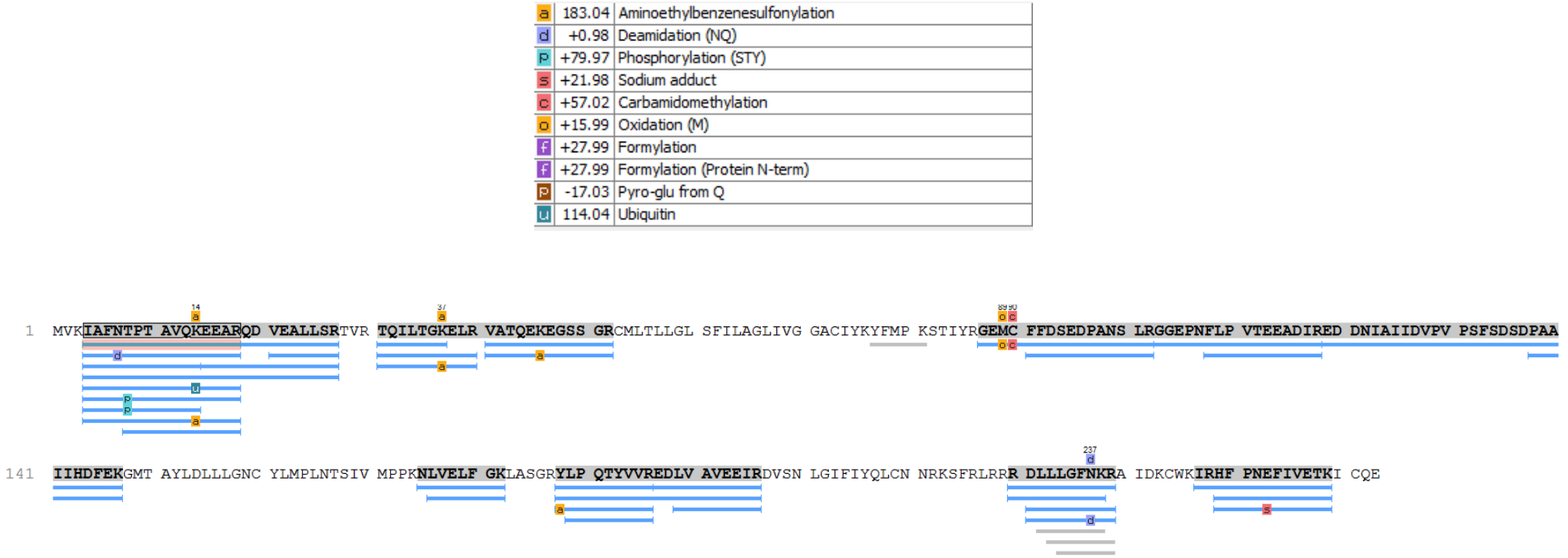

Figure 6.12 Mass spectrometry analysis of ITM2A immunoprecipitates

Top: Legend for the identified post translational modifications. Bottom: Amino acid sequenced of ITM2A with identified post translational modifications. Sample was digested with trypsin. Blue lines represent the coverage.

STRING analysis reveals a highly significant clustering (p= 1 x10-16) of over 90% of the proteins identified **(Figure 6.13)**, with the existence of sub-clusters related to the ER protein quality control, mitochondria membrane protein translocation and stress granules. Some of the proteins identified play important roles in the recognition of defective mitochondria for clearance by mitophagy (prohibitin and prohibitin-2, ADACT3, HSPA1B). This snapshot of ITM2A interactome suggest that it might function at ER-mitochondria contacts to regulate mitophagy. This selective type of autophagy has been shown to play an important role during mitochondrial network remodelling in myogenic differentiation and could explain the regulatory role of Itm2a in C2C12 cells (Baechler et a;., 2019).

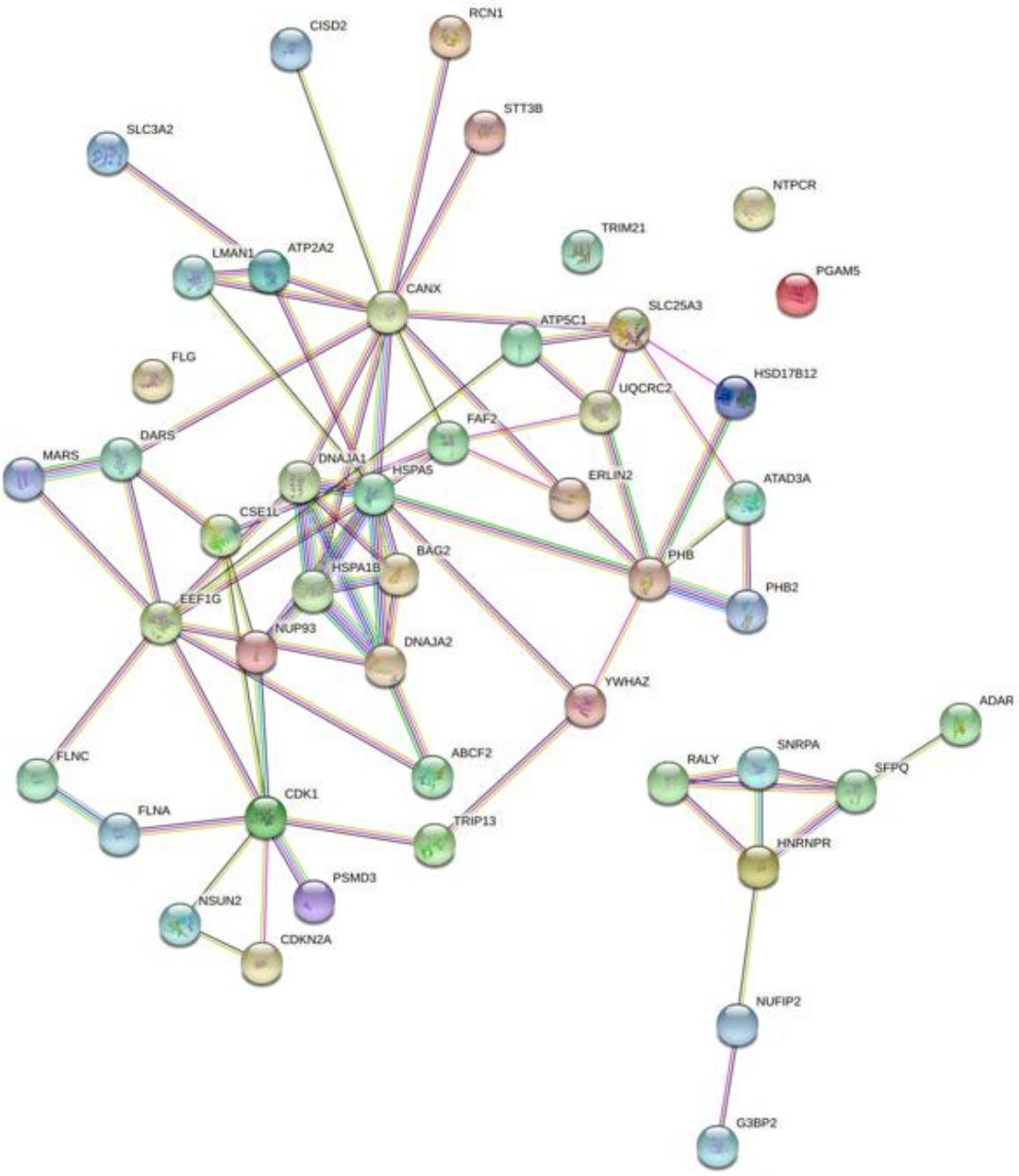

Figure 6.13 Unsupervised STRING clustering of proteins identified in ITM2A immunoprecipitates from HEK293 cells

The number of connecting lines increases with experimental evidence of physical or functional interaction. Known interactions=light blue and pink lines; predicted interactions=green, red and dark blue; textmining=yellow; co-expression=black; protein homology=purple (Szklarczyk et al., 2019).

6.4 Discussion

6.4.1 ITM2A effect in PTCH1 expression

The results presented in the previous chapter show that expression of ITM2A downregulates PTCH1 levels, suggesting that it reduces its stability. Considering that ITM2A expression is affecting PTCH1 stability, it was no surprise that in the C2C12 cells that have a higher expression of endogenous ITM2A, the endogenous levels of ITM2A were sufficient to inhibit the autophagy phenotype observed when PTCH1 is transfected in HEK293 and HeLa cells (Chen et al, 2018). When C2C12 cells with reduced ITM2A levels were transfected, the overexpression of PTCH1 generated the previously described blocking effect on the autophagic flux, although not to the extent seen in HEK293 and HeLa cells (Chen et al, 2018). It is important to consider that the knockdown efficiency obtained for the C2C12 cell line was only 40% at an mRNA level.

These results strengthen the hypothesis that the expression of ITM2A has a negative effect on the stability of PTCH1, causing its degradation.

6.4.2 Cell cycle regulation by ITM2A

Myoblasts express genes from the bHLH family of transcription factors, which mediate the expression of muscle specific genes upon induction of differentiation. Alongside the gene expression, cells also exit the cell cycle permanently (Franklin and Xiong, 1996; Williamson et al., 2009). Although the regulation of the muscle-specific gene expression has been widely studied, there is still much left to uncover about the cell cycle withdrawal which is necessary for the initiation and maintenance of differentiation (Franklin and Xiong, 1996). D-type cyclins act in the G1 phase of the cell cycle and they have the same interacting capacity with

CDK4 and they all can activate it at the same degree *in vitro* during cellular proliferation. However, studies show that cyclin D3 also plays a role during myogenic differentiation. On the contrary to cyclin D1 and cyclin D2, the expression levels of cyclin D3 increase upon differentiation induction (Bartkova et al., 1998; Cenciarelli et al., 1999). Results presented in this chapter show that, when *Itm2a* expression is partially silenced in C2C12 cells, the expression of cyclin D3 is downregulated during myogenic differentiation. Therefore, it is possible that expression of Itm2a in C2C12 cells is involved in the upregulation of the expression of cyclin D3 during differentiation, and in this way indirectly related to establishment and maintenance of myogenic differentiation.

Studies show that upon initiation of the differentiation process, the increase in cyclin D3 levels is accompanied by an increase in the expression of the p21 in different myogenic cell lines, among them C2C12 (Franklin and Xiong, 1996; Duronio and Xiong, 2013). The increase in the levels of cyclin D3 during differentiation promotes the formation of the CDK4-cyclin D3 complex, which then interacts with p21. The induction of p21 inhibits the progression of the cells into the S phase where the DNA synthesis takes place (Cenciarelli et al., 1999; Williamson et al., 2009). However, the maintenance of the upregulation of p21 during differentiation is not necessary for the maintenance of the cell cycle withdrawal. p21 is unstable with a half-life of 30 minutes, and acts quickly on the cell cycle, while the CDKIs that belong to the INK4 family have half-lives in the range of 4 to 6 hours and produce long-term cycle arrest (Franklin and Xiong, 1996; Duronio and Xiong, 2013). Therefore, it would be necessary to study the expression of the different CDKIs during the differentiation of the C2C12 after *ITM2A* silencing to understand if ITM2A could be involved in their regulation.

Intriguingly, CDKN2A (also known as $p16^{INK4}$) was identified as an ITM2A-interacting protein by mass spectrometry. Given the role of Itm2a in C2C12 differentiation, it is possible that it can directly stimulate the function of this CDK4/6 inhibitor to accelerate cell cycle exit. Analysis of $p16^{INK4}$ levels in scramble and shItm2a cells will be necessary to explore if they are mechanistically related.

These results suggest that the expression of Itm2a in the C2C12 cell line plays an important role in the expression of cell cycle regulators. Particularly, the delay in differentiation of C2C12 cells with reduced Itm2a might be attributed to failure to upregulate cyclin D3 levels. However, this can only be suggested as this analysis has not been confirmed with biological replicas. Further studies should be carried out to understand if Itm2a is involved indirectly in the stabilization of the main complexes involved in the maintenance of the cell cycle withdrawal required for the differentiation of myoblasts into myotubes. The potential physical interaction with CDKN2 suggested by the proteomics analysis, is an attractive starting point to further investigate this process. More studies would allow the identification of the specific regulatory mechanisms involved in the changes of the cell cycle induced by *ITM2A* silencing.

To have a better understanding on how the silencing of Itm2a is modifying the cell cycle progression, flow cytometry studies could be carried out in actively cycling myoblasts and during differentiation into myotubes to elucidate changes in the cell cycle phase distribution modulated by Itm2a levels.

Chapter 7

Final conclusions

Chapter 7

Final conclusions

Our published research shows that the CTD of PTCH1 mediates an autophagic flux blockade through interaction with ATG101 (Chen et al., 2018). The results that I generated, presented in Chapter 3, were used in the published paper to demonstrate that endogenous PTCH1 downregulates autophagic flux. This is relevant as it suggests that the mutations characterised in the next chapter could modify autophagy when expressed at endogenous levels.

Continuing with this investigation, I generated constructs encoding three different somatic mutations in the CTD of PTCH1 that are overrepresented in colorectal, stomach and endometrial cancer and showed that the interaction between PTCH1 and ATG101 occurs in the region comprising amino acids 1308-1447. Nevertheless, the CTD construct that, although validated by Sanger sequencing, was not detected by western blot, needs to be generated for future analysis of different PTCH1-interactin proteins. A new cloning strategy could include the addition of an N-terminal tag instead of the current C-terminal, or the use of a different tag unable to form polyproline helixes in the context of a proline-rich sequence.

Of importance, the results presented in Chapter 4 suggest that the cancer mutations in the CTD of PTCH1 that loss the ability to interact with ATG101, also lose their ability to inhibit the autophagic flux. Therefore, these mutations could be giving an advantage for cancer cells to survive without the restrictive role of PTCH1 on the regulation of autophagy. Further studies in more relevant cell lines and animal models are required to understand the pathological consequences of

these somatic mutations. Nevertheless, the results presented in Chapter 4 strongly suggest that the tumour suppressor role of PTCH1 is not limited to its inhibitory action on SMO and highlights the importance of the investigation of mutations in the CTD of PTCH1 that have not been previously appreciated, as they are not involved in the activation of the Hh canonical pathway. In the future, the identification of these mutations could be used as a biomarker for specific cancers (colorectal, stomach and endometrial). Also, as these mutations potentially enhance survival of cancer cells by stimulating autophagy, the use of autophagy inhibitors could be considered for treatment.

I first started investigating the function of ITM2A with the hypothesis that it was a mediator of the autophagic flux regulated by PTCH1. Results in Chapter 5 show that even when PTCH1 and ITM2A interact with each other, they block autophagic flux independently of each other. Strikingly, expression of ITM2A caused a downregulation of PTCH1 expression, suggesting an unforeseen function of ITM2A in the regulation of PTCH1 stability and, importantly, in the regulation of the canonical Hh pathway. The effect of ITM2A on PTCH1 stability was observed in the different cell lines. Therefore, the first step toward elucidating the function of ITM2A in the Hh signalling pathway would be the generation of complete ITM2A knockouts in different cell lines, particularly in the ones with higher ITM2A endogenous levels. CRISPR/Cas 9 technology could be used for obtaining ITM2A knockout, now that the technology is widely used in the lab. It would also be relevant to generate an ITM2A knockout cell line in NIH3T3 cells to further study the effect of ITM2A in the Hh canonical pathway.

The findings reported here (Chapter 5 and 6), as well as the studies published elsewhere, clearly show that the effects of the expression of ITM2A depend greatly on the cell type that is being investigated. Results obtained by a different group showed that the loss of ITM2A in samples from invasive serous ovarian cancer was highly common. Loss of ITM2A was a characteristic of around 45% of the analysed tissue samples. The expression of ITM2A in patient samples, as well as on ovarian cancer cell lines, revealed that expression of ITM2A was directly related to cell growth. While higher expression levels of ITM2A caused a reduction in cell growth and a reduction in cell colony formation. Importantly, the expression of ITM2A render the ovarian cancer cells more susceptible to the chemotherapy agents Paclitaxel and Carboplatin (Nguyen et al., 2016). This study is in line with the results presented in Chapter 5 corresponding to HeLa cells, in which the silencing of ITM2A caused a statistically significant decrease in the cells doubling time. This suggests that ITM2A could potentially be playing a positive role in the proliferation of HeLa cells or reducing their apoptotic index. However, further studies are necessary to understand the changes in the kinetics of cell proliferation and apoptosis in HeLa cells regulated by ITM2A.

The results presented in Chapter 6, showing the changes in the expression of cyclin D3 during myogenic differentiation of C2C12 myoblasts after *Itm2a* silencing correspond to a single biological replica, and therefore, biological repeats are required to validate the reproducibility of results, to draw conclusions and to have a better understanding of how to move forward to further analyse the role of Itm2a and myogenic differentiation. The results from the proteomic

analysis also provide a good starting point for future analysis of potential interacting partners and the processes affected.

It would also be important to optimise the conditions for the mass spectrometry analysis of ITM2A. The PTM analysis showed in Chapter 6 was obtained using only trypsin to digest the ITM2A pulldowns. A future analysis using different proteases would provide a higher coverage percentage of the protein and therefore the identification of potential PTMs that can be modified to explore the function of ITM2A.

Overall, this thesis shows a tumour suppressor role of PTCH1 that is independent of its role as SMO repressor, and also a new exciting role of ITM2A in the regulation of the Hh signalling pathway.

Bibliography

Ahlberg, J. and Glaumann, H. 1985. Uptake—Microautophagy—and degradation of exogenous proteins by isolated rat liver lysosomes: Effects of pH, ATP, and inhibitors of proteolysis. *Experimental and Molecular Pathology*. **42**(1), pp.78–88.

Alcedo, J., Ayzenzon, M., Von Ohlen, T., Noll, M. and Hooper, J.E. 1996. The Drosophila smoothened gene encodes a seven-pass membrane protein, a putative receptor for the hedgehog signal. *Cell*. **86**(2), pp.221–232.

Allen, B.L., Tenzen, T. and McMahon, A.P. 2007. The Hedgehog-binding proteins Gas1 and Cdo cooperate to positively regulate Shh signaling during mouse development. *Genes and development*. **21**(10), pp.1244–1257.

Anders, L., Ke, N., Hydbring, P., Choi, Y.J., Widlund, H.R., Chick, J.M., Zhai, H., Vidal, M., Gygi, S.P., Braun, P. and Sicinski, P. 2011. A systematic screen for CDK4/6 substrates links FOXM1 phosphorylation to senescence suppression in cancer cells. *Cancer cell*. **20**(5), pp.620–634.

Arstila A.U. and Trump B.F. 1968. Studies on cellular autophagocytosis. The formation of autophagic vacuoles in the liver after glucagon administration. *The American Journal of Pathology*. **53**(5), pp.687-733.

Assoian, R.K. and Zhu, X. 1997. Cell anchorage and the cytoskeleton as partners in growth factor dependent cell cycle progression. *Current opinion in cell biology*. **9**(1), pp.93–98.

Axe, E., Walker, S., Manifava, M., Chandra, P., Roderick, H., Habermann, A., Griffiths, G. and Ktistakiset, N. 2008. Autophagosome Formation from Membrane Compartments Enriched in Phosphatidylinositol 3-Phosphate and Dynamically

Connected to the Endoplasmic Reticulum. *The Journal of Cell Biology*. **182**(4), pp.685-701.

Baechler, B.L., Bloemberg, D. and Quadrilatero, J. 2019. Mitophagy regulates mitochondrial network signaling, oxidative stress, and apoptosis during myoblast differentiation. *Autophagy*. **15**(9), pp.1606–1619.

Banerjee, B., Corless, C.L, Miettinen, M.M., Noh, S., Ustoy, R., Davis, J.L., Tang, C.M., Yebra, M., Burgoyne , A.M. and Sicklick, J.K. 2019. Loss of the PTCH1 tumor suppressor defines a new subset of plexiform fibromyxoma. *Journal of Translational Medicine*. **17**(1), pp.246–246.

Bangs, F. and Anderson, K.V. 2017. Primary Cilia and Mammalian Hedgehog Signaling. *Cold Spring Harbor perspectives in biology*. **9**(5), pp.a028175.

Barnes, E.A., Kong, M., Ollendorff, V. and Donoghue, D.J. 2001. Patched1 interacts with cyclin B1 to regulate cell cycle progression. *The EMBO journal*. **20**(9), pp.2214–2223.

Barth, S., Glick, D. and Macleod, K. 2010. Autophagy: assays and artifacts. *The Journal of Pathology*. **221**(2), pp.117–124.

Bartkova, J., Lukas, J., Strauss, M., and Bertek, J. 1998. Cyclin D3: requirement for G1/S transition and high abundance in quiescent tissues suggest a dual role in proliferation and differentiation. *Oncogene*. **17**(8), pp.1027–1037.

Beachy, P.A., Hymowitz, S.G., Lazarus, R.A., Leahy, D.J. and Siebold, C. 2010. Interactions between Hedgehog proteins and their binding partners come into view. *Genes & development*. **24**(18), pp.2001–2012.

Bento, C.F., Renna, M., Ghislat, G., Puri, C., Ashkenazi, A., Vicinanza, M., Menzies, F.M. and Rubinsztein, D.C. 2016. Mammalian Autophagy: How Does It Work?. *Annual review of biochemistry*, **85**, pp.685–713.

Bhutia, S.K., Mukhopadhyay, S., Sinha, N., Das, D.N., Panda, P.K., Patra, S.K., Maiti, T.K., Mandal, M., Dent, P., Wang, X.Y., Das, S. K., Sarkar, D. and Fisher, P.B. 2013. Autophagy: cancer's friend or foe?. Advances in cancer research, 118, 61–95.

Bitgood, M.J., Shen, L. and McMahon, A.P. 1996. Sertoli cell signaling by Desert hedgehog regulates the male germline. *Current biology*. **6**(3), pp.298–304.

Bjørkøy, G., Lamark, T., Brech, A., Outzen, H., Perander, M., Øvervatn, A., Stenmark, H. and Johansen, T. 2005. p62/SQSTM1 Forms Protein Aggregates Degraded by Autophagy and Has a Protective Effect on Huntingtin-Induced Cell Death. *The Journal of Cell Biology*. **171**(4), pp.603–614.

Blommaart, E., Luiken, J. and Meijer, A. 1997. Autophagic proteolysis: control and specificity. *The Histochemical Journal*. **29**(5), pp.365–385.

Bonam, S.R., Bayry, J., Tschan, M.P. and Muller, S. 2020. Progress and Challenges in The Use of MAP1LC3 as a Legitimate Marker for Measuring Dynamic Autophagy In Vivo. *Cells*. **9**(5), pp.1321.

Brennan, D., Chen, X., Cheng, L., Mahoney, M. and Riobo, N.A. 2012. Noncanonical Hedgehog signaling. *Vitamins and hormones*. **88**, pp.55–72.

Briscoe, J. and Thérond, P.P. 2013. The mechanisms of Hedgehog signalling and its roles in development and disease. *Nature reviews*. **14**(7), pp.416–429.

Brown, E.J., Albers, M.W., Shin, T.B., Ichikawa, K., Keith, C.T., Lane, W.S. and Schreiber, S.L. 1994. A mammalian protein targeted by G1-arresting rapamycin-receptor complex. *Nature*. **369**(6483), pp.756–758.

Bumcrot, D.A., Takada, R. and McMahon, A.P. 1995. Proteolytic processing yields two secreted forms of sonic hedgehog. Molecular and cellular biology, 15(4), 2294–2303.

Burke, R., Nellen, D., Bellotto, M., Hafen, E., Senti, K.A., Dickson, B.J. and Basler, K. 1999. Dispatched, a novel sterol-sensing domain protein dedicated to the release of cholesterol-modified hedgehog from signaling cells. *Cell*. **99**(7), pp.803–815.

Cai, C., Thorne, J. and Grabel, L. 2008. Hedgehog serves as a mitogen and survival factor during embryonic stem cell neurogenesis. *Stem cells*. **26**(5), pp.1097–1108.

Capdevila, J., Pariente, F., Sampedro, J., Alonso, J.L. and Guerrero, I. 1994. Subcellular localization of the segment polarity protein patched suggests an interaction with the wingless reception complex in Drosophila embryos. *Development*. **120**(4), pp.987–998.

Carballo, G.B., Honorato, J.R., de Lopes, G.P.F. and Spohr, T.C.L. 2018. A highlight on Sonic hedgehog pathway. *Cell Communication and Signaling*. **16**(1), p.11.

Cenciarelli, C., De Santa, F., Puri, P.L., Mattei, E., Ricci, L., Bucci, F., Felsani, A. and Caruso, M. 1999. Critical Role Played by Cyclin D3 in the MyoD-Mediated Arrest of Cell Cycle during Myoblast Differentiation*. Molecular and Cellular Biology*. **19**(7), pp.5203–5217.

Chen, C. H., von Kessler, D.P., Park, W., Wang, B., Ma, Y. and Beachy, P.A. 1999. Nuclear trafficking of Cubitus interruptus in the transcriptional regulation of Hedgehog target gene expression. *Cell*. **98**(3), pp.305–316.

Chen, J.K., Taipale, J., Young, K.E., Maiti, T. and Beachy, P.A. 2002. Small molecule modulation of Smoothened activity. *Proceedings of the National Academy of Sciences of the United States of America*. **99**(22), pp.14071–14076.

Chen, X., Morales-Alcala, C.C. and Riobo-Del Galdo, N.A. 2018. Autophagic Flux Is Regulated by Interaction Between the C-terminal Domain of PATCHED1 and ATG101. *Molecular cancer research.* **16**(5), pp.909–919.

Chen, X.L., Chinchilla, P., Fombonne, J., Ho, L., Guix, C., Keen, J.H., Mehlen, P., and Riobo, N.A. 2014. Patched-1 proapoptotic activity is downregulated by modification of K1413 by the E3 ubiquitin-protein ligase Itchy homolog. *Molecular and cellular biology*. **34**(20), pp.3855–3866.

Chen, Y. and Struhl, G. 1996. Dual roles for patched in sequestering and transducing Hedgehog. *Cell*. **87**(3), pp.553–563.

Cheng, L., Al-Owais, M., Covarrubias, M. L., Koch, W. J., Manning, D. R., Peers, C. and Riobo-Del Galdo, N. A. 2018. Coupling of Smoothened to inhibitory G proteins reduces voltage-gated K+ currents in cardiomyocytes and prolongs cardiac action potential duration. *The Journal of biological chemistry*. **293**(28), pp.11022–11032.

Chiang, H.L. and Dice, J.F. 1988. Peptide sequences that target proteins for enhanced degradation during serum withdrawal. *The Journal of Biological Chemistry*. **263**(14), pp.6797–6805.

Chinchilla, P., Xiao, L., Kazanietz, M.G. and Riobo, N.A. 2010. Hedgehog proteins activate pro-angiogenic responses in endothelial cells through non-canonical signaling pathways. *Cell cycle*. **9**(3), pp.570–579.

Choi, S.C., Kim, J., Kim, T.H., Cho, S.Y., Park, S.S., Kim, K.D. and Lee, S.H. 2001. Cloning and Characterization of a Type II Integral Transmembrane Protein Gene, Itm2c, That Is Highly Expressed in the Mouse Brain. *Molecules and Cells*. **12**(3), pp.391-397.

Cicchini, M., Karantza, V. and Xia, B. 2015. Molecular pathways: autophagy in cancer--a matter of timing and context. *Clinical cancer research*. **21**(3), pp.498–504.

Cohen-Kaplan, V., Livneh, I., Avni, N., Fabre, B., Ziv, T., Kwon, Y.T. and Ciechanover, A. 2016. p62- and ubiquitin-dependent stress-induced autophagy of the mammalian 26S proteasome. *Proceedings of the National Academy of Sciences – PNAS*. **113**(47), pp.E7490–E7499.

Cuervo, A. and Dice, J. 1998. Lysosomes, a meeting point of proteins, chaperones, and proteases. *Journal of Molecular Medicine.* **76**(1), pp.6–12.

Dai, P., Akimaru, H., Tanaka, Y., Maekawa, T., Nakafuku, M. and Ishii, S. 1999. Sonic Hedgehog-induced activation of the Gli1 promoter is mediated by GLI3. *The Journal of biological chemistry*. **274**(12), pp.8143–8152.

De Duve, C. and Wattiaux, R. 1966. Functions of lysosomes. *Annual Review of Physiology.* **28**(1), pp435-492.

de la Roche, M., Ritter, A. T., Angus, K. L., Dinsmore, C., Earnshaw, C. H., Reiter, J. F. and Griffiths, G. M. 2013. Hedgehog signaling controls T cell killing at the immunological synapse. *Science*. **342**(6163), pp.1247–1250.

Deleersnijder, W., Hong, G., Cortvrindt, R., Poirier, C., Tylzanowski, P., Pittois, K., Van Marck, E., & Merregaert, J. 1996. Isolation of markers for chondro-osteogenic differentiation using cDNA library subtraction. Molecular cloning and characterization of a gene belonging to a novel multigene family of integral membrane proteins. *The Journal of Biological Chemistry*. **271**(32), pp.19475–19482.

Delorme-Axford, E. and Klionsky, D. 2019. On the edge of degradation: Autophagy regulation by RNA decay. *Wiley Interdisciplinary Reviews. RNA*. **10**(3), pp.e1522–n/a.

Denton, D., Xu, T. and Kumar, S. 2015. Autophagy as a pro-death pathway. *Immunology and cell biology*. **93**(1), pp. 35-42

Deretic V. 2008. Autophagosome and phagosome. Methods in molecular biology. **445**, pp.1–10.

Devereaux, K., Dall'Armi, C., Alcazar-Roman, A., Ogasawara, Y., Zhou, X., Wang, F., Yamamoto, A., De Camilli, P. and Di Paolo, G. 2013. Regulation of mammalian autophagy by class II and III PI 3-kinases through PI3P synthesis. *PloS one*. **8**(10), p.e76405.

Dunlop, E. and Tee, A. 2014. mTOR and autophagy: A dynamic relationship governed by nutrients and energy. *Seminars in Cell & Developmental Biology*. **36**, pp.121–129

Dunn, W.A. 1990(a). Studies on the Mechanisms of Autophagy: Formation of the Autophagic Vacuole. *The Journal of Cell Biology*. **110**(6), pp.1923–1933.

Dunn, W.A. 1990(b). Studies on the mechanisms of autophagy: maturation of the autophagic vacuole. *The Journal of cell biology*. **110**(6), pp.1935–1945.

Duronio, R.J and Xiong, Y. 2013. Signaling pathways that control cell proliferation. *Cold Spring Harbor Perspectives in Biology*. **5**(3), pp.a008904–a008904.

Echelard, Y., Epstein, D.J., St-Jacques, B., Shen, L., Mohler, J., McMahon, J.A. and McMahon, A.P. 1993. Sonic hedgehog, a member of a family of putative signaling molecules, is implicated in the regulation of CNS polarity. *Cell*. **75**(7), pp.1417–1430.

Epstein E.H. 2008. Basal cell carcinomas: attack of the hedgehog. Nature reviews. *Cancer*. **8**(10), pp.743–754.

Fleet, A., Lee, J. P., Tamachi, A., Javeed, I. and Hamel, P. A. 2016. Activities of the Cytoplasmic Domains of Patched-1 Modulate but Are Not Essential for the Regulation of Canonical Hedgehog Signaling. *The Journal of biological chemistry*. **291**(34), pp.17557–17568.

Franklin, D. and Xiong, Y. 1996. Induction of p18INK4c and its predominant association with CDK4 and CDK6 during myogenic differentiation. *Molecular Biology of the Cell*. **7**(10), pp.1587–1599.

Gailani M.R., Stahle-Backdahl M., Leffell D.J., Glynn M., Zaphiropoulos P.G., Pressman C., Unde´n A.B., Dean M., Brash D.E., Bale A.E. and Toftgardet, R. 1996. The role of the human homologue of Drosophila patched in sporadic basal cell carcinomas. *Nature Genetics*. **14**(1), pp78–81.

Galluzzi, L., Baehrecke, E.H., Ballabio, A., Boya, P., Bravo-San Pedro, J.M., Cecconi, F., Choi, A.M., Chu, C.T., Codogno, P., Colombo, M.I., Cuervo, A M., Debnath, J., Deretic, V., Dikic, I., Eskelinen, E.L., Fimia, G.M., Fulda, S., Gewirtz, D.A., Green, D.R., Hansen, M., Harper J.W., Jäättelä, M., Johansen. T., Juhasz, G., Kimmelman, A.C, Kraft, C., Ktistakis, N.T., Kumar, S., Levine, B., Lopez-Otin, C.,

Madeo, F., Martens, S., Martinez, J., Melendez, A., Mizushima, N., Münz, C., Murphy, L.O., Penninger, J.M., Piacentini, M., Reggiori, F., Rubinsztein, D.C., Ryan, K.M., Santambrogio, L., Scorrano, L., Simon, A.K., Simon, H.U., Simonsen, A., Tavernarakis, N., Tooze, S.A., Yoshimori, T., Yuan, J., Yue, Z., Zhong, Q. and Kroemer, G. 2017. Molecular definitions of autophagy and related processes. *The EMBO journal*. **36**(13), pp.1811–1836.

Galluzzi, L., Pietrocola, F., Bravo-San Pedro, J.M., Amaravadi, R.K., Baehrecke, E.H., Cecconi, F., Codogno, P., Debnath, J., Gewirtz, D.A., Karantza, V., Kimmelman, A., Kumar, S., Levine, B., Maiuri, M.C., Martin, S.J., Penninger, J., Piacentini, M., Rubinsztein, D.C., Simon, H.U., Simonsen, A., Thorburn, A.M., Velasco, G., Ryan, K.M. and Kroemer, G. 2015. Autophagy in malignant transformation and cancer progression. *The EMBO journal*. **34**(7), pp.856–880.

Ganley, I.G., Lam, D., Wang, J., Ding, X., Chen, S. and Jiang, X. 2009. ULK1.ATG13.FIP200 complex mediates mTOR signaling and is essential for autophagy. *The Journal of biological chemistry*. **284**(18), pp.12297–12305.

Gautier, J., Norbury, C., Lohka, M., Nurse, P. and Maller, J. 1988. Purified maturation-promoting factor contains the product of a Xenopus homolog of the fission yeast cell cycle control gene cdc2^{+}. *Cell*. **54**(3), pp.433–439.

Glickman, M.H. and Ciechanover, A. 2002. The Ubiquitin-Proteasome Proteolytic Pathway: Destruction for the Sake of Construction. *Physiological Reviews*. **82**(2), pp.373–428.

Goodrich, L.V., Johnson, R.L., Milenkovic, L., McMahon, J.A and Scott, M.P.1996. Conservation of the hedgehog/patched signaling pathway from flies to mice:

induction of a mouse patched gene by Hedgehog. *Genes & Development*. **10**(3), pp.301–312.

Goodrich, L.V., Milenković, L., Higgins, K.M. and Scott, M.P. 1997. Altered neural cell fates and medulloblastoma in mouse patched mutants. *Science*. **277**(5329), pp.1109–1113.

Guertin, D.A. and Sabatini, D.M. 2007. Defining the role of mTOR in cancer. *Cancer cell*. **12**(1), pp.9–22.

Gurung, R., and Parnaik, V. 2012. Cyclin D3 promotes myogenic differentiation and Pax7 transcription. *Journal of Cellular Biochemistry*. **113**(1), pp.209–219.

Hahn, H., Wicking, C., Zaphiropoulous, P.G., Gailani, M.R., Shanley, S., Chidambaram, A., Vorechovsky, I., Holmberg, E., Unden, A.B., Gillies, S., Negus, K., Smyth, I., Pressman, C., Leffell, D.J., Gerrard, B., Goldstein, A.M., Dean, M., Toftgard, R., Chenevix-Trench, G., Wainwright, B. and Bale, A.E. 1996. Mutations of the human homolog of Drosophila patched in the nevoid basal cell carcinoma syndrome. *Cell*. **85**(6), pp.841–851.

Halevy, O., Novitch, B.G., Spicer, D.B., Skapek, S.X., Rhee, J., Hannon, G.J., Beach, D. and Lassar, A.B. 1995. Correlation of terminal cell cycle arrest of skeletal muscle with induction of p21 by MyoD. *Science*. **267**(5200), pp.1018–1021.

Hamasaki, M., Furuta, N., Matsuda, A., Nezu, A., Yamamoto, A., Fujita, N., Oomori, H., Noda, T., Haraguchi, T., Hiraoka, Y., Amano, A. and Yoshimori, T. 2013. Autophagosomes form at ER-mitochondria contact sites. *Nature*, **495**(7441), pp.389–393.

Hammerschmidt, M., Brook, A. and McMahon, A.P. 1997. The world according to hedgehog. *Trends in genetics*. **13**(1), pp.14–21.

Hara, T. and Mizushima, N. 2009. Role of ULK-FIP200 complex in mammalian autophagy: FIP200, a counterpart of yeast Atg17? *Autophagy*. **5**(1), pp.85–87.

Hara, T., Takamura, A., Kishi, C., Iemura, S., Natsume, T., Guan, J.L. and Mizushima, N. 2008. FIP200, a ULK-Interacting Protein, Is Required for Autophagosome Formation in Mammalian Cells. *The Journal of Cell Biology*. **181**(3), pp.497–510.

Heitman, J., Movva, N.R. and Hall, M.N. 1991. Targets for cell cycle arrest by the immunosuppressant rapamycin in yeast. *Science*. **253**(5022), pp.905–909.

Hernández-Hernández, J.M., García-González, E.G., Brun, C.E. and Rudnicki, M.A. 2017. The myogenic regulatory factors, determinants of muscle development, cell identity and regeneration. *Seminars in cell & developmental biology*. **72**, pp.10–18.

Hidalgo, A. and Ingham, P. 1990. Cell patterning in the Drosophila segment: spatial regulation of the segment polarity gene patched. *Development*. **110**(1), pp.291–301.

Hosokawa, N., Hara, T., Kaizuka, T., Kishi, C., Takamura, A., Miura, Y., Iemura, S., Natsume, T., Takehana, K., Yamada, N., Guan, J.L., Oshiro, N. and Mizushima, N. 2009(a). Nutrient-dependent mTORC1 association with the ULK1-Atg13-FIP200 complex required for autophagy. *Molecular biology of the cell*. **20**(7), pp.1981–1991.

Hosokawa, N., Sasaki, T., Iemura, S., Natsume, T., Hara, T. and Mizushima, N. 2009(b). Atg101, a novel mammalian autophagy protein interacting with Atg13. *Autophagy*. **5**(7), pp.973–979.

Huangfu, D. and Anderson, K.V. 2006. Signaling from Smo to Ci/Gli: conservation and divergence of Hedgehog pathways from Drosophila to vertebrates. *Development*. **133**(1), pp.3–14.

Humke, E. W., Dorn, K.V., Milenkovic, L., Scott, M.P. and Rohatgi, R. 2010. The output of Hedgehog signaling is controlled by the dynamic association between Suppressor of Fused and the Gli proteins. *Genes & development*. **24**(7), pp.670–682.

Hunter, T. and Pines, J. 1994. Cyclins and cancer. II: Cyclin D and CDK inhibitors come of age. *Cell*. **79**(4), pp.573–582.

Hwang, S.Y., Kang, Y.J., Sung, B., Kim, M., Kim, D.H., Lee, Y., Yoo, M.A., Kim, C.M., Chung, H.Y. and Kim, N.D. 2015. Folic acid promotes the myogenic differentiation of C2C12 murine myoblasts through the Akt signaling pathway. *International journal of molecular medicine*. **36**(4), pp.1073–1080.

Ingham P.W. 1991. Segment polarity genes and cell patterning within the Drosophila body segment. *Current opinion in genetics & development*. **1**(2), pp.261–267.

Ingham, P.W. and McMahon, A.P. 2001. Hedgehog Signaling in Animal Development: Paradigms and Principles. *Genes & Development*. **15**(23), pp.3059–3087.

Ingham, P.W., Taylor, A.M. and Nakano, Y. 1991. Role of the Drosophila patched gene in positional signalling. *Nature*. **353**(6340), pp.184–187.

Isogai, S., Morimoto, D., Arita, K., Unzai, S., Tenno, T., Hasegawa, J., Sou, Y., Komatsu, M., Tanaka, K., Shirakawa, M. and Tochio, H. 2011. Crystal structure of the ubiquitin-associated (UBA) domain of p62 and its interaction with ubiquitin. *The Journal of Biological Chemistry*. **286**(36), pp.31864–31874.

Izzi, L., Lévesque, M., Morin, S., Laniel, D., Wilkes, B.C., Mille, F., Krauss, R.S., McMahon, A.P., Allen, B.L. and Charron, F. 2011. Boc and Gas1 each form distinct Shh receptor complexes with Ptch1 and are required for Shh-mediated cell proliferation. *Developmental cell*. **20**(6), pp.788–801.

Jahreiss, L., Menzies, F.M. and Rubinsztein, D.C. 2008. The itinerary of autophagosomes: from peripheral formation to kiss-and-run fusion with lysosomes. *Traffic*. **9**(4), pp.574–587.

Jenkins D. 2009. Hedgehog signalling: emerging evidence for non-canonical pathways. *Cellular signalling*. **21**(7), pp.1023–1034.

Johnson, R.L., Rothman, A.L., Xie, J., Goodrich, L.V., Bare, J.W., Bonifas, J.M., Quinn, A.G., Myers, R.M., Cox, D.R., Epstein, E.H., Jr, and Scott, M.P. 1996. Human homolog of patched, a candidate gene for the basal cell nevus syndrome. *Science*. **272**(5268), pp.1668–1671.

Johnson, R.L., Zhou, L. and Bailey, E.C. 2002. Distinct consequences of sterol sensor mutations in Drosophila and mouse patched homologs. *Developmental biology*. **242**(2), pp.224–235.

Kaur, J. and Debnath, J. 2015. Autophagy at the crossroads of catabolism and anabolism. *Nature Reviews*. **16**(8), pp.461–472.

Kawamura, S., Hervold, K., Ramirez-Weber, F.A. and Kornberg, T.B. 2008. Two Patched Protein Subtypes and a Conserved Domain of Group I Proteins That Regulates Turnover. *The Journal of Biological Chemistry*. **283**(45), pp.30964–30969.

Kennedy, B.K. and Lamming, D.W. 2016. The Mechanistic Target of Rapamycin: The Grand ConducTOR of Metabolism and Aging. *Cell metabolism*. **23**(6), pp.990–1003.

Kerr, J.F., Wyllie, A.H., & Currie, A.R. 1972. Apoptosis: a basic biological phenomenon with wide-ranging implications in tissue kinetics. *British journal of cancer*. **26**(4), pp.239–257.

Kihara, M., Kiyoshima, T., Nagata, K., Wada, H., Fujiwara, H., Hasegawa, K., Someya, H., Takahashi, I. and Sakai, H. 2014. Itm2a expression in the developing mouse first lower molar, and the subcellular localization of Itm2a in mouse dental epithelial cells. *PloS One*. **9**(7), pp.e103928–e103928.

Kim, D., Sarbassov, D., Ali, S., Latek, R., Guntur, K., Erdjument-Bromage, H., Tempst, P. and Sabatini, D. 2003. GβL, a Positive Regulator of the Rapamycin-Sensitive Pathway Required for the Nutrient-Sensitive Interaction between Raptor and mTOR. *Molecular Cell*. **11**(4), pp.895–904.

Kim, D.H., Sarbassov, D.D., Ali, S.M., King, J.E., Latek, R.R., Erdjument-Bromage, H., Tempst, P. and Sabatini, D. M. 2002. mTOR interacts with raptor to form a nutrient-sensitive complex that signals to the cell growth machinery. *Cell*. **110**(2), pp.163–175.

Kim, J., and Klionsky, D. 2000. Autophagy, cytoplasm-to-vacuole targeting pathway, and pexophagy in yeast and mammalian cells. *Annual Review of Biochemistry*. **69**(1), pp.303–342.

Kinzler, K.W., Ruppert, J.M., Bigner, S.H. and Vogelstein, B. 1988. The GLI gene is a member of the Kruppel family of zinc finger proteins. *Nature*. **332**(6162), pp.371–374.

Kirchner, J. and Bevan, M. 1999. ITM2A is induced during thymocyte selection and T cell activation and causes downregulation of CD8 when overexpressed in CD4(+)CD8(+) double positive thymocytes. *The Journal of Experimental Medicine*. **190**(2), pp.217–228.

Kirkin, V., McEwan, D., Novak, I. and Dikic, I. 2009. A Role for Ubiquitin in Selective Autophagy. *Molecular Cell*. **34**(3), pp.259–269.

Kiyokawa, H., Richon, V.M., Rifkind, R.A. and Marks, P.A. 1994. Suppression of cyclin-dependent kinase 4 during induced differentiation of erythroleukemia cells. *Molecular and cellular biology*. **14**(11), pp.7195–7203.

Klionsky, D. 2005. The molecular machinery of autophagy: unanswered questions. *Journal of Cell Science*. **118**(Pt 1), pp.7–18.

Klionsky, D. 2008. Autophagy revisited: A conversation with Christian de Duve. *Autophagy*. **4**(6), pp.740–743.

Klionsky, D., Mizushima, N., Cuervo, A. and Levine, B. 2008. Autophagy fights disease through cellular self-digestion. *Nature*. **451**(7182), pp.1069–1075.

Klionsky, D.J., Abdel-Aziz, A.K., Abdelfatah, S., Abdellatif, M., Abdoli, A., Abel, S., Abeliovich, H., Abildgaard, M.H., Abudu, Y.P., Acevedo-Arozena, A., Adamopoulos, I.E., Adeli, K., Adolph, T.E., Adornetto, A., Aflaki, E., Agam, G., Agarwal, A., Aggarwal, B.B., Agnello, M., Agostinis, P., … Tong, C.K. 2021. Guidelines for the use and interpretation of assays for monitoring autophagy (4th edition)1. *Autophagy*. **17**(1), pp.1–382.

Köchl, R., Hu, X., Chan, E. and Tooze, S. 2006. Microtubules Facilitate Autophagosome Formation and Fusion of Autophagosomes with Endosomes. *Traffic*. **7**(2), pp.129–145.

Kogerman, P., Krause, D., Rahnama, F., Kogerman, L., Unden, A.B., Zaphiropoulos, P.G. and Toftgard, R. 2002. Alternative first exons of PTCH1are differentially regulated in vivo and may confer different functions to the PTCH1 protein. *Oncogene*. **21**(39), pp.6007–6016.

Koleva, M., Kappler, R., Vogler, M., Herwig, A., Fulda, S. and Hahn, H. 2005. Pleiotropic effects of sonic hedgehog on muscle satellite cells. *Cellular and Molecular Life Sciences: CMLS.* **62**(16), pp.1863–1870.

Lagha, M., Mayeuf-Louchart, A., Chang, T., Montarras, D., Rocancourt, D., Zalc, A., Kormish, J., Zaret, K.S., Buckingham, M.E. and Relaix, F. 2013. Itm2a is a Pax3 target gene, expressed at sites of skeletal muscle formation in vivo. *PloS one*. **8**(5), p.e63143.

Lamb, C. A., Yoshimori, T. and Tooze, S. A. 2013. The autophagosome: origins unknown, biogenesis complex. *Nature reviews*. **14**(12), pp.759–774.

Lassar, A.B., Skapek, S.X. and Novitch, B. 1994. Regulatory mechanisms that coordinate skeletal muscle differentiation and cell cycle withdrawal. *Current opinion in cell biology*. **6**(6), pp.788–794.

Lauth, M. and Toftgård, R. 2007. Non-Canonical Activation of GLI Transcription Factors: Implications for Targeted Anti-Cancer Therapy. *Cell Cycle*. **6**(20), pp.2458–2463.

Lee, D.K. 2002. Androgen receptor enhances myogenin expression and accelerates differentiation. *Biochemical and Biophysical Research Communications*. **294**(2), pp.408–413.

Lee, E.J., Jan, A.T., Baig, M.H., Ahmad, K., Malik, A., Rabbani, G., Kim, T., Lee, I. K., Lee, Y.H., Park, S.Y. and Choi, I. 2018. Fibromodulin and regulation of the

intricate balance between myoblast differentiation to myocytes or adipocyte-like cells. *FASEB journal*. **32**(2), pp.768–781.

Lee, J.J., Ekker, S.C., von Kessler, D.P., Porter, J.A., Sun, B.I. and Beachy, P.A. 1994. Autoproteolysis in hedgehog protein biogenesis. *Science*. **266**(5190), pp.1528–1537.

Levine, B. and Kroemer, G. 2008. Autophagy in the pathogenesis of disease. *Cell*. **132**(1), pp.27–42.

Levine, B. and Kroemer, G. 2019. Biological Functions of Autophagy Genes: A Disease Perspective. *Cell*. **176**(1-2), pp.11–42.

Li, W., Li, J. and Bao, J. 2012. Microautophagy: lesser-known self-eating. *Cellular and Molecular Life Sciences : CMLS*. **69**(7), pp.1125–1136.

Lodish, H., Berk, A., Zipursky, S.L., Matsudaira, P., Baltimore, P. and Darnell, J. Molecular Cell Biology. 2000. *Interaction and Regulation of Signaling Pathways*. 4th edition. New York: W. H. Freeman [Accessed 23 March 2021] Available from: https://www.ncbi.nlm.nih.gov/books/NBK21659/

Loewith, R., Jacinto, E., Wullschleger, S., Lorberg, A., Crespo, J., Bonenfant, D., Oppliger, W., Jenoe, P. and Hall, M. 2002. Two TOR Complexes, Only One of which Is Rapamycin Sensitive, Have Distinct Roles in Cell Growth Control. *Molecular Cell*. **10**(3), pp.457–468.

Loftus, S.K., Morris, J.A., Carstea, E.D., Gu, J.Z., Cummings, C., Brown, A., Ellison, J., Ohno, K., Rosenfeld, M.A., Tagle, D.A., Pentchev, P.G. and Pavan, W.J. 1997. Murine model of Niemann-Pick C disease: mutation in a cholesterol homeostasis gene. *Science*. **277**(5323), pp.232–235.

Lopes, J.L., Miles, A.J., Whitmore, L. and Wallace, B.A. 2014. Distinct circular dichroism spectroscopic signatures of polyproline II and unordered secondary structures: applications in secondary structure analyses. *Protein science*. **23**(12), pp.1765–1772.

Lu, X., Liu, S. and Kornberg, T. 2006. The C-terminal tail of the Hedgehog receptor Patched regulates both localization and turnover. *Genes and development*. **20**(18), pp.2539–2551.

Luedde, T., Rodriguez, M.E., Tacke, F., Xiong, Y., Brenner, D.A. and Trautwein, C. 2003. p18(INK4c) collaborates with other CDK-inhibitory proteins in the regenerating liver. *Hepatology*. **37**(4), pp.833–841.

Lum, L., Yao, S., Mozer, B., Rovescalli, A., Von Kessler, D., Nirenberg, M. and Beachy, P.A. 2003. Identification of Hedgehog pathway components by RNAi in Drosophila cultured cells. *Science*. **299**(5615), pp.2039–2045.

Ma, Y., Erkner, A., Gong, R., Yao, S., Taipale, J., Basler, K. and Beachy, P.A. 2002. Hedgehog-mediated patterning of the mammalian embryo requires transporter-like function of dispatched. *Cell*. **111**(1), pp.63–75.

Malumbres, M. 2014. Cyclin-dependent kinases. *Genome Biology*. **15**(6), pp.122–122.

Malumbres, M. and Barbacid, M. 2009. Cell cycle, CDKs and cancer: a changing paradigm. *Nature reviews Cancer*. **9**(3), pp.153–166.

Mann, S.S. and Hammarback, J.A. 1994. Molecular characterization of light chain 3. A microtubule binding subunit of MAP1A and MAP1B. *The Journal of Biological Chemistry*. **269**(15), pp.11492–11497.

Martinelli, D.C. and Fan, C.M. 2007. Gas1 extends the range of Hedgehog action by facilitating its signaling. *Genes & development*. **21**(10), pp.1231–1243.

Marzella, L., Ahlberg, J. and Glaumann, H. 1981. Autophagy, heterophagy, microautophagy and crinophagy as the means for intracellular degradation. *Virchows Archiv. Abteilung B. Zellpathologie.* **36**(1), pp.219–234.

Massey, A., Kiffin, R., and Cuervo, A. 2004. Pathophysiology of chaperone-mediated autophagy. *International Journal of Biochemistry and Cell Biology*, **36**(12), pp.2420–2434.

Massey, A.C., Zhang, C., and Cuervo, A.M. 2006. Chaperone-mediated autophagy in aging and disease. *Current Topics in Developmental Biology*. **73**, pp.205–235.

Mauvezin, C., Nagy, P., Juhász, G., & Neufeld, T. P. 2015. Autophagosome-lysosome fusion is independent of V-ATPase-mediated acidification. *Nature communications*. **6**, p.7007.

McMahon, A.P., Ingham, P.W. and Tabin, C.J. 2003. Developmental roles and clinical significance of hedgehog signaling. *Current topics in developmental biology*. **53**, pp.1–114.

Melia, T., Lystad, A. and Simonsen, A. 2020. Autophagosome biogenesis: From membrane growth to closure. *The Journal of Cell Biology*. **219**(6), pp.e202002085.

Mercer, C.A., Kaliappan, A. and Dennis, P.B. 2009. A novel, human Atg13 binding protein, Atg101, interacts with ULK1 and is essential for macroautophagy. *Autophagy*. **5**(5), pp.649–662.

Mijaljica, D., Prescott, M. and Devenish, R. 2012. The intriguing life of autophagosomes. *International Journal of Molecular Sciences*. **13**(3), pp.3618–3635.

Mille, F., Thibert, C., Fombonne, J., Rama, N., Guix, C., Hayashi, H., Corset, V., Reed, J. C. and Mehlen, P. 2009. The Patched dependence receptor triggers apoptosis through a DRAL-caspase-9 complex. *Nature cell biology*. **11**(6), pp.739–746.

Mizushima, N. 2005. The pleiotropic role of autophagy: from protein metabolism to bactericide. *Cell death and differentiation*. **12**(2), pp.1535–1541.

Mizushima, N. and Komatsu, M. 2011. Autophagy: renovation of cells and tissues. *Cell*. **147**(4), pp.728–741.

Mizushima, N., Ohsumi, Y. and Yoshimori, T. 2002. Autophagosome Formation in Mammalian Cells. *Cell Structure and Function*. **27**(6), pp.421–429.

Mizushima, N., Yoshimori, T. and Levine, B. 2010. Methods in Mammalian Autophagy Research. *Cell.* **140**(3), pp.313–326.

Mortimore, G.E., Hutson, N.J. and Surmacz, C.A. 1983. Quantitative Correlation between Proteolysis and Macro- and Microautophagy in Mouse Hepatocytes during Starvation and Refeeding. *Proceedings of the National Academy of Sciences – PNAS*. **80**(8), pp.2179–2183.

Munafó, D.B. and Colombo, M.I. 2001. A novel assay to study autophagy: regulation of autophagosome vacuole size by amino acid deprivation. *Journal of cell science*. **114**(Pt 20), pp.3619-3629

Nakano, Y., Guerrero, I., Hidalgo, A., Taylor, A., Whittle, J. R., and Ingham, P. W. 1989. A protein with several possible membrane-spanning domains encoded by the Drosophila segment polarity gene patched. *Nature.* **341**(6242), pp.508–513.

Namkoong, S., Lee, K., Lee, J., Park, R., Lee, E., Jang, I., and Park, J. 2015. The integral membrane protein ITM2A, a transcriptional target of PKA-CREB, regulates autophagic flux via interaction with the vacuolar ATPase. *Autophagy*. **11**(5), pp.756–768.

Neufeld, T.P. 2010. TOR-dependent control of autophagy: biting the hand that feeds. *Current opinion in cell biology*. **22**(2), pp.157–168.

Nguyen, T., Shin, I., Lee, T., Park, J., Kim, J., Park, M. and Lee, E. 2015. Loss of ITM2A, a novel tumor suppressor of ovarian cancer through G2/M cell cycle arrest, is a poor prognostic factor of epithelial ovarian cancer. *Gynecologic Oncology*. **140**(3), pp.545–553.

Noda, T., Kirisako, T., Mizushima, N., Ueno, T., Yoshimori, T., Kabeya, Y., Kominami, E., Ohsumi, Y. and Yamamoto, A. 2000. LC3, a mammalian homologue of yeast Apg8p, is localized in autophagosome membranes after processing. *The EMBO Journal*. **19**(21), pp.5720–5728.

Norbury, C. and Nurse, P. 1992. Animal Cell Cycles and Their Control. *Annual Review of Biochemistry*. **61**(1), pp.441–468.

Nozawa, Y. I., Lin, C. and Chuang, P. T. 2013. Hedgehog signaling from the primary cilium to the nucleus: an emerging picture of ciliary localization, trafficking and transduction. *Current opinion in genetics & development*. **23**(4), pp.429–437.

Okada, A., Charron, F., Morin, S., Shin, D.S., Wong, K., Fabre, P.J., Tessier-Lavigne, M. and McConnell, S.K. 2006. Boc is a receptor for sonic hedgehog in the guidance of commissural axons. *Nature*. **444**(7117), pp.369–373.

Orenstein, S.J., and Cuervo, A.M. (2010). Chaperone-mediated autophagy:molecular mechanisms and physiological relevance. *Semin.Cell Dev. Biol*. **21**, pp.719–726.

Orsi, A., Razi, M., Dooley, H., Robinson, D., Weston, A., Collinson, L. and Tooze, S. 2012. Dynamic and transient interactions of Atg9 with autophagosomes, but not membrane integration, are required for autophagy. *Molecular Biology of the Cell*. **23**(10), pp.1860–1873.

Otto, T. and Sicinski, P. 2017. Cell cycle proteins as promising targets in cancer therapy. Nature reviews. *Cancer*. **17**(2), pp.93–115.

Pan, Y., Bai, C.B., Joyner, A. L. and Wang, B. 2006. Sonic hedgehog signaling regulates Gli2 transcriptional activity by suppressing its processing and degradation. *Molecular and cellular biology*. **26**(9), pp.3365–3377.

Pan, Y., Wang, C. and Wang, B. 2009. Phosphorylation of Gli2 by protein kinase A is required for Gli2 processing and degradation and the Sonic Hedgehog-regulated mouse development. *Developmental biology*. **326**(1), pp.177–189.

Pankiv, S., Clausen, T.H., Lamark, T., Brech, A., Bruun, J., Outzen, H., Øvervatn, A., Bjørkøy, G. and Johansen, T. 2007. p62/SQSTM1 Binds Directly to Atg8/LC3 to Facilitate Degradation of Ubiquitinated Protein Aggregates by Autophagy. *The Journal of Biological Chemistry*. **282**(33), pp.24131–24145.

Parker, S.B., Eichele, G., Zhang, P., Rawls, A., Sands, A.T., Bradley, A., Olson, E.N., Harper, J. W. and Elledge, S.J. 1995. p53-independent expression of p21Cip1 in muscle and other terminally differentiating cells. *Science*. **267**(5200), pp.1024–1027.

Pathi, S., Pagan-Westphal, S., Baker, D.P., Garber, E.A., Rayhorn, P., Bumcrot, D., Tabin, C.J., Blake Pepinsky, R. and Williams, K.P. 2001. Comparative biological responses to human Sonic, Indian, and Desert hedgehog. *Mechanisms of development*. **106**(1-2), pp.107–117.

Pavlidou, T., Rosina, M., Fuoco, C., Gerini, G., Gargioli, C., Castagnoli, L., and Cesareni, G. 2017. Regulation of myoblast differentiation by metabolic perturbations induced by metformin. *PloS One*. **12**(8), pp.e0182475–e0182475.

Pepinsky, R.B., Zeng, C., Wen, D., Rayhorn, P., Baker, D.P., Williams, K.P., Bixler, S.A., Ambrose, C.M., Garber, E.A., Miatkowski, K., Taylor, F.R., Wang, E.A. and Galdes, A. 1998. Identification of a Palmitic Acid-modified Form of Human Sonic hedgehog. *The Journal of Biological Chemistry*. **273**(22), pp.14037–14045.

Peppard, J.V., Rugg, C., Smicker, M., Dureuil, C., Ronan, B., Flamand, O., Durand, L. and Pasquier, B. 2014. Identifying Small Molecules which Inhibit Autophagy: a Phenotypic Screen Using Image-Based High-Content Cell Analysis. *Current chemical genomics and translational medicine*. **8**(Suppl1), pp.3-15.

Perry, R.L. and Rudnick, M.A. 2000. Molecular mechanisms regulating myogenic determination and differentiation. *Front Biosci*. **5**, pp.750-767.

Petrova, R. and Joyner, A. L. 2014. Roles for Hedgehog signaling in adult organ homeostasis and repair. *Development*. **141**(18), pp.3445–3457.

Pfeifer, U., Werder, E. and Bergeest, H. 1978. Inhibition by Insulin of the Formation of Autophagic Vacuoles in Rat Liver: A Morphometric Approach to the Kinetics of Intracellular Degradation by Autophagy. *The Journal of Cell Biology*. **78**(1), pp.152–167.

Pietrobono, S., Gagliardi, S. and Stecca, B. 2019. Non-canonical Hedgehog Signaling Pathway in Cancer: Activation of GLI Transcription Factors Beyond Smoothened. *Frontiers in genetics*. **10**, p.556.

Pines, J. 1995. Cyclins and cyclin-dependent kinases: a biochemical view. *The Biochemical journal*. **308**(Pt 3), pp.697–711.

Polizio, A.H., Chinchilla, P., Chen, X., Kim, S., Manning, D.R. and Riobo, N.A. 2011. Heterotrimeric Gi proteins link Hedgehog signaling to activation of Rho small GTPases to promote fibroblast migration. *The Journal of biological chemistry*. **286**(22), pp.19589–19596.

Porter, J.A., von Kessler, D.P., Ekker, S.C., Young, K.E., Lee, J.J., Moses, K. and Beachy, P.A. 1995. The product of hedgehog autoproteolytic cleavage active in local and long-range signalling. *Nature*. **374**(6520), pp.363–366.

Porter, J.A., Young, K.E. and Beachy, P.A. 1996. Cholesterol modification of hedgehog signaling proteins in animal development. *Science*. **274**(5285), pp.255–259.

Prosser, S.L., and Morrison, C.G. 2015. Centrin2 regulates CP110 removal in primary cilium formation. *The Journal of cell biology*. **208**(6), pp.693–701.

Qi, X., Schmiege, P., Coutavas, E. and Li, X. 2018. Two Patched molecules engage distinct sites on Hedgehog yielding a signaling-competent complex. *Science*. **362**(6410), p.eaas8843.

Rabinowitz, J.D. and White, E. 2010. Autophagy and Metabolism. *Science*. **330**(6009), pp.1344–1348.

Rao, S.S., Chu, C. and Kohtz, D.S. 1994. Ectopic expression of cyclin D1 prevents activation of gene transcription by myogenic basic helix-loop-helix regulators. *Molecular and cellular biology*. **14**(8), pp.5259–5267.

Richards, A., Eckhardt, M., and Krogan, N. 2021. Mass spectrometry-based protein–protein interaction networks for the study of human diseases. *Molecular Systems Biology*. **17**(1), pp.e8792–n/a.

Riddle, R.D., Johnson, R.L., Laufer, E. and Tabin, C. 1993. Sonic hedgehog mediates the polarizing activity of the ZPA. *Cell*. **75**(7), pp.1401–1416.

Riobo N.A. 2012. Cholesterol and its derivatives in Sonic Hedgehog signaling and cancer. *Current opinion in pharmacology*. **12**(6), pp.736–741.

Robbins, D.J., Fei, D.L. and Riobo, N.A. 2012. The Hedgehog signal transduction network. *Science signaling*. **5**(246), p.re6.

Robbins, D.J., Nybakken, K.E., Kobayashi, R., Sisson, J.C., Bishop, J.M. and Thérond, P.P. 1997. Hedgehog elicits signal transduction by means of a large complex containing the kinesin-related protein costal2. *Cell*. **90**(2), pp.225–234.

Rohatgi, R., Milenkovic, L. and Scott, M.P. 2007. Patched1 regulates hedgehog signaling at the primary cilium. *Science*. **317**(5836), pp.372–376.

Ruiz i Altaba, A. 1999. Gli proteins and Hedgehog signaling: development and cancer. *Trends in Genetics*. **15**(10), pp.418–425.

Russell, R., Tian, Y., Yuan, H., Park, H., Chang, Y., Kim, J., Kim, H., Neufeld, T., Dillin, A. and Guan, K. 2013. ULK1 induces autophagy by phosphorylating Beclin-1 and activating VPS34 lipid kinase. *Nature Cell Biology*. **15**(7), pp.741–750.

Sabatini, D.M., Erdjument-Bromage, H., Lui, M., Tempst, P. and Snyder, S.H. 1994. RAFT1: a mammalian protein that binds to FKBP12 in a rapamycin-dependent fashion and is homologous to yeast TORs. *Cell*. **78**(1), pp.35–43.

Sánchez-Pulido, L., Devos, D. and Valencia, A. 2002. BRICHOS: a conserved domain in proteins associated with dementia, respiratory distress and cancer. *Trends in biochemical sciences*. **27**(7), pp.329–332.

Sarbassov, D.D., Ali, S.M. and Sabatini, D.M. 2005. Growing roles for the mTOR pathway. *Current opinion in cell biology*. **17**(6), pp.596–603.

Sasaki, H., Nishizaki, Y., Hui, C., Nakafuku, M. and Kondoh, H. 1999. Regulation of Gli2 and Gli3 activities by an amino-terminal repression domain: implication of Gli2 and Gli3 as primary mediators of Shh signaling. *Development.* **126**(17), pp.3915–3924.

Schafer, K.A. 1998. The cell cycle: a review. *Veterinary pathology*. **35**(6), pp.461–478.

Schworer, C.M., Shiffer, K.A. and Mortimore, G.E. 1981. Quantitative relationship between autophagy and proteolysis during graded amino acid deprivation in perfused rat liver. *The Journal of Biological Chemistry*. **256**(14), pp.7652–7658.

Seibenhener, M.L., Babu, J.R., Geetha, T., Wong, H.C., Krishna, N.R. and Wooten, M.W. 2004. Sequestosome 1/p62 Is a Polyubiquitin Chain Binding Protein Involved in Ubiquitin Proteasome Degradation. *Molecular and Cellular Biology*. **24**(18), pp.8055–8068.

Sherr, C.J. and Roberts, J.M. 1999. CDK inhibitors: positive and negative regulators of G1-phase progression. *Genes & development*. **13**(12), pp.1501–1512.

Simpson, F., Kerr, M.C. and Wicking, C. 2009. Trafficking, development and hedgehog. *Mechanisms of development*. **126**(5-6), pp.279–288.

Skapek, S.X., Rhee, J., Spicer, D.B. and Lassar, A.B. 1995. Inhibition of myogenic differentiation in proliferating myoblasts by cyclin D1-dependent kinase. *Science*. **267**(5200), pp.1022–1024.

Stinchcombe, J.C. and Griffiths, G.M. 2014. Communication, the centrosome and the immunological synapse. *Philosophical transactions of the Royal Society of London. Series B, Biological sciences*. **369**(1650), p.20130463.

Stone, D.M., Hynes, M., Armanini, M., Swanson, T.A., Gu, Q., Johnson, R.L., Scott, M.P., Pennica, D., Goddard, A., Phillips, H., Noll, M., Hooper, J.E., de Sauvage, F. and Rosenthal, A. 1996. The tumour-suppressor gene patched encodes a candidate receptor for Sonic hedgehog. *Nature*. **384**(6605), pp.129–134.

Suzuki, K. and Ohsumi, Y. 2010. Current knowledge of the pre-autophagosomal structure (PAS). *FEBS letters*. **584**(7), pp.1280–1286.

Sveen, A., Johannessen, B., Tengs, T., Danielsen, S.A., Eilertsen, I.A., Lind, G. E., Berg, K., Leithe, E., Meza-Zepeda, L.A., Domingo, E., Myklebost, O., Kerr, D., Tomlinson, I., Nesbakken, A., Skotheim, R.I., & Lothe, R.A. 2017. Multilevel genomics of colorectal cancers with microsatellite instability-clinical impact of JAK1 mutations and consensus molecular subtype 1. *Genome medicine*. **9**(1), p.46.

Szklarczyk, D., Gable, A.L., Lyon, D., Junge, A., Wyder, S., Huerta-Cepas, J., Simonovic, M., Doncheva, N.T., Morris, J.H., Bork, P., Jensen, L.J. and Mering, C.V. 2019. STRING v11: protein-protein association networks with increased coverage, supporting functional discovery in genome-wide experimental datasets. *Nucleic acids research*. **47**(D1), pp.D607–D613.

Tai, T., Pai, S., and Ho, I. 2014. Itm2a, a target gene of GATA-3, plays a minimal role in regulating the development and function of T cells. *PloS One*. **9**(5), pp.e96535–e96535.

Taipale, J., Cooper, M.K., Maiti, T. and Beachy, P.A. 2002. Patched acts catalytically to suppress the activity of Smoothened. *Nature*. **418**(6900), pp.892–897.

Tang, J., He, A., Yan, H., Jia, G., Liu, G., Chen X., Cai, J., Tian, G., Shang, H. and Zhao, H. 2018. Damage to the myogenic differentiation of C2C12 cells by heat stress is associated with up-regulation of several selenoproteins. *Scientific Reports*. **8**(1), pp.10601–10609.

Tanida, I., Minematsu-Ikeguchi, N., Ueno, T. and Kominami, E. 2005. Lysosomal Turnover, but Not a Cellular Level, of Endogenous LC3 is a Marker for Autophagy. *Autophagy*. **1**(2), pp.84–91.

Tenzen, T., Allen, B.L., Cole, F., Kang, J.S., Krauss, R.S. and McMahon, A.P. 2006. The cell surface membrane proteins Cdo and Boc are components and targets of the Hedgehog signaling pathway and feedback network in mice. *Developmental cell*. **10**(5), pp.647–656.

Thibert, C., Teillet, M.A., Lapointe, F., Mazelin, L., Le Douarin, N.M. and Mehlen, P. 2003. Inhibition of neuroepithelial patched-induced apoptosis by sonic hedgehog. *Science*. **301**(5634), pp.843–846.

Thu, K.L., Soria-Bretones, I., Mak, T. W. and Cescon, D.W. 2018. Targeting the cell cycle in breast cancer: towards the next phase. *Cell cycle*. **17**(15), pp.1871–1885.

Tuckermann, J., Pittois, K., Partridge, N., Merregaert, J. and Angel, P. 2000. Collagenase-3 (MMP-13) and Integral Membrane Protein 2a (Itm2a) are Marker Genes of Chondrogenic/Osteoblastic Cells in Bone Formation: Sequential Temporal, and Spatial Expression of Itm2a, Alkaline Phosphatase, MMP-13, and Osteocalcin in the Mouse. *Journal of Bone and Mineral Research*. **15**(7), pp.1257–1265.

Tuson, M., He, M. and Anderson, K.V. 2011. Protein kinase A acts at the basal body of the primary cilium to prevent Gli2 activation and ventralization of the mouse neural tube. *Development*. **138**(22), pp.4921–4930.

Vadlamudi, R. K., Joung, I., Strominger, J.L. and Shin, J. 1996. p62, a phosphotyrosine-independent ligand of the SH2 domain of p56lck, belongs to a new class of ubiquitin-binding proteins. *The Journal of Biological Chemistry*. **271**(34), pp.20235–20237.

Valdespino-Gómez, V.M., Valdespino-Castillo, P.M. and Valdespino-Castillo, V.E. 2015. Interacción de las vías de señalización intracelulares participantes en la proliferación celular: potencial blanco de intervencionismo terapéutico [Cell signaling pathways interaction in cellular proliferation: Potential target for therapeutic interventionism]. *Cirugia y cirujanos*. **83**(2), pp.165–174.

van den Heuvel, M. and Ingham, P.W. 1996. smoothened encodes a receptor-like serpentine protein required for hedgehog signalling. *Nature*. **382**(6591), pp.547–551.

Van den Plas, D. and Merregaert, J. 2004a. Constitutive overexpression of the integral membrane protein Itm2A enhances myogenic differentiation of C2C12 cells. *Cell Biology International*. **28**(3), pp.199–207.

Van den Plas, D., and Merregaert, J. 2004b. In vitro studies on Itm2a reveal its involvement in early stages of the chondrogenic differentiation pathway. *Biology of the Cell*. **96**(6), pp.463–470.

Vermeulen, K., Van Bockstaele, D.R. and Berneman, Z.N. 2003. The cell cycle: a review of regulation, deregulation and therapeutic targets in cancer. *Cell proliferation*. **36**(3), pp.131–149.

Vézina, C., Kudelski, A. and Sehgal, S.N. 1975. Rapamycin (AY-22,989), a new antifungal antibiotic. I. Taxonomy of the producing streptomycete and isolation of the active principle. *The Journal of antibiotics*. **28**(10), pp.721–726.

Walsh, K. and Perlman, H. 1997. Cell cycle exit upon myogenic differentiation. *Current Opinion in Genetics & Development*. **7**(5), pp.597–602.

Wang, C. and Klionsky, D. 2003. The molecular mechanism of autophagy. *Molecular Medicine*. **9**(3-4), pp.65–76.

Wang, G., Amanai, K., Wang, B. and Jiang, J. 2000. Interactions with Costal2 and suppressor of fused regulate nuclear translocation and activity of cubitus interruptus. *Genes & development*, **14**(22), pp.2893–2905.

Wang, Y., Peterson, S.E. and Loring, J.F. 2014. Protein post-translational modifications and regulation of pluripotency in human stem cells. *Cell Research*. **24**(2), pp.143-160.

Wen, X. and Klionsky, D. J. 2016. An overview of macroautophagy in yeast. *Journal of molecular biology*. **428**(9 Pt A), pp.1681–1699.

White, E. 2012. Deconvoluting the context-dependent role for autophagy in cancer. *Nature reviews. Cancer*. **12**(6), pp.401–410.

Wieschaus, E. and Nüsslein-Volhard, C. 1980. Mutations affecting segment number and polarity in Drosophila. *Nature*. **287**(5785), pp.795–801.

Williamson, D.L., Butler, D.C. and Always, S.E. 2009. AMPK inhibits myoblast differentiation through a PGC-1α-dependent mechanism. *American Journal of Physiology – Endocrinology And Metabolism*. **297**(2), pp.304–314.

Wong, P.M., Puente, C., Ganley, I.G. and Jiang, X. 2013. The ULK1 complex: sensing nutrient signals for autophagy activation. *Autophagy*. **9**(2), pp.124–137.

Xie, Z., Nair, U. and Klionsky, D. 2008. Atg8 controls phagophore expansion during autophagosome formation. *Molecular Biology of the Cell.* **19**(8), pp.3290–3298.

Yaffe, D. and Saxel, O. 1977. Serial passaging and differentiation of myogenic cells isolated from dystrophic mouse muscle. *Nature.* **270**(5639), pp.725–727.

Yamamoto, A., Masaki, R. and Tashiro, Y. 1990. Characterization of the isolation membranes and the limiting membranes of autophagosomes in rat hepatocytes by lectin cytochemistry. *The journal of histochemistry and cytochemistry*. **38**(4), pp.573–580.

Yang, J., Andre, P., Ye, L. and Yang, Y.Z. 2015. The Hedgehog signalling pathway in bone formation*. International journal of oral science*. **7**(2), pp.73–79.

Yang, Z. and Klionsky, D. J. 2010. Eaten alive: a history of macroautophagy. *Nature cell biology*. **12**(9), pp.814–822.

Yao, S., Lum, L. and Beachy, P. 2006. The ihog cell-surface proteins bind Hedgehog and mediate pathway activation. *Cell*. **125**(2), pp.343–357.

Yorimitsu, T. and Klionsky, D.J. 2005. Autophagy: molecular machinery for self-eating. *Cell death and differentiation*, **12 Suppl 2**(Suppl 2), pp.1542–1552.

Yoshii, S.R. and Mizushima, N. 2017. Monitoring and Measuring Autophagy. *International journal of molecular sciences*. **18**(9), p.1865.

Young, A., Chan, E., Hu, X., Köchl, R., Crawshaw, S., High, S., Hailey, D., Lippincott-Schwartz, J. and Tooze, S. 2006. Starvation and ULK1-dependent cycling of

mammalian Atg9 between the TGN and endosomes. *Journal of Cell Science*. **119**(Pt 18), pp.3888–3900.

Young, K., Lee, E., Litingtung, Y., Westphal, H., Beachy, P., Corden, J. and Chiang, C. 1996. Cyclopia and defective axial patterning in mice lacking Sonic hedgehog gene function. *Nature*. **383**(6599), pp.407–413.

Yu, L., Chen, Y. and Tooze, S.A. 2018. Autophagy pathway: Cellular and molecular mechanisms. *Autophagy*. **14**(2), pp.207–215.

Zachari, M. and Ganley, I. 2017. The mammalian ULK1 complex and autophagy initiation. *Essays in Biochemistry*. **61**(6), pp.585–596.

Zarrinpar, A., Bhattacharyya, R.P. and Lim, W.A. 2003. The structure and function of proline recognition domains. *Science's STKE : signal transduction knowledge environment*. **2003**(179), pp.RE8.

Zeng, X., Overmeyer, J. and Maltese, W. 2006. Functional specificity of the mammalian Beclin-Vps34 PI 3-kinase complex in macroautophagy versus endocytosis and lysosomal enzyme trafficking. *Journal of Cell Science*. **119**(Pt 2), pp.259–270.

Zhang, J., Waeber, C., Pérez-Sala, D., Baek, S., Stang, M., et al. 2016. Guidelines for the use and interpretation of assays for monitoring autophagy (3rd edition). *Autophagy*. **12**(1), pp.1-222

Zhao, Y., Tong, C. and Jiang, J. 2007. Hedgehog regulates smoothened activity by inducing a conformational switch. *Nature*. **450**(7167), pp.252–258.

Zhao, Y.G. and Zhang, H. 2019. Autophagosome maturation: An epic journey from the ER to lysosomes. *The Journal of cell biology*, **218**(3), pp.757–770.

Zheng, X., Mann, R.K., Sever, N., & Beachy, P.A. 2010. Genetic and biochemical definition of the Hedgehog receptor. *Genes & development*. **24**(1), pp.57–71.

Zhou, C., Wang, M., Yang, J., Xiong, H., Wang, Y. and Tang, J. 2019. Integral membrane protein 2A inhibits cell growth in human breast cancer via enhancing autophagy induction. *Cell Communication and Signaling*. **17**(1), pp.105–105.

Zhu, J., Nakamura, E., Nguyen, M. T., Bao, X., Akiyama, H. and Mackem, S. 2008. Uncoupling Sonic hedgehog control of pattern and expansion of the developing limb bud. *Developmental cell*. **14**(4), pp.624–632.